PROCESS AND CULTIVATION STRATEGIES FOR THE HUMAN INDUSTRIAL CELL LINE AGE1.HN

Vom Promotionsausschuss der
Technischen Universität Hamburg-Harburg

zur Erlangung des akademischen Grades

Doktor-Ingenieur (Dr.-Ing.)

genehmigte Dissertation

von

Oscar Ben-Jail Platas Barradas

aus

Xalapa, Veracruz, Mexiko

2014

Gutachter:

Prof. Dr.-Ing. Ralf Pörtner

Prof. Dr. rer. nat. An-Ping Zeng

Prof. Dr. rer. nat. Thomas Scheper

Prüfungsvorsitzender:

Prof. Dr.-Ing. Michael Schlütter

Tag der mündlichen Prüfung:

10. Januar 2014

Danksagung

Mein besonderer Dank gilt meinem Doktorvater Herr Prof. Dr.-Ing. Ralf Pörtner für das mir entgegengebrachte Vertrauen während der Durchführung meiner Promotion, für die konstruktiven Diskussionen und für die mir gegönnte Freiheit bei der Bearbeitung der Promotionsthemen.

Ebenso bedanke ich mich herzlich bei Herrn Prof. Dr. An-Ping Zeng, Leiter des Instituts für Bioprozess- und Biosystemtechnik (IBB) und des Verbundprojektes SysLogics, für die Motivation während meiner Experimente und die immer angenehmen Diskussionen.

Herrn Prof. Dr. Thomas Scheper danke ich für die Prüfung meiner Arbeit und die enge Zusammenarbeit mit seinen Mitarbeitern innerhalb des Projektes SysLogics. Herrn Prof. Dr.-Ing. Michael Schlütter danke ich für die Übernahme der Prüfungsvorsitzenderfunktion.

Ein besonderer Dank gilt an Herrn Dr. Uwe Jandt, der während der Durchführung meiner Versuche immer an meiner Seite stand und mit großem Interesse, Tat und Kraft das Prozessleitsystem im Zellkulturlabor auf den neuen Stand der Technik brachte.

Ich bedanke mich auch bei Frau Dr. Christiane Goepfert, die immer für mich ein offenes Ohr hatte und mich jederzeit selbstverständlich bei der Organisation der Synchronisationsversuche unterstützt hat.

Grit Blume, Kerstin Michael, Katharina Wiegandt und Janina Bahnemann danke ich für das stets angenehme Arbeitsklima und die fruchtbare Zusammenarbeit im Zellkulturbereich.

Meinen Studenten Martin Schaletzky, Linh Da Minh Phan, Berkan Ünal, Olga Rivas, Anja Dittmann, Mario Eduardo Villanueva, Onur Serçinoğlu, Daniel Vázquez Ramírez, Sebastian Schubert, Simon Kern, Max Becker und Mostafa Aasif danke ich herzlichst für Ihr Engagement und für das Interesse bei der Durchführung der Versuche.

Herrn Cord Heineking von der Forschungswerkstatt Maschinenbau (FWM) und Herrn Frank Sokolinski und Herrn Werner Knutzen von der Forschungswerkstatt Elektrotechnik (FWE) danke ich für die Fertigung von zahlreichen Stahl- und Elektroausrüstungen für Forschung und Praktika innerhalb des IBBs.

A mis padres Emma Barradas Palmeros y Pablo Platas Hernández

Abstract

This work focuses on the development of process and cultivation strategies for a systematic characterization and optimization of mammalian cell cultures, especially for the novel human industrial cell line AGE1.HN. This cell line was studied within the collaborative project SysLogics -Systems Biology of Cell Culture for Biologics- with the final goal of generating quantitative and systematic data on mammalian cell metabolism.

In the first part of this work optimal operation windows in lab-scale mammalian cell culture are identified, which should also allow for comparability of results generated during cultivations in geometrically different bioreactor systems. Power input, mixing time, maximum fluid velocity and Reynolds number were systematically compared for the cultivation of AGE1.HN cells in shake flasks as well as in five different benchtop bioreactor systems. Proper operation ranges were identified for all systems using the maximal cell-specific growth rate (μ_{max}) as an indicator. Specific operation ranges in bioreactors were identified for the impeller tip speed, whereas the power input and the Reynolds number allow for comparability in shake flask cultivations. Furthermore, maximum cell growth was found in both systems when mixing time was used as the comparison parameter. The average standard deviation of μ_{max} for the process operation ranges studied was reduced to 25 % (absolute) of its initial value in both the bioreactors and shake flasks. These results intend to guarantee consistency of the results within partner laboratories.

The second part of this work aimed at developing a strategy for cell synchronization which should allow for a quantitative study of cell cycle dependent metabolic pathways. This kind of research requires not only the synchronization of a cell population within the cell cycle, but also further synchronous growth under physiological conditions. Physical methods including temperature shift and countercurrent centrifugal elutriation were evaluated and experimentally tested for synchronization of AGE1.HN cells. Cell-size distribution, DNA-content and the number of synchronous divisions were used for comparison of the methods. Our results showed, that a temperature shift allowed for an enrichment of a whole cell population in the S phase (up to 80 %). Furthermore, using the countercurrent flow centrifugal elutriation, different subpopulations were obtained with synchrony yields close to 95 % and 75 % in the G_1 and G_2/M phases respectively. Further cultivation of the synchronous cells in bioreactors allowed for a physiological growth state and solved the need for high cell numbers for analytics.

The third part aimed at reducing the time needed for the evaluation of feeding strate-

gies with mammalian cells during fed-batch culture. Although fed-batch cultivation of mammalian cells is a well established and reliable strategy for achieving high cell density and product titer during culture, the selection and configuration of feeding strategies has been mostly based on empirical approaches. In order to evaluate different feeding strategies for the industrial cell line AGE1.HN, a MATLAB®-based software tool was developed for the simulation of cell growth for different fed-batch strategies. It enables an easy-to-perform determination of kinetic parameters, which are afterwards set into a kinetic growth model. After verification of the model in laboratory, a constant linear feeding profile was tested as a proof of concept for the proposed strategy. The results showed consistent data prediction and an average difference of 17 % between simulated and experimental data. This strategy can be implemented in order to reduce the number of experiments during discretization of fed-batch strategies in mammalian cell cultures.

The strategies developed in this work establish a solid basis for systematic studies with mammalian production cell lines, by allowing for their characterization from an engineering point of view, and the implementation of results in systems biology research.

Keywords: process standardization, bioreactor, shake flask, cell-cycle synchronization, synchronous growth, elutriation, dialysis bioreactor, fed-batch, software tool, feeding strategy.

First Author Publications

Platas Barradas, O., Jandt, U., Becker, M., Bahnemann, J., Pörtner, R. and Zeng, A.-P. Synchronized mammalian cell culture: Part I – A physical strategy for synchronized cultivation under physiological conditions. Accepted for publication in Biotechnology Progress.

Platas Barradas, O., Jandt, U., Minh Phan, L. D., Villanueva, M. E., Schaletzky, M., Rath, A., Freund, S., Reichl, U., Skerhutt, E., Scholz, S., Noll, T., Sandig, V., Pörtner, R. and Zeng, A.-P. (2012), Evaluation of criteria for bioreactor comparison and operation standardization for mammalian cell culture. Eng. Life Sci., 12: 518528. doi: 10.1002/elsc.201100163.

Platas Barradas, O., Jandt, U., Phan, L.D.M., Villanueva, M., Rath, A., Reichl, U., Schräder, E., Scholz, S., Noll, T., Sandig, V., Pörtner, R., Zeng, A.-P. (2011). Criteria for bioreactor comparison and operation standardisation during process development for mammalian cell culture. BMC Proceedings, 5(Suppl 8):P47.

Platas Barradas, O., Jandt, U., Hass, R., Kasper, C., Sandig, V., Pörtner, R., Zeng, A.-P. (2011). Physical methods for synchronization of a human production cell line. BMC Proceedings, 5(Suppl 8):P49.

Conference Presentations

Synchronization of an Eukaryotic Industrial Cell Line for Systems Biology Research. GVC/DECHEMA Conference: Biopharmazeutische Produktion, Freiburg, Germany.

Bioreactor Design Parameters for the Cultivation of a Human Industrial Cell Line in Laboratory Scale. GVC/DECHEMA Conference: Bioprozessorientiertes Anlagendesign, Nürnberg, Germany.

Contents

Symbols and Abbreviations

Symbols

a_b	baffle depth [m]
A	cross-sectional area [m^2]
b_b	baffle width [m]
C	concentration [$mol\,L^{-1}$, $g\,L^{-1}$]
C_1, C_2	constants [-]
d_b	shake flask diameter at flask bottom [m]
d_i	impeller diameter, maximum shake flask diameter [m]
$d_{i,mod}$	modified shake flask diameter [m]
d_o	shaking diameter [m]
$d_{p,i}$	particle diameter [μm]
d_T	vessel diameter [m]
$\Delta\, h$	impeller interspacing [m]
η	dynamic viscosity [Pa s]
F	flow rate [$m^3\,s^{-1}$]
Fl	Flow Number, $QN^{-1}\,d_i^{-3}$ [-]
Fr_a	axial Froude number [-]
φ_i	osmotic coefficient [-]
g	gravitational force constant = 9.81 [$m\,s^{-2}$]
H	liguid height from bioreactor bottom to filling surface [m]
h	height of the liquid at shake-flask wall [m]
h_T	height of the shake flask [m]
h_1	lower-impeller distance to tank bottom [m]
k	constant [-]
$K_{H_{cp}}$	Henry coefficient [$mol\,m^{-3}\,Pa^{-1}$]
$k_L\,a$	volumetric oxygen transfer coefficient [h^{-1}]
l_i	blade length [m]
M	mixing degree [%]
μ_{max}	specific growth rate [d^{-1}]
N	agitation speed, shaking velocity [min^{-1}]
$N_{\Omega,\mathrm{par}}$	percentage of parental cells in the same cell cycle phase [%]

N_Ω	percentage of cells in the same cell cycle phase within a subpopulation (synchrony degree) [%]
n_i	number of impeller blades [-]
n_b	number of baffles [-]
Np	power number, $Np = P/\rho N^3 d_i^5$ [-]
Np'	modified Power Number [-]
$N\Theta_M$	mixing number [-]
ω=2πN/60	centrifugal velocity [s^{-1}]
P_o	shake flask's outer perimeter [m]
Pg	gassed power [$W\,m^{-3}$]
P/V	specific (volumetric) power input [$W\,m^{-3}$]
p	propeller pitch [m]
p_{abs}	absolute pressure [bar]
q_{Glc}	specific glucose uptake rate [$mmol\,cell^{-1}\,h^{-1}$]
q_{Lac}	specific lactate production rate [$mmol\,cell^{-1}\,h^{-1}$]
q_{O_2}	specific oxygen consumption rate [$mmol\,cell^{-1}\,h^{-1}$]
R	centrifugal radius [m], gas constant = 8.314 [$J\,K^{-1}\,mol^{-1}$]
Re	Reynolds number [-]
r_p	particle (cell) radius [μm]
ρ	density [$kg\,m^{-3}$]
s_w	standard deviation of the mean cell diameter [μm]
s_{wall}	wall thickness [mm]
T	Temperature [°C, K]
t	time [h]
t_d	doubling time [h]
Θ_M	mixing time [s]
u_i	maximum fluid velocity, impeller tip speed [$m\,s^{-1}$]
V_{sG}	settling velocity [$cm\,min^{-1}$]
V_T	total volume [m^3]
V_w	working volume [m^3]
w_b	baffle width [m]
w_i	impeller blade width [m]
X_v	viable cell density [cells mL^{-1}]

X_t	total cell density [cells mL^{-1}]
X_w	mean cell diameter [μm]
$Y_{X/Glc}$	biomass-to-substrate yield coefficient [10^{10} cells mmol_{Glc}^{-1}]
Y_{sync}	enrichment factor [-]
y_{O_2}	oxygen partial pressure [-]
z	number of impellers [-]

Abbreviations

3-MP	3-blade marine propeller
3-S	3-blade segment impeller
4-PBT	4-pitch-blade turbine
6-RT	6-blade radial-discharging impeller (Rushton)
DO	Dissolved Oxygen
FSC	Forward Scatter Channel
MS	Measured Signal
OTR	Oxygen Transfer Rate [$\mathrm{mmol\,L^{-1}\,h^{-1}}$]
OUR	Oxygen Uptake Rate [$\mathrm{mmol\,L^{-1}\,h^{-1}}$]
PDH	Pyruvate Dehydrogenase
PBS	Phosphate Buffer Saline
PI	Propidium Iodide
RS	Ring Sparger
rpm	revolutions per minute [min^{-1}]
SSC	Side Scatter Channel
TCD	Total Cell Density
VCD	Viable Cell Density

List of Figures

List of Tables

1 Motivation and Objectives

The joint project "SysLogics"[1] aimed at the adaptation and development of methods specific to systems biology, and tools for the mathematical modelling and analysis of key metabolic and regulatory processes in mammalian cell culture, used for the production of biologics. Specifically, the dynamics of central metabolism and the cell cycle and their interactions during growth and product formation of a novel human cell line were studied so that the performance of cells under varied physiological conditions or with genetic modifications could be analysed and eventually predicted [Zeng and Pörtner (2013)].

The object of this research was the industrial cell line AGE1.HN, a suspendable cell line which was generated from human neural tissue and transfected with adenovirus 5 E1A and B genes for immortalization. AGE1.HN grows in serum-free medium and has shown reduced nutrient consumption rates and a low accumulation of toxic byproducts. Furthermore it is capable of producing complex and highly fucosylated proteins, e.g. the human protease inhibitor alpha-1-antitrypsin (A1AT). A1AT produced in AGE1.HN cells has shown the same biological activity compared to that isolated from human serum [Blanchard et al. (2011)]. This makes the AGE1.HN cell line potentially interesting for research and industrial applications.

The systems biology study of the central metabolism and of cell cycle dependent reactions requires the collaboration of different research groups for the development and application of various methods for the generation of metabolic data. One of the first objectives within this project was to contribute from a biochemical engineering standpoint with a basis for consistency of data by means of comparing cell growth in five geometrically different bioreactors as well as in two shake flask systems within the research groups. By using geometric relevant parameters and operating conditions from each culture system, dimensionless numbers can be calculated for each system during culture. A dependency of cell growth on the dimensionless parameters is expected, where comparable cell growth for the different systems might be found.

Within further systems biology goals of this project, reproducible synchronous cell

[1]Systems Biology of Cell Culture for Biologics. Participating Institutions: ProBioGen AG, Berlin, CeBiTec/Bielefeld University, Bielefeld; Leibniz University Hannover, Hannover; Max Planck Institute for Dynamics of Complex Technical Systems, Magdeburg; Hamburg University of Technology, Hamburg; and Saarland University, Saarland. Supported by the German Federal Ministry of Education and Research (BMBF), Project Nr. 0315275A.

growth of AGE1.HN cells under physiological conditions was set as a requirement for the systematic study of the cell-cycle dependent metabolism. Furthermore, synchronous growth should not be affected by other variables in the cell surrounding millieu (limitation, inhibition, etc.), since this would affect the dynamics of cell metabolism. In this way the motivation for the implementation of a cell synchronization process is to select and implement a method, which allows for a low perturbation of metabolism as well as for exponential cell growth over many population doublings. As a proof of concept, the developed protocol will be applied for the synchronization of an industrial CHO-K1 cell line.

Finally, the choice for industrial cultivation of AGE1.HN cells can be analyzed by the development of a reliable method for the evaluation of feeding strategies in fed-batch culture. For the evaluation of feeding strategies a software tool can be developed based in a first instance in a simple kinetic growth model. If the model is kept simple, the complexity of the experiments for determination of the model's kinetic parameters can be also reduced e.g. from simple shake flask culture. The development of a strategy of this kind might contribute to a faster and less expensive method for the evaluation of feeding profiles during fed-batch culture.

The following chapters are dedicated to the development of the three mentioned tasks. Due to their individuality, each task is introduced, developed and concluded in its respective chapter.

2 Evaluation of Process Parameters in Shake Flasks and Bioreactor Systems[2]

2.1 Technical and Theoretical Background

2.1.1 Comparability in Different Cultivation Systems

Comparability and reproducibility of results obtained in different cultivation systems or bioreactors are key factors for reliable data generation during research. They also represent a prerequisite for interdisciplinary studies, e.g. in systems biology projects involving different laboratories. However, differences in cultivation facilities might hinder the participants in achieving comparable results.

Within the project SysLogics, five participating institutions in Germany committed themselves to generate quantitative data on cell metabolism from shake flask and bioreactor culture, with the aim of data collection for further modelling tasks. Shake flask and bioreactor cultures were to be performed in different cultivation systems depending on the participant laboratory. Figure 2.1 displays the cultivation systems at the project partners' laboratories, part of the scientific consortium.

After a series of initial cultivations in each laboratory with standard culture parameters (rpm, pH and DO) and culture handling, the specific growth rate (μ_{max}) of each growth curve was calculated. The average μ_{max} as well as its respective standard deviation are shown in Figure 2.2.A for 27 bioreactor cultures. Figure 2.2.B shows as well, the average μ_{max} and its corresponding $s_{\mu_{max}}$ of 19 shake flask experiments performed in our laboratory.

The standard deviations shown in Figure 2.2.A and B would result in a maximum doubling time difference of 22 h. Considering the standard doubling time of AGE1.HN cells in culture, $t_d = 40$ h, some cultures would show differences in cell density during growth of over 100 %.

Such marked growth differences might also have an impact on all levels of cell metabolism. Figure 2.3 shows the dependency of three main biochemical param-

[2]Part of this chapter has been published in: Platas Barradas, O., Jandt, U., Phan, L. D. M., Villanueva, M. E., Schaletzky, M., Rath, A., Freund, S., Reichl, U., Skerhutt, E., Scholz, S., Noll, T., Sandig, V., Pörtner, R. and Zeng, A.-P., *Engineering in Life Sciences*, 2012, 12, 5. doi: 10.1002/elsc.201100163.

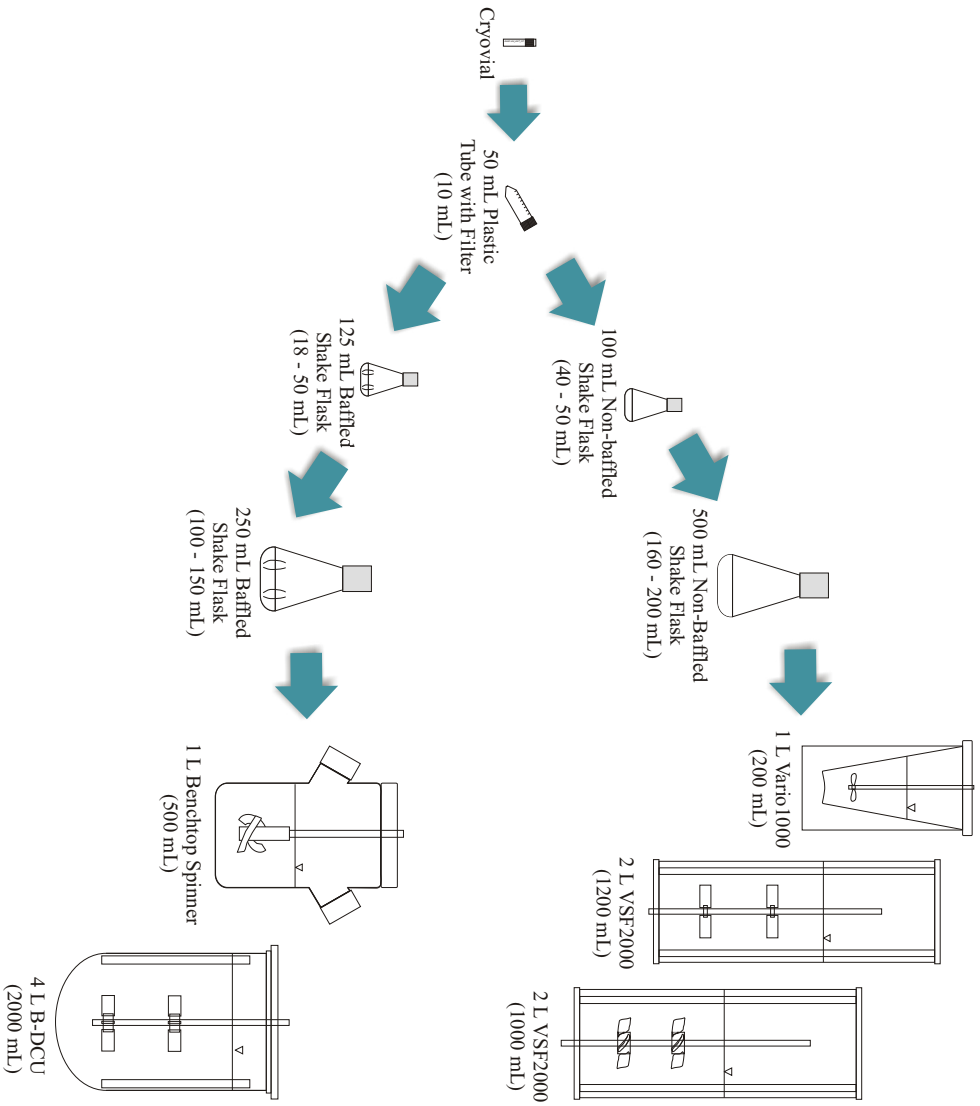

Figure 2.1: Shake flask and bioreactor culture steps used during the project SysLogics for the cultivation of the human industrial cell line AGE1.HN.

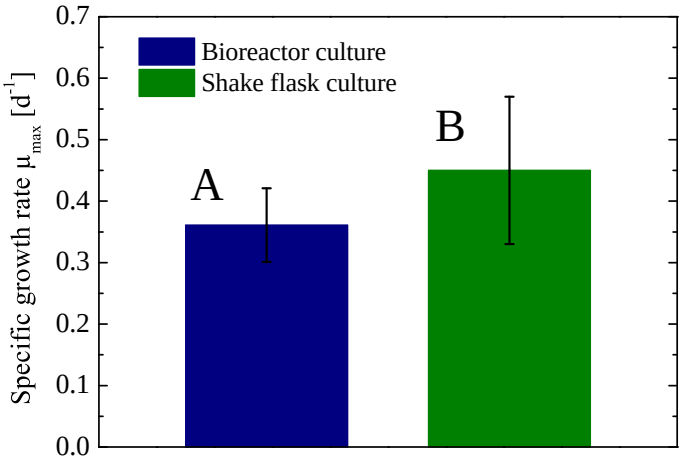

Figure 2.2: Average specific growth rate μ_{max} and standard deviation $s_{\mu_{max}}$ of 27 bioreactor (A) and 19 shake flask (B) AGE1.HN runs. Data belong to cultivations performed prior to culture standardization.

eters on the specific growth rate of AGE1.HN cells in bioreactor (filled symbols) and shake flask culture (open symbols)[3]. All data points belong to cultures with identical initial conditions ($Glc_{t=0}$, $Gln_{t=0}$, $Lac_{t=0}$). Variations in μ_{max} are therefore a result of the variation of the process parameters used during cultivation.

According to the figure, the higher the μ_{max} value, the lower would be the specific glucose uptake (q_{Glc}) as well as the lactate production (q_{Lac}). Furthermore, cells would seem to metabolize glucose in a more efficient manner by yielding more cells per mol of consumed glucose ($Y_{X/Glc}$). According to the data fit, the lower the μ_{max} values the more abrupt is the change in the biochemical parameters of the cells, whereas at higher μ_{max}, data seem to flatten and reach a plateau at maximum μ_{max} values. Most probably at this point, cells grow completely unperturbed from the surrounding conditions.

The dramatic differences in μ_{max} observed after the first cultivations of AGE1.HN cells might be the result of the cell-growth dependency on the bioreactor geometry-related hydrodynamic parameteres. To this point, the fact of having different cultivation facilities with proved differences in culture performance, set up a challenge to reduce culture differences by minimizing their standard deviation. A maximum standard deviation for μ_{max} of 0.05 was set as a reference for standardization of each culture system, which corresponds to the average standard deviation of the historical μ_{max} data of the shake-flask maintenance cultures. Culture standardization should

[3]A similar time span was taken into account for calculation of $Y_{X/Glc}$, q_{Glc} and q_{Lac}, which considers the first 48 h of cultivation.

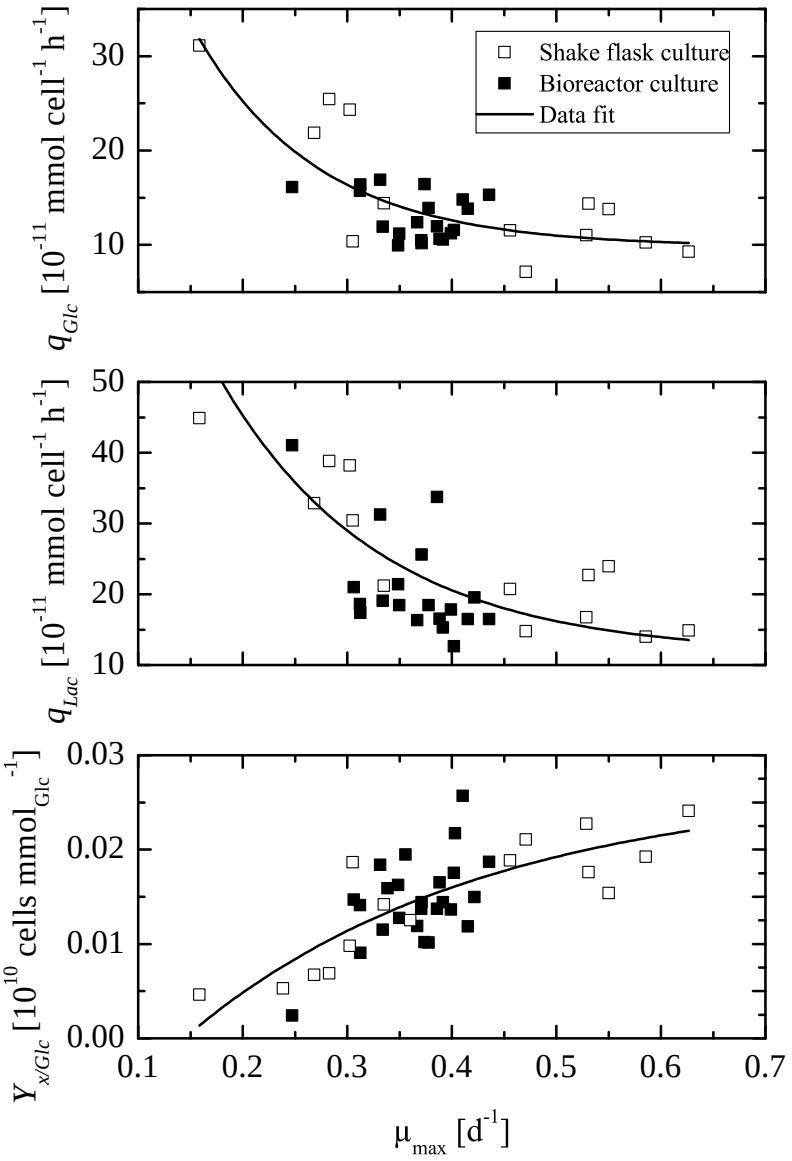

Figure 2.3: Dependency of the biochemical parameters q_{Glc}, q_{Lac} *and* $Y_{X/Glc}$ on the specific growth rate (μ_{max}) of AGE1.HN cells.

be performed through process characterization of the corresponding culture steps with a desirable further identification of process parameter ranges for comparable growth.

2.1.2 Criteria for Process Comparability in Mammalian Cell Culture

There is a plenty of literature detailing scale-up issues in bioreactors [Ju and Chase (1992), Junker (2004), Xing et al. (2009), Amanullah et al. (2004)]. These studies, however, concentrate on the analysis of scale-up criteria for a specific type of bioreactor, where geometric similarity is maintained. If this is not the case, selection of an appropriate criterion for process comparability requires a detailed analysis, even for bioreactors at similar scale. The following comments and statements refer to common criteria for comparability and scale-up between bioreactors.

Specific Power Input (P/V) in Bioreactors

The specific power input is one of the most accepted criteria for scale-up and process transfer between bioreactors. Power input can be measured by using special equipment. Otherwise the calculation of this parameter relies on the dimensionless power number (Np), the value of which accounts for a series of relationships among geometric parameters and the impeller diameter as the reference length [Bates and Fondy (1963)] (see Equation 2.1).

$$Np = \frac{P}{\rho\, N^3\, d_i^5} = k_1 \left(\frac{\rho\, N\, d_i^2}{\eta}\right)^{x_1} \left(\frac{N^2 d_i}{g}\right)^{x_2} \left(\frac{d_T}{d_i}\right)^{x_3} \left(\frac{H}{d_i}\right)^{x_4} \left(\frac{h_1}{d_i}\right)^{x_5} \left(\frac{p}{d_i}\right)^{x_6} \left(\frac{w_i}{di}\right)^{x_7} \left(\frac{l_i}{d_i}\right)^{x_8} \left(\frac{n_{i,2}}{n_{i,1}}\right)^{x_9} \tag{2.1}$$

The first dimensionless group in Equation 2.1 is the Reynolds Number (Re), the second corresponds to the Froude Number (Fr). The further terms represent the dimensionless ratio of the tank diameter (d_T), liquid height (H), lower-impeller distance to tank bottom (h_1), propeller pitch (p), impeller blade width (w_i) and blade length (l_i), to the impeller diameter (d_i). n_i refers to the number of impeller blades. Since the effect on Np due to variation of these geometric parameters has been mostly studied in reference vessels with specific geometries, correlations existing in literature [Henzler (1982), Einsele (1978), Rushton et al. (1950a), Rushton et al. (1950b), Chudacek (1985), Markopoulos and Pantuflas (2001)] in the form of $Np = f(Re)$ are most of the times specific for the studied vessel form and a defined range of

geometric variations.

For this reason, the more a bioreactor deviates from the so called standard geometry, the less information on power input is available. Since the construction of model vessels for power input measurements can be very time demanding, a detailed theoretical evaluation of power input while dealing with geometrically dissimilar bioreactors might be beneficial. This includes a careful analysis of the impeller and vessel geometry, as well as the necessary geometry corrections for the impeller interspacing, and the baffle number and size. The effect of aeration on power input should also be considered, since power consumption in gassed systems (Pg) tend to differ from unaerated systems depending on the flow regime and the gas dynamics in the vessel [Amanullah et al. (2004)]. Power input values of bioreactors during the cultivation of mammalian cells can be found in different publications [Smith and Greenfield (1992), Al-Rubeai et al. (1995), Chisti (2001), Czermak (2008)], with values up to 1000 $\mathrm{W\,m^{-3}}$ depending on the bioreactor scale.

Specific Power Input (P/V) in Shake Flasks

Büchs et al. [Büchs et al. (2000a), Büchs et al. (2000b)] analyzed power consumption in shake flasks and presented a correlation for a modified Power Number (Np') as a function of the Reynolds number at the thin liquid layer at the flask wall (see Equation 2.2). In analogy to a stirrer blade inside a bioreactor, this equation considers the dimensionless parameter w_i/d_i (see Equation 2.1), which is changed for shake flasks by the relationship between the height of the liquid in the flask during rotation and the shake flask maximum inner diameter (h/d_i).

$$Np' = Np\,\frac{d}{h} = \frac{P}{\rho\,N^3\,d_i^4\,h} = C_1\,\pi^4\,f(Re) \tag{2.2}$$

A simplification of Equation 2.2 considers the quantity $h \propto V_L^{1/3}$ to describe a characteristic length scale for the friction area between liquid and flask wall (see Equation 2.3). In turbulent conditions in a hydrodynamic undisturbed system the correlation $f(Re) = C_2 Re^{-0.2}$ [Schlichting (1979)] can be applied [Büchs et al. (2000a)], in which case Equation 2.3 would lead to Equation 2.4:

$$Np' = \frac{P}{\rho\,N^3\,d_i^4\,{V_L}^{1/3}} = C_1\,\pi^4\,f(Re) \tag{2.3}$$

$$Np' = \frac{P}{\rho\, N^3\, d_i^4\, {V_L}^{1/3}} = C_1\, \pi^4\, C_2 Re^{-0.2} \tag{2.4}$$

When the liquid in the flask doesn't rotate in synchrony with the shaker's movement, the hydrodynamics of the system is affected, which leads to a decrease in power consumption, an increase in mixing time, and a decrease in the volumetric oxygen transfer coefficient, $k_L a$. This phenomenon is called by Büchs et al. as *out-of-phase*, and it is often found at low shaking frequencies, high viscosities, low filling volumes, short shaking diameters and high liquid viscosities. Figure 2.4 shows experimental measurements depicting the behavior of *Np'* for *in-* and *out-of-phase* conditions [Büchs et al. (2000b)]. This deviating behavior is based on the studies by Deiber and Cerro, and Semena and Khmelëv [Büchs et al. (2000b)] for a rotating horizontal drum.

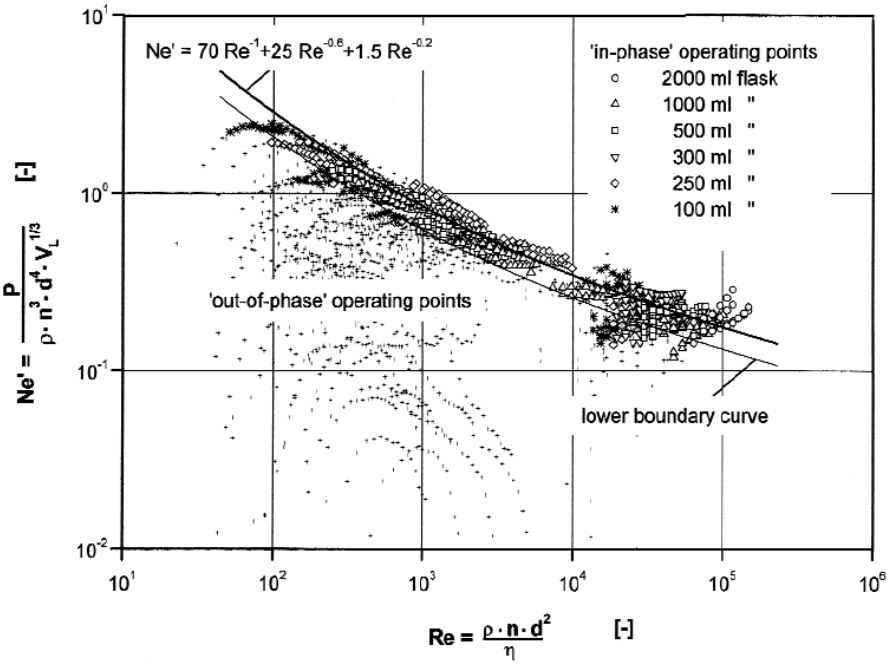

Figure 2.4: Dependency of the modified Power Number (here *Ne'*) on the flask Reynolds number with variation of flask size, liquid viscosity, shaking diameter and shaking frequency [Büchs et al. (2000b)].

The *in-phase* points of Figure 2.4 obey the following fit (see Equation 2.5):

$$Np' = 70Re^{-1} + 25Re^{-0.6} + 1.5Re^{-0.2} \tag{2.5}$$

According to Büchs et al., the equation to determine the boundary up to which the liquid remains *in-phase*, *Ph*, is the following:

$$Ph = \frac{d_o}{d_i}\left(1 + 3log_{10}(Re_f)\right) > 1.26 \tag{2.6}$$

where Re_f is the liquid-film Reynolds number:

$$Re_f = Re\frac{\pi}{2}\left(1 - \sqrt{1 - \frac{4}{\pi}\left(\frac{V_L^{1/3}}{d_i}\right)^2}\right)^2 \tag{2.7}$$

In a different approach, Kato et al. [Kato et al. (1995)] determined the power consumption in horizontally shaking cylindrical vessels by using the average energy consumption of the shaking machine for different flask and shaking diameters ($d_i = 0.140$ - 0.206 m and $d_o = 0.01$ - 0.04 m, respectively), and shaking velocities (102 - 198 rpm), at higher viscosity values ($9{\cdot}10^{-4}$ - 1 Pa s). The experimental data on torque measurement were fitted to a *Re* and *Fr* dependent correlation (see Equation 2.8). In contrast to Büchs et al., Kato et al. use the shaking diameter, d_o, for calculation of the Reynolds number.

$$Np = 934Fr^{3/2}Re^{-1/4}\left(\frac{d_o}{d_i}\right)^{3/2} \tag{2.8}$$

with

$$Fr = \frac{N^2\, d_i}{g} \tag{2.9}$$

and

$$Re = \frac{\rho\, N\, d_o^2}{\eta} \tag{2.10}$$

A region for mixing efficiency is defined with *Fr* and *Re* as:

$$0.135Re^{-0.176} < Fr < 0.135Re^{0.186}\ (Re{>}1)$$

Mixing Time (Θ_M)

Although reaction rates in mammalian cell cultures are slower than those in chemical or microbial systems, the importance of a well-mixed environment has been clearly pointed out in view of the effects of cell agglomeration, cell suspension, pH gradients, oxygen supply and CO_2 removal [Amanullah et al. (2004), Ozturk (1996), Lara et al. (2006)]. The time needed for a defined volume of substance to reach a determined degree of homogeneity after adding a pulse of a tracer is defined as the mixing time; its value depends on the desired degree of mixing M (Equation 2.11):

$$M = 1 - \frac{|C_{t=\infty} - C_t|}{C_{t=\infty} - C_{t=0}} \tag{2.11}$$

where C is the local concentration of the tracer at the time after its addition ($C_{t=0}$), during the mixing process (C_t), and after reaching homogenity (C_∞). Methods for determination of mixing time in bioreactors and shake flasks might be based on the measurement of temperature, conductivity, refraction index, fluorescence, color, radioactivity, etc.; their advantages and drawbacks are extensively explained in literature [Kraume (2003), Lübbert (1992), Mavros (2001), Tan et al. (2011)]. Up to now, the colorimetric method is the simplest and easiest method used to ascertain the optimal mixing time. A common colorimetric method employs Lugol's solution, which consists of elemental iodine and potassium iodide (I/KI) in a starch solution, and sodium thiosulfate NaS_2O_3 as a titration agent (see Equation 2.12).

$$2I + 2S_2O_3^{-2} \longrightarrow 2I^- + S_4O_6^{-2} \tag{2.12}$$

The dissapearance of the intense blue color can be followed by a camera and further analyzed manually or with appropriate software. In this way, this method allows for an easy visualization of the decolourization process as well as for identification of local death zones. Moreover the experimental determination of the mixing time with this method is not affected by the reaction time of the measuring probes. For experimental purposes, the mixing time is considered at 95 - 98 % of the final equilibrium concentration (C_∞).

Due to the increase in mixing time with bioreactor scale, mixing time has not played an important role as a scale-up criterion, neither for bioreactors nor for shake flasks. Junker [Junker (2004)] presented a comparison of mixing times for bioreactor volumes ranging from 10 to 120 000 L for yeast and bacterial cultures. The average

increase in mixing time for these production bioreactors was approximately 17 seconds per order of magnitude during increase of bioreactor volume. A summary of mixing times in bioreactors for processes with microorganisms, plant and mammalian cells depicts its increase with bioreactor scale [Lara et al. (2006)].

At laboratory scale the known problems during mixing time determination such as location of tracer addition, location of probes, response time of probes, etc. might not play such an important role as they do in large scale. For this reason, Θ_M can be regarded as an important process transfer criterion in laboratory scale bioreactors.

Dimensionless equations for describing the mixing efficiency in bioreactors are e.g. the Mixing Number $N\Theta_M$, which describes the number of turns a stirrer needs in order to reach a certain fluid homogeneity in a system; and the Flow Number $Fl = QN^{-1}d_i^{-3}$, which considers the off-blade discharged volumetric liquid flow Q for a determined impeller diameter [Nienow (1997)].

Maximum fluid velocity (u_i)
In bioreactors this parameter is defined by the impeller tip speed, whereas in shake flasks the maximum liquid velocity is reached at the flask wall.

$$u_i = \pi\, N\, d_i \tag{2.13}$$

Reynolds Number (Re)
Maximum Reynolds numbers are calculated for bioreactors at the impeller tip. As well as for u_i this number is calculated in shake flasks at the flask wall.

$$Re = \frac{\rho\, N\, d_i^2}{\eta} \tag{2.14}$$

According to Kato et al. [Kato et al. (1995)], the Reynolds Number for shaken systems is calculated using the shaking diameter of the shaking machine, d_o (see Equation 2.10).

Both u_i and Re have not been used universally for scale-up issues in bioreactors, since their value depends only on both impeller diameter and agitation speed, but it is independent of impeller type, energy input or mixing behavior. However, they are of critical importance during fermentations of shear sensitive organisms [Ju and Chase (1992)]. Critical impeller-tip-speed values for many types of mammalian cells

have been presented by Amanullah et al. [Amanullah et al. (2004)], Chisti [Chisti (2001)], and Czermak [Czermak (2008)].

2.2 Materials and Methods

2.2.1 Cell Line

Cell Line: Two clones of the human industrial cell line AGE1.HN (ProBioGen AG, Berlin, Germany) were used. One of the AGE1.HN clones produces α-1-antitrypsin (AGE1.HN$_{AAT}$); the second clone is the non-producing cell line. Both cell lines proved to show similar growth and substrate uptake rates in shake flask culture under same culture conditions. For this reason, no difference between clones will be made in this work. This cell line grows in a chemically defined medium (42-Max-UB, TeutoCell AG, Germany), which was supplemented with L-Glutamine at a final concentration of 5 mM. A detailed description of this cell line can be found elsewhere [Niklas et al. (2011)].

2.2.2 Preculture

Preculture was carried out in unbaffled 100 and 500 mL glass Erlenmeyer shake flasks (DIN 12385, Schott Duran, Wertheim am Main, Germany) described in Table 2.2 with working volumes of 50 and 200 mL, respectively. These preculture steps were carried out on an orbital shaker at $N = 225\,\mathrm{rpm}$ with shaking diameter $d_o = 10\,\mathrm{mm}$ (GFL3005, Omnilab, Germany). Incubator atmosphere was controlled during shake flask culture at 36.8±0.2 °C (Heraeus Heracell, Germany). As an additional reference measurement, an incubator thermometer (VWR, Germany) was placed on the surface of the shaker.

The CO_2 partial pressure was set at an initial value of 5 %. The pH of the cultures was measured externally (CG 822, Schott AG, Mainz, Germany) during sampling. A scheduled reduction of the CO_2 partial pressure was carried out routinely according to the measured pH value in culture: $CO_2 = 5\,\%$ for pH > 7.3, 3 % for $7.1 <$ pH ≤ 7.3, and 0 % for pH ≤ 7.1. Exponential growth was always observed at a pH range of 7.0 - 7.4. This schedule was easy to follow and allowed for exponential growth at all preculture steps.

Cell counting and viability measurements were performed manually on a Neubauer

Haemocytometer (Laboroptik, Friedrichsdorf, Germany) using the trypan blue exclusion method.

The other participating groups, who kindly contributed with growth data for the bioreactors 2 and 4, carried out the preculture in 125 and 250 mL polycarbonate Erlenmeyer flasks with volumes ranging between 18 - 50 mL, and 100 - 150 mL, respectively. For these flasks, an agitation rate of 185 rpm with shaking diameter of 50 mm was used (ES-X, Kuhner Shaker, Switzerland). Cell counting here was done by image analysis (Roche Innovatis, Germany).

2.2.3 Bioreactor and Shake Flask Experiments

Cells growing exponentially in the preculture were centrifuged (125 g, 5 min) and inoculated at an initial cell density of $0.4{\cdot}10^6$ cells mL^{-1} for the non-producing cell line and $1{\cdot}10^6$ cells mL^{-1} for the A1AT-producing cell line.

In the bioreactors, the pH was controlled at 7.15 (CO_2 / 0.5 M Na_2CO_3), whereas DO was set to 25 - 40 % of air saturation (pH and DO probes from Mettler Toledo AG, Germany). In this DO range no differences in growth have been observed for this cell line (data not shown). The total gas flow during bioreactor culture (N_2 + CO_2 + O_2) was either fixed or controlled at a maximum of 0.06 vvm. Off-line sampling was performed at least once per day. The agitation rate was kept constant unless otherwise indicated.

In the shake flasks, the pH was controlled as described for the preculture steps. The shaking velocity was set constant for all cultivations (values shown in Section 2.3) . For assuring consistence of data, the shaking frequency of the shaking machines as well as the agitation speed of the bioreactors were calibrated prior to the start of the experiment.

2.2.4 Characterization of Bioreactor and Shake Flask Hydrodynamics

Bioreactors' geometric characteristics

The following bioreactors were used in this work: VARIO1000 [4] (medorex e.K., Germany), Benchtop Spinner 0.5 L [5] (DASGIP AG, Germany), VSF2000 [4] (Bioengi-

[4]Hamburg University of Technology, Hamburg

[5]Max Planck Institute for Dynamics of Complex Technical Systems, Magdeburg.

neering, Switzerland) in two different geometry configurations, and Biostat B-DCU [6] (Sartorius Stedim Biotech GmbH, Germany) (see Figure 2.5). The geometric characteristics of these bioreactors were obtained from the participating project partners and used for the calculation of the various dimensionless numbers. Relevant numbers and geometric data are summarized in Table 2.1.

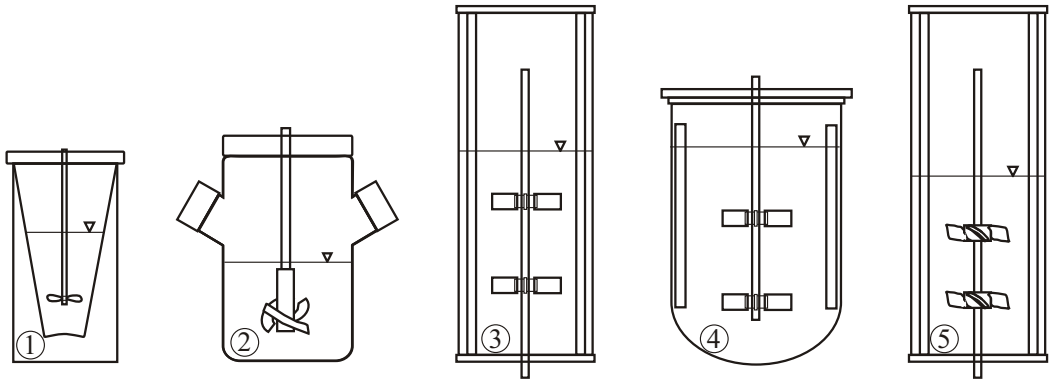

Figure 2.5: Benchtop bioreactors employed during the cultivation of the human industrial cell line AGE1.HN: (1) VARIO1000 (medorex e.K., Germany), (2) Benchtop Spinner 0.5 L (DASGIP AG, Germany), (3) and (5) VSF2000 (Bioengineering, Switzerland) in two different geometrical configurations, and (4) Biostat B-DCU (Sartorius Stedim Biotech GmbH, Germany).

The impeller types of each bioreactor are depicted in Figure 2.6.

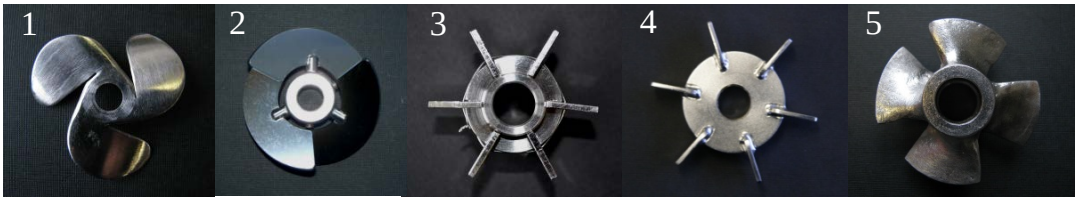

Figure 2.6: Impeller types of the bioreactors depicted in Figure 2.5. 1: 3-blade marine propeller; 2: 3-blade segment impeller; 3 and 4: 6-blade radial-discharging impeller (Rushton); 5: 4-pitch-blade turbine.

Shake Flask Geometry

The geometric characteristics of the baffled and unbaffled glass shake flasks included in this study (DIN 12385, Schott Duran, Wertheim am Main, Germany) are displayed in Figure 2.7, and in Table 2.2. The characterization of the hydrodynamics in shake flasks includes relevant difficulties related to the shake flask geometry. Depending on the manufacturer and production batch, the flask, and the form and size

[6] Bielefeld University, Bielefeld.

Table 2.1: Bioreactor geometric characteristics

Bioreactors	V_w	d_T	H/d_T	Bottom	Impeller	z	d_i	w_i	d_i/d_T	Δh	h_1/d_T	n_b	w_b	Gas Inlet
	[10^{-3}m^3]	[m]	[-]			[-]	[m]	[m]	[-]	[m]	[-]	[m]	[m]	
1 Vario1000	0.2	0.065[a]	1.52	Truncated cone	3-MP	1	0.035	0.021	0.53	-	0.69	0	-	RS (0.3)
2 Benchtop spinner	0.5	0.100	0.75	Curved	3-S	1	0.054	0.056	0.54	-	0.35	0	-	Open tube
3 VSF2000	1.2	0.104	1.92	Flat	6-RT	2	0.048	0.012	0.46	0.060	0.61	2	0.015	RS (0.5)
4 Biostat B-DCU	2.0	0.130	1.23	Dished	6-RT	2	0.053	0.010	0.41	0.050	0.23	4	0.012	RS (0.6)
5 VSF2000	1.0	0.104	1.60	Flat	4-PBT	2	0.048	0.024	0.46	0.048	0.48	2	0.015	RS (0.5)

[a] Due to the conical shape of this bioreactor, calculation of vessel diameter was done at impeller height. V_w, working volume; d_T, vessel diameter; H, liquid height from bioreactor bottom to filling surface; 3-MP, 3-blade marine propeller; 3-S, 3-blade segment impeller; 6-RT, 6-blade radial-discharging impeller (Rushton); 4-PBT, 4-pitch-blade turbine; z, number of impellers; d_i, impeller diameter; w_i, impeller-blade width; Δh, impeller interspacing; h_1, lower-impeller distance from tank bottom; n_b, number of baffles; w_b, baffle width; RS, ring sparger (orifice diameter in mm).

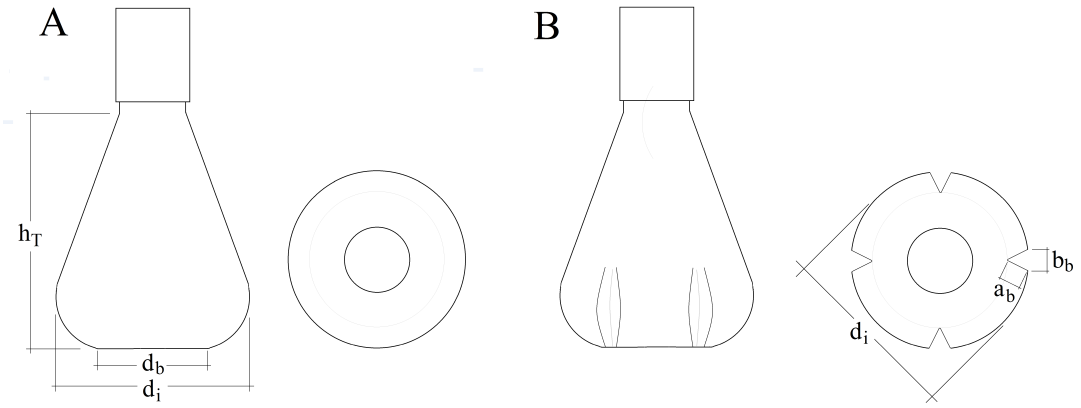

Figure 2.7: Geometric characteristics of the A: unbaffled shake flasks and B: baffled shake flasks.

Table 2.2: Shake flask geometric characteristics.

V_T [mL]	V_w [mL]	n_b [-]	d_b [mm]	d_i [mm]	P_o [mm]	$d_{i,mod}$ [mm]	a_b [mm]	b_b [mm]	h_T [mm]
100	40	-	40	64	207	64	-	-	105
100	40	4	40	64	226	70	10	15	105
500	180	-	75	105	336	105	-	-	180
500	180	4	75	105	377	118	15	23	180

V_T, total volume; V_w, working volume; n_b, baffle number; d_b, shake flask diameter at flask bottom; $d_{i,mod}$, modified shake flask diameter; a_b, baffle depth; b_b, baffle width; h_T, shake flask height.

of the baffles might vary, making the transfer of results during characterization work cumbersome. In an attempt to overcome the difficulties for comparing baffled and unbaffled shake flasks, a modified shake flask diameter, $d_{i,mod}$, is introduced here, which accounts for the size of the baffles (see Equation 2.15). The baffle depth, a_b, is included into the flask perimeter (P_o), from which $d_{i,mod}$ can be calculated. As a result, the higher the baffle size, the higher will be $d_{i,mod}$ compared to d_i. This will lead to higher values of the calculated process parameters (P/V, Re and u_i) at a determined agitation speed in comparison to unbaffled shake flasks. Therefore, $d_{i,mod}$, accounts in this work for the increase in turbulence due to baffle presence in shake flasks.

$$d_{i,mod} = \frac{P_o}{\pi} - 2 \cdot s_{wall} \tag{2.15}$$

Here, P_o is the shake flask's outer perimeter and s_{wall} the shake flask's wall thickness (here 1 mm). For practical purposes P_o can be measured at the maximum flask

outer diameter.

The following process parameters were evaluated for all cultivation systems: (1) Specific power input *(P/V)*, (2) Mixing time at $M = 95\,\%$ (Θ_{95}), (3) Maximum fluid velocity (u_i) and (4) Reynolds number (Re). Depending on the criterion, the values were calculated or determined experimentally. The density and the viscosity of the protein-free medium 42-Max-UB was taken as that of water at 37 °C. For this consideration, the rheological effect of the cells in culture is neglected.

Power Input in Bioreactors

The determination of the power input was performed by using empirical correlations. An experimental method for P/V determination (e.g. torque measurement), would have implied the construction of model vessels with following adaptation of stirrer shafts to the vessels and to the measurement system.

The calculation was carried out as follows:

1. Power numbers were obtained from $Np = f(Re)$ graphic correlations available in literature [Bates and Fondy (1963)], [Rushton et al. (1950a)], [Rushton et al. (1950b)]. The search for suitable graphs, equations and corrections was based on similarity to our systems, for which the geometry of the vessel i.e. H/d_T, d_i/d_T, presence and number of baffles n_b, type of impeller, and vessel shape, were considered. Although there is more recent literature on power input data, the closest similarity between the studied systems was given by the publications mentioned in this work. A constant liquid volume (and therefore constant H) was assumed for determination of Np values.

2. A difference in power input of two impellers compared to one, Np_2/Np_1, has been observed for two impeller systems at $\Delta h/d_T < 0.75$ and $\Delta h < 1.65\ d_i$ [Henzler (1982)], [Markopoulos and Pantuflas (2001)], [Hudcova et al. (1989)]. This effect has been presented as a function of impeller interspacing, H, and d_i/d_T [Hudcova et al. (1989)], see Figure 2.8. The relationship Np_2/Np_1 (in Figure 2.8 shown as P_2/P_1) was determined graphically and multiplied by the single-impeller Np value.

3. A further correction for Np accounts for the deviation from a standard baffled system, which contemplates four baffles equidistant at vessel wall with size $w_b = 0.1 \cdot d_T$ [Hemrajani and Taterson (2004)]. This correction takes into account the baffle num-

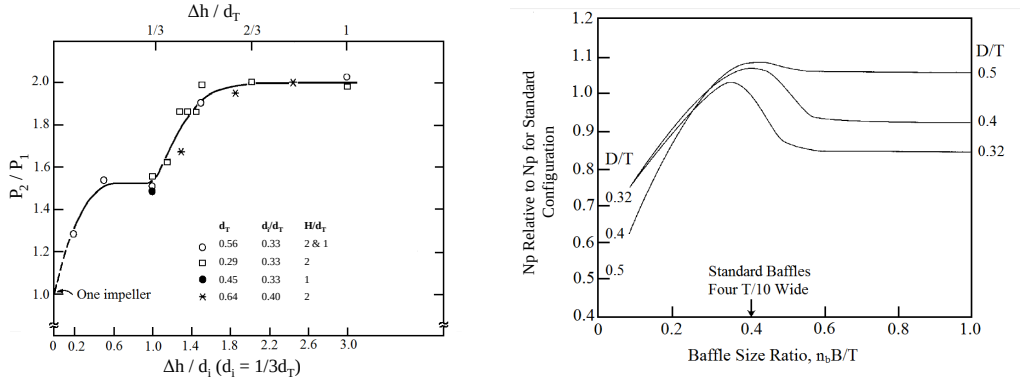

Figure 2.8: A: *Np* correction due to impeller interspacing [Hudcova et al. (1989)], B: *Np* correction for baffling [Hemrajani and Taterson (2004)].

ber (n_b), the baffle width (w_b) and the ratio d_i/d_T, and was calculated graphically according to Hemrajani and Tatterson [Hemrajani and Taterson (2004), Figure 2.8] for two-baffled systems (bioreactors 3 and 5).

4. Power input values were calculated with the obtained *Np* values according to Equation 2.1. Volume change due to sampling was taken into account for determination of P/V. Thus, P/V data shown in this work are average values during culture.

Power Input in Shake Flasks

Np was calculated according to the methods presented in Section 2.1.2, p. 8, for shake flasks [Büchs et al. (2000a), Büchs et al. (2000b), Kato et al. (1995)] under the following considerations:

a. The use of higher working volumes in this work ($V_w \triangleq 30\text{-}50\,\%$ compared to $V_w \triangleq 4\text{-}20\,\%$ in Büchs et al.; percent values related to nominal volume) might influence *Np* calculation, as a higher volume would account for a higher friction area considered by the term $h \propto V_L^{1/3}$ in Equation 2.3. However, since the working volume and the shaking diameter were kept fairly constant within a determined flask size, the friction area inside a flask could be regarded as a constant throughout the cell culture period. For this reason *Np* calculation in established turbulent conditions can be calculated according to Equation 2.5.

b. The shaking diameter differences ($d_o = 1$ cm in this work compared to $d_o \triangleq 1.25\text{-}5$ cm in Büchs et al.) were neglected during *Np* calculations, since only a slight influence of d_o during P/V measurements has been observed in an established turbulent regime [Büchs et al. (2000a)]. This was also the case for *Np* calculation based

on Kato et al.'s equation [Kato et al. (1995)], where slightly different conditions were used ($d_i \triangleq 0.140$ - 0.206 m, $d_o \triangleq 0.01$ - 0.04 m, $N \triangleq 102$ - 198 rpm).

c. The validity of both procedures was assessed by calculation of the boundary conditions for an *in-phase* regime [Büchs et al. (2000a)] and for efficient mixing [Kato et al. (1995)].

The following procedure was used for calculation:

1. Measurement and calculation of the geometric characteristics (see Table 2.2).

2. Calculation of *Np'* according to Equation 2.5, considering the Reynolds number as shown in Equation 2.14.

3. Calculation of P/V according to Eq. 2.3.

4. The *in-phase* boundaries were calculated according to Equations 2.6 and 2.7.

5. $d_{i,mod}$ was used for calculations in baffled flasks (see Equation 2.15).

6. For the calculation of the specific power consumption according to Kato et al., *Np* was calculated according to Equation 2.8, with *Fr* and *Re* according to Equations 2.9 and 2.10 respectively.

7. Calculations were verified to be in the region of mixing efficiency defined by Kato et al. (See Section 2.1.2 p. 10).

Mixing time

The decolourization method with a mixture of iodine and potassium iodide, and sodium thiosulfate as titration agent, was used [Kraume (2003)]. Following solutions were prepared: 1 M I and KI ($250\,\mathrm{g\,L^{-1}}$ and $128\,\mathrm{g\,L^{-1}}$ respectively, Merck), 1 M $Na_2S_2O_3$ (Merck) and 1 % w/v soluble starch (Merck). For dissolving the starch water was preheated to a temperature close to its boiling point; prior to adding starch, the water was taken out of the heat source. 2 g L^{-1} benzoic acid were added to the starch solution to avoid contamination. The I/KI solution was first titrated against $Na_2S_2O_3$. Afterwards, the shake flasks and bioreactors were filled to working volume (see Tables 2.2 and 2.1); 1 % (v/v) of starch solution was added.

After complete mixing, the K/KI solution (0.01 % v/v) was added carefully. After reaching a homogeneous intense blue color N was set according to the experiment. A volume corresponding to a molar excess of 5 % of $Na_2S_2O_3$ (from previous titration) was added from the top of the bioreactor into the liquid (1 - 5 cm above liquid) while keeping a relatively constant addition time (ca. 1 s). The molar excess of 5 % $Na_2S_2O_3$ allows for determination of mixing time at a mixing degree of 95 %. Digital camera recording (Canon Powershot S5IS, Japan) was used to follow the decolourization reaction. Mixing time determinations were performed as triplicates. In order to avoid subjectiveness during determination of the decolourization time in bioreactors, computer video analysis of the decolourization process was carried out by measuring the loss of saturation of the complete vessel image. Therefore, the measurement is based on a desaturation signal, which is proportional to the concentration of the colorless redox products (I^- and $S_4O_6^{-2}$), and Equation 2.16 can be expressed as:

$$M = 1 - \frac{MS_\infty - MS_t}{MS_\infty - MS_0} \tag{2.16}$$

where MS is the measured signal during desaturation. The videos were converted and processed using the ImageJ image processing software suite (National Institutes of Health, USA) and GNU C++. The desaturation process might become noisy towards its end due to the movement of stirrer. To avoid noise the desaturation process was considered to be finished at 99.5 %. Thus, the mixing times determined in this study for bioreactors correspond to a real degree of mixing $M = (0.95)\,(0.995) = 94.5\,\%$.
The influence of tubings and probes on the mixing time is more relevant at a smaller scale whenever standard invasive probes are used for measurement of pH and DO. In order to minimize this influence in bioreactor 1, which was the bioreactor with the smallest vessel, the probes were placed at a distance equal to d_i above impeller height.

Maximum Fluid Velocity and Reynolds number were calculated according to Equations 2.13 and 2.14.

Analysis of the Dependency of μ_{max} on Culture's Process Parameters
The specific growth rate μ_{max} was used as an indicator for comparison of culture performance. Data pairs from each culture were plotted (t,lnX_v) and linearly fitted in the form y = mx + b. The slope of the line (m) corresponds to μ (see Equation 2.17). For the calculation of μ_{max} those data pairs which yielded a slope with a

minimum linear regression coefficient $R^2 = 0.98$ were selected. The highest R^2 was chosen when discretizing between μ_{max} values.

$$ln\,(X_{v,n+1}) - ln\,(X_{v,n}) = \mu\,(t_{n+1} - t_n) \tag{2.17}$$

Relevant biochemical coefficients like $Y_{X/Glc}$, q_{Glc} and q_{Lac} were calculated for most of the cultivations. However, the rapid change of their values in culture just after entering the exponential growth rate generates significant deviations, which makes statistical comparisons problematic. μ_{max} on the other side, shows only a small reduction in its value during the first 70 hours during AGE1.HN culture [Rath (2012)] and allows for high linear regression coefficients.

OUR vs OTR in Shake Flask Culture

In order to focus on the dependency of μ_{max} on only process parameters in shake flask cultures, other parameters which might lead to erroneous conclusions should be excluded, such as possible limiting oxygen concentrations due to the lack of DO-control. In case the cells in a shake flask enter into limiting DO values, which might occur at low agitation speeds or during exponential growth, then μ_{max} would be dependent on the oxygen supply to the cells but not on the process parameters on study. To avoid this, the oxygen uptake rate (OUR) of the AGE1.HN cells was determined and compared to the oxygen transfer rate (OTR) of the shaking flasks in which culture took place.

For OUR calculation the dynamic method with cells growing under controlled conditions was used: the air supply of a bioreactor with exponentially growing cells was stopped during cultivation. Equations 2.18 and 2.19 describe the change in the oxygen concentration of the system. In absence of oxygen transfer ($OTR = 0$), OUR can be calculated from the time change in oxygen concentration (measured as a signal) at different cell density values (see Equation Eq. 2.20). This procedure was performed repeatedly during the exponential cell growth phase. The calculated OUR values were plotted against their corresponding cell density at every measured time point. After linear regression, the slope of the plotted values corresponded to the specific oxygen uptake rate, q_{O_2}, (see Equation 2.20).

$$\frac{dC_{O_2}}{dt} = OTR - OUR \tag{2.18}$$

$$\frac{dC_{O_2}}{dt} = k_L a \, \Delta C_{O_2} - q_{O_2} \, X_v \tag{2.19}$$

when OTR = 0,

$$\frac{dC_{O_2}}{dt} = -OUR = -q_{O_2} \, X_v = K_{H_{cp}} \, p_{abs} \frac{y_{O_{2,2}} - y_{O_{2,1}}}{\Delta t} \tag{2.20}$$

with $K_{H_{cp}}$ as the Henry coefficient of the system, which relates the oxygen concentration (C_{O_2}) to its partial pressure (y_{O_2}) at the boundary layer in equilibrium. The dependency of the Henry coefficient on the temperature was calculated according to the following equation:

$$K_{H_{cp}} = K^{\ominus}_{H_{cp}} \cdot exp\left(\frac{-\Delta H_{soln}}{R}\left(\frac{1}{T} - \frac{1}{T^{\ominus}}\right)\right) \tag{2.21}$$

where $K^{\ominus}_{H_{cp}}$ is the Henry coefficient at standard conditions ($T^{\ominus} = 298$ K), ΔH_{soln} is the enthalpy of solution and R the gas constant. In this work $K_{H_{cp}} = 1.283{\cdot}10^{-5}$ mol m^{-3} Pa^{-1} with $\Delta H_{soln}/R = 1700$ K [Sander (1999) from Dean (1992)].
The influence of salts on the solubility of oxygen can be described by a "salting out" constant. Takagi and Ueda calculated this constant for MEM Medium [Takagi and Ueda (1994)] and concluded, that the solubility of oxygen is reduced to 0.92 compared to its normal value in water. The oxygen concentration in water at saturation can be calculated as follows (see Eq. 2.22):

$$C^*_{O_2} = K_{H_{cp}} \, p_{abs} \, y_{O_2} \cdot 0.92 \tag{2.22}$$

with p_{abs} as the absolute pressure and y_{O_2} as the partial pressure of oxygen in the gas phase. The specific oxygen uptake rate is defined by Equation 2.23:

$$q_{O_2} = \frac{OUR}{X_v} \tag{2.23}$$

The calculation of the oxygen transfer rate (OTR) is also based on equation 2.18. When no oxygen is consumed in the system, the change in oxygen concentration is

defined as:

$$\frac{dC_{O_2}}{dt} = OTR = k_L a \, (C^*_{O_2} - C_{O_2}) \tag{2.24}$$

A polarographic probe (Mettler Toledo, Germany) was used in bioreactors for DO and OUR measurements. This probe was calibrated after being mounted in the bioreactor filled with water, and run at experimental conditions. DO = 0 % was calibrated by nitrogen sparging, whereas air was used for 100 % of air saturation.

DO was measured in shake flasks by means of the dynamic luminiscence quenching method. In this method a luminophore is intermittently excited by a light ray. During luminiscence, collision with oxygen molecules will decrease the luminophore's luminiscence. The received signal at the measuring device (Fibox 3, PreSens GmbH, Germany) is inversely proportional to the oxygen concentration in the solution. For the sensor calibration, the liquid in the flasks (37 °C) was actively gassed with nitrogen by introducing a thin silicon tubing into the flask's headspace (DO = 0 %). For DO = 100 %, the headspace was aerated until the signal was constant.

After separation of variables and integration, Equation 2.24 develops into Eq. 2.25:

$$ln\frac{C^*_{O_2} - C_{O_2,t=0}}{C^*_{O_2} - C_{O_2,t}} = k_L a \, t \tag{2.25}$$

By having a measured signal (MS) that is proportional to the oxygen concentration in the liquid phase, Equation 2.25 can be rewritten into 2.26:

$$ln\frac{MS^*_{O_2} - MS_{O_2,t=0}}{MS^*_{O_2} - MS_{O_2,t}} = k_L a \, t \tag{2.26}$$

where $k_L a$ is the slope of the change in the measured signal between t = 0 ($MS_{O_2,t=0}$) and oxygen saturation ($MS^*_{O_2}$), related to the whole saturation curve ($MS^*_{O_2}$ - $MS_{O_2,t=0}$).

$k_L a$ experiments were performed in a model medium, which consisted of a solution with a similar salt composition as it can be found in common cell culture media (7 g NaCl, 1.2 g $NaHCO_3$ and 0.312 g KCl per Liter deionized water). This salt content corresponds to that of a 1:1 DMEM/Ham's F12 medium. These experiments were not performed in culture medium to ensure comparability with other contributions on this topic.

The gassing-in method was employed for the $k_L a$ determination. The calculated $k_L a$ values consider the oxygen transfer from the incubator's atmosphere into the model medium inside the flask, by simplification of the different resistances to oxygen transport. These resistances include the aluminium cap, the variable oxygen partial pressure in the flask's headspace due to O_2 uptake, CO_2 accumulation, foam formation, etc.

After calibration, the culture system was gassed with N_2 until reaching DO = 0 %. After stopping the N_2 gassing the time was started. Neither active elimination of N_2 in the headspace nor aeration of the flasks took place. The oxygen signal $MS_{O_2,t}$ was continuously recorded until the end of the saturation curve. The saturation concentration of oxygen at the liquid boundary layer inside the flask ($C^*_{O_2}$) was considered as constant.

For practical purposes (avoiding response time of probes, saturation noise, etc.) a data range (MS_t) between 20 - 80 % DO was used for regression analysis during k_La determination.

Finally, OTR can be calculated as follows:

$$\frac{dC_{O_2}}{dt} = OTR = k_L a \; K_{H_{cp}} \; p_{abs} \left(y_{O_{2,2}} - y_{O_{2,1}} \right) \cdot 0.92 \tag{2.27}$$

2.3 Results and Discussion

2.3.1 Dependency of μ_{max} on Process Parameters in Bioreactor Cultures

The relationship between μ_{max} and the power input, mixing time, impeller tip speed, and Reynolds number in benchtop bioreactors is shown in Table 2.3 and Figure 2.9. According to Figure 2.9, the specific growth rate shows a clear dependency on the four criteria analyzed. Moreover, the fact that the fitted μ_{max} curves reach different maximum values within a same criterion, shows its dependency on bioreactor geometry.

For power input (Figure 2.9.A) the μ_{max} data can be separated into three cases, which seem to be well described by the fitted curves. The first includes experiments performed in bioreactors 1 (3-MP) and 2 (3-S) with maximum specific growth rates below $P/V = 75\ \mathrm{W\,m^{-3}}$. The second is found in bioreactor 5 (4-PBT) with maximum growth rates between P/V values of 50 and 200 $\mathrm{W\,m^{-3}}$. The third case is related to bioreactor 3, for which maximum growth rates are observed between 125 and 550 $\mathrm{W\,m^{-3}}$. An additional experiment performed in this bioreactor at $P/V = 1068\ \mathrm{W\,m^{-3}}$ (450 rpm) showed a reduction of only 20 % in μ_{max}, which confirms the fact that cells are able to grow at higher power input values [Ma et al. (2003)]. Therefore, the reduction of μ_{max} in bioreactors 1 and 5 is not due to power input, but most probably due to the impeller tip speed.

In all cases, during a theoretical power input determination minimum deviations from the proposed stirrer geometry might lead to significant variations of the power number [Kraume and Zehner (2001)]. However, due to the notorious geometrical differences in the studied stirrers in this work, deviations of the calculated *Np* values of even ± 20 % would not change dramatically the conclusions drawn here for power input.

The use of air for oxygen supply to the cells during cultivation is known to affect the estimated power consumption. To avoid this, a maximum aeration rate of only 0.06 vvm was set in all bioreactors. This value might lead to maximum differences between gassed and non-gassed power input of only 5 - 10 % according to Amanullah et al. [Amanullah et al. (2004)].

Interestingly, according to our results there is a region for mixing time (Figure 2.9.B)

Table 2.3: Process parameters and maximum specific growth rates of AGE1.HN cultivated in different bioreactors [Platas et al. (2012)].

Bioreactor	Impeller[a]	N [min^{-1}]	Np[c] [-]	P/V [$W\,m^{-3}$]	$\Theta_{94.5}$ [s]	u_i [$m\,s^{-1}$]	Re [-]	μ_{max} [d^{-1}]	s_μ [d^{-1}]
		200		2.9	18.5	0.37	5826	0.43	0.040
		300		9.7	14.8	0.55	8739	0.43	0.020
1		474		40.1	11.8	0.87	13797	0.42	0.024
Vario1000	3-MP↑	530	0.29	53.7	10.8	0.97	15438	0.41	0.029
		566		74.0	10.1	1.09	16487	0.39	0.014
		670		111.7	9.42	1.23	19516	0.20	0.016
		120		5.3	11.0	0.34	8321	0.39	0.009
2		120		5.3	11.0	0.34	8321	0.37	0.004
Benchtop	3-S↓	125	0.70	5.9	10.7	0.35	8667	0.37	0.030
Spinner		125		5.9	10.7	0.35	8667	0.37	0.015
		125		5.9	10.7	0.35	8667	0.39	0.019
		170		62.9	17.8	0.43	9292	0.25	0.012
		190		88.2	14.5	0.47	10315	0.33	0.028
		220		137.5	12.2	0.56	12181	0.39	0.017
3		232		161.2	12.0	0.58	12710	0.40	0.020
VSF2000	6-RT↔	261	11.90	212.0	10.7	0.66	14299	0.39	0.024
		310		350.3	9.2	0.78	16984	0.39	0.020
		350		552.3	8.2	0.88	19175	0.38	0.040
		450		1068.2	6.5	1.13	24653	0.32	0.029
4		100		7.3	21.2	0.28	6680	0.31	0.029
Biostat	6-RT↔	100 - 130[b]	7.56	9.3	21.2	0.30	7125	0.23	0.011
B-DCU		100 - 180[b]		25.1	16.0	0.39	9447	0.31	0.014
		250		40.2	18.0	0.63	13697	0.35	0.031
5		300		69.4	12.1	0.75	16436	0.41	0.002
VSF2000	4-PBT↓	350	2.16	110.2	10.0	0.88	19175	0.40	0.019
		420		190.4	8.5	1.06	23010	0.40	0.010
		500		322.6	7.6	1.26	27393	0.33	0.012

[a] 3-MP: 3-blade marine propeller, 3-S: 3-blade segment impeller, 6-RT: 6-blade radial-discharging impeller (Rushton), 4-PBT: 4-pitch-blade turbine. The arrows display the pumping direction of the impeller: ↑ upwards, ↓ downwards, ↔ radial.

[b] During these cultivations, agitation speed was varied in order to prevent further cell agglomeration. Process transfer criteria are therefore, averaged values.

[c] Values shown for power number consider impeller type and number, and bioreactor configuration. N, shaking velocity; Np, power number; P/V, specific power input; Θ_{95}, mixing time; u_i, impeller tip speed; Re, Reynolds number; μ_{max}, specific growth rate; s_μ, estimated error of the slope.

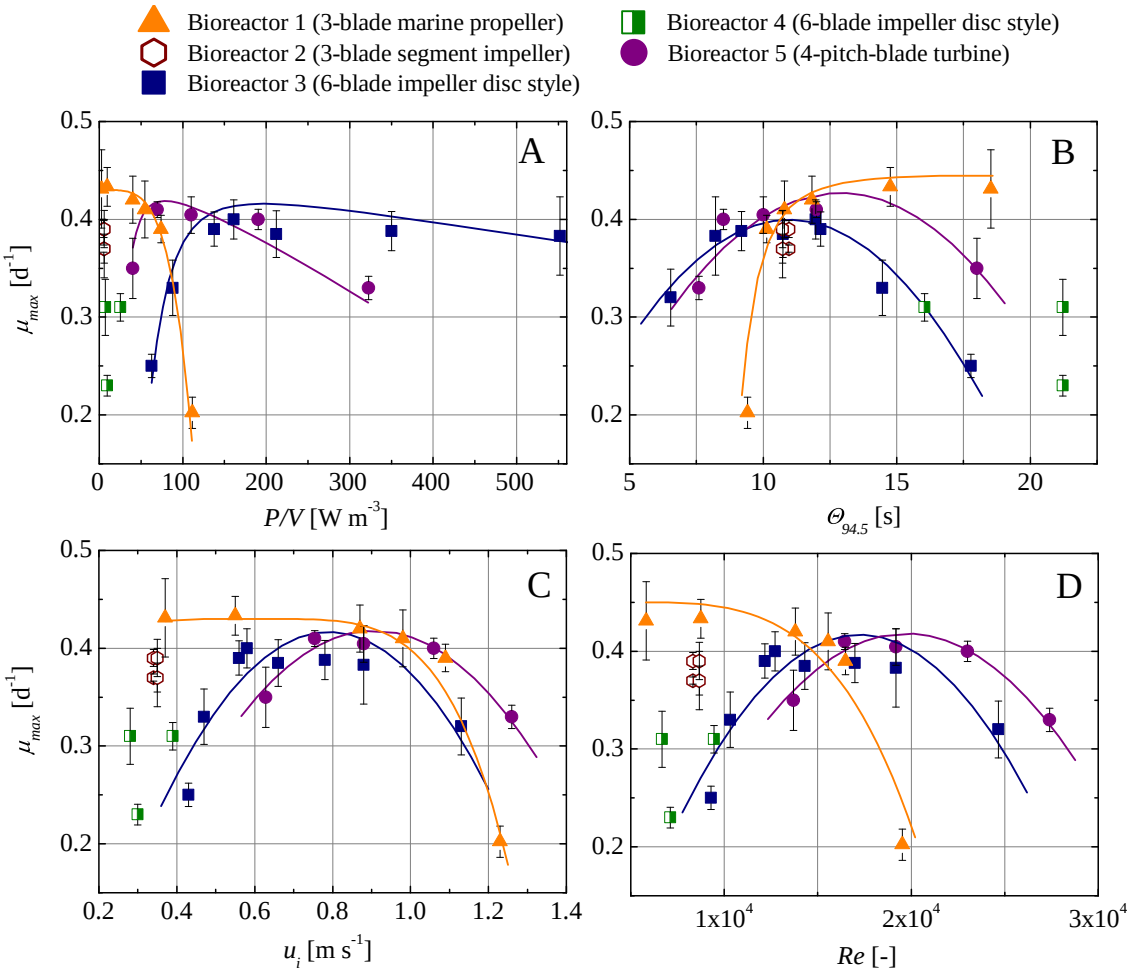

Figure 2.9: Dependency of μ_{max} on process parameters during the cultivation of AGE1.HN cells in benchtop bioreactors. A: power input, B: mixing time at mixing degree of 94.5 %, C: impeller tip speed, D: Reynolds number [Platas et al. (2012)].

where maximum μ_{max} values match at a common of $\Theta_{94.5} = 10$ - 12.5 s for the different bioreactors analyzed in this study. In this region, the maximum difference between μ_{max} values is reduced from a maximum of 0.19 to 0.05 d^{-1}. The steep decrease in μ_{max} in bioreactor 1 at $\Theta_{94.5}$ below 10 seconds cannot be explained by the mixing characteristic of this bioreactor, for which higher agitation speeds over 600 rpm have an almost irrelevant effect on the mixing time. This reduction in μ_{max} is probably a consequence of the impeller tip speed (u_i), which approaches to a value of 1.2 $m\,s^{-1}$ above 600 rpm.

The fact of an existing common region for mixing time with maximum μ_{max} values in these different bioreactors would explain two noteworthy phenomena; first, the high μ_{max} value of 0.37 - 0.39 d^{-1} in bioreactor 2 (3-S) at a power input value of only 5 $W\,m^{-3}$. This value is up to 0.15 d^{-1} higher than the μ_{max} reached in bioreactor

4 at a very similar power input value. However, as shown in Figure 2.9.B, at this power input range, the mixing time in bioreactor 2 was 11 s, whereas its value in bioreactor 4 was already above 20 s. A second observation considers the offset of the fitted μ_{max} curves of the bioreactors for P/V (see Figure 2.9.A). Considering bioreactor 3, μ_{max} would fall below 0.2 d^{-1} at P/V below 50 $W\,m^{-3}$. In this bioreactor agitation speeds above 170 rpm ($P/V = 63$ $W\,m^{-3}$) would be needed in order to avoid cell growth between the baffles and the bioreactor wall as well as around the bottom borders. The corresponding $\Theta_{94.5}$ in bioreactor 3 at this condition is 18 s. At this value, a reduction of μ_{max} for bioreactor 5 can be observed in Figure 2.9.B as well. Strong cell agglomeration was also observed in bioreactor 1 at $\Theta_{94.5} = 18.5$ s, which confirms the reduction in μ_{max} at $\Theta_{94.5} > 18$ s. The flat profile of the fitted μ_{max} data seem at $\Theta_{94.5} > 18$ s relies on the fact, that the agglomerated cells were also counted during analytics for this bioreactor. Without having considered the agglomerated cells, μ_{max} would have been clearly reduced. Finally, a tendency for cell agglomeration was also observed for bioreactor 4 at the similar region for mixing time. In two experiments with bioreactor 4 the agitation rate was increased after agglomeration was detected, in order to reduce the rate of agglomerated cells. Although agglomeration was reduced, this didn't lead to higher growth rates even though $\Theta_{94.5}$ approached common optimum values for all bioreactors. This behavior might be attributed to cell metabolism after agglomeration and to the formation of gradients which might lead the cells to reduced growth. Cell agglomeration was not observed during shake flask experimentation, since at the time those experiments were performed the agglomeration had been diminished by a slight medium modification (salt content) indicated by the project partner in charge of medium production.

The measurable consequences of the physical and chemical environment surrounding cells in culture have been reviewed by Ammanullah et al. [Amanullah et al. (2004)] and Ozturk [Ozturk (1996)]. Gradients which occur during cell cultivation might lead to cell agglomeration or sedimentation as well as to substrate and oxygen limitations. At mixing times (in this work $\Theta_{94.5} > 18$ s), cells might experience the so called pH excursions [Amanullah et al. (2004)], where cells move in streams of higher pH values for a longer time, in which their metabolism might be affected. The use of higher concentration of base for pH regulation might lead to the formation of necrotic droplets or the so called snow balls [Ozturk (1996)].

For u_i (Figure 2.9.C) there is a clear interval between 0.7 to 1.0 $m\,s^{-1}$ for com-

mon maximum specific growth rates in bioreactors 1, 3 and 5. At lower u_i values, only bioreactors 1 and 2 seem to keep a well mixed environment for the cells and allow for highest μ_{max}, probably due to their low cultivation volume. Beyond $u_i = 1\,\mathrm{m\,s^{-1}}$ a reduction in μ_{max} can be seen in all bioreactors.

For *Re* (Figure 2.9.D) it seems to be an overlapping of curves more than a common maximum, as it was the case during calculation of *Re* in shake flasks using the shake flask diameter as reference variable. Here, while bioreactors 3 and 5 might find their range for highest μ_{max} between $Re = 13000$ and 17000, a steep decrease in μ_{max} takes place within this range in bioreactor 2.

2.3.2 Dependency of μ_{max} on Process Parameters in Shake Flask Cultures

A range between 120 and 287 rpm was selected for the verification of the dependency of μ_{max} on the process parameters in shake flask culture. Surprisingly, there seems to be a very clear common region for high values of μ_{max} between 175 and 250 rpm for the four shake flasks analyzed here (Figure 2.10.A). In this range the AGE1.HN cells reached growth rate values between 0.49 and $0.59\,\mathrm{d^{-1}}$. These values have been only observed in these experiments; otherwise precultures showed a common growth rate of $0.40\pm0.05\ \mathrm{d^{-1}}$ in over 100 culture runs. These preculture runs were carried out at a working volume (V_w) ranging between 50 and 200 mL under the same culture conditions. The μ_{max} value of $0.40\pm0.05\ \mathrm{d^{-1}}$ is also the common optimal value for AGE1.HN growth in bioreactors as shown in the last section. It is worthy to mention two hints about the accelerated cell growth compared to the preculture:

a. Variability between medium charges: all cultures shown in Figure 2.10 were carried out with the same medium batch. Although two experiments were performed as nonparallel duplicates (100 mL baffled and 500 mL unbaffled, $N = 214$ and 215 rpm, and different operators for counting), both runs were carried out in the same medium. Therefore, a possible variation in the medium charge cannot be excluded.
b. Oxygen supply: repeated sampling in shake flask culture leads to different oxygen concentration profiles during culture. Accelerated cell growth was mostly observed in experiments, in which sampling took place twice per day (sampling of preculture was performed only once per day). In order to exclude any possible oxygen limitation from the preculture steps, the oxygen transfer capacity of the shake flasks was

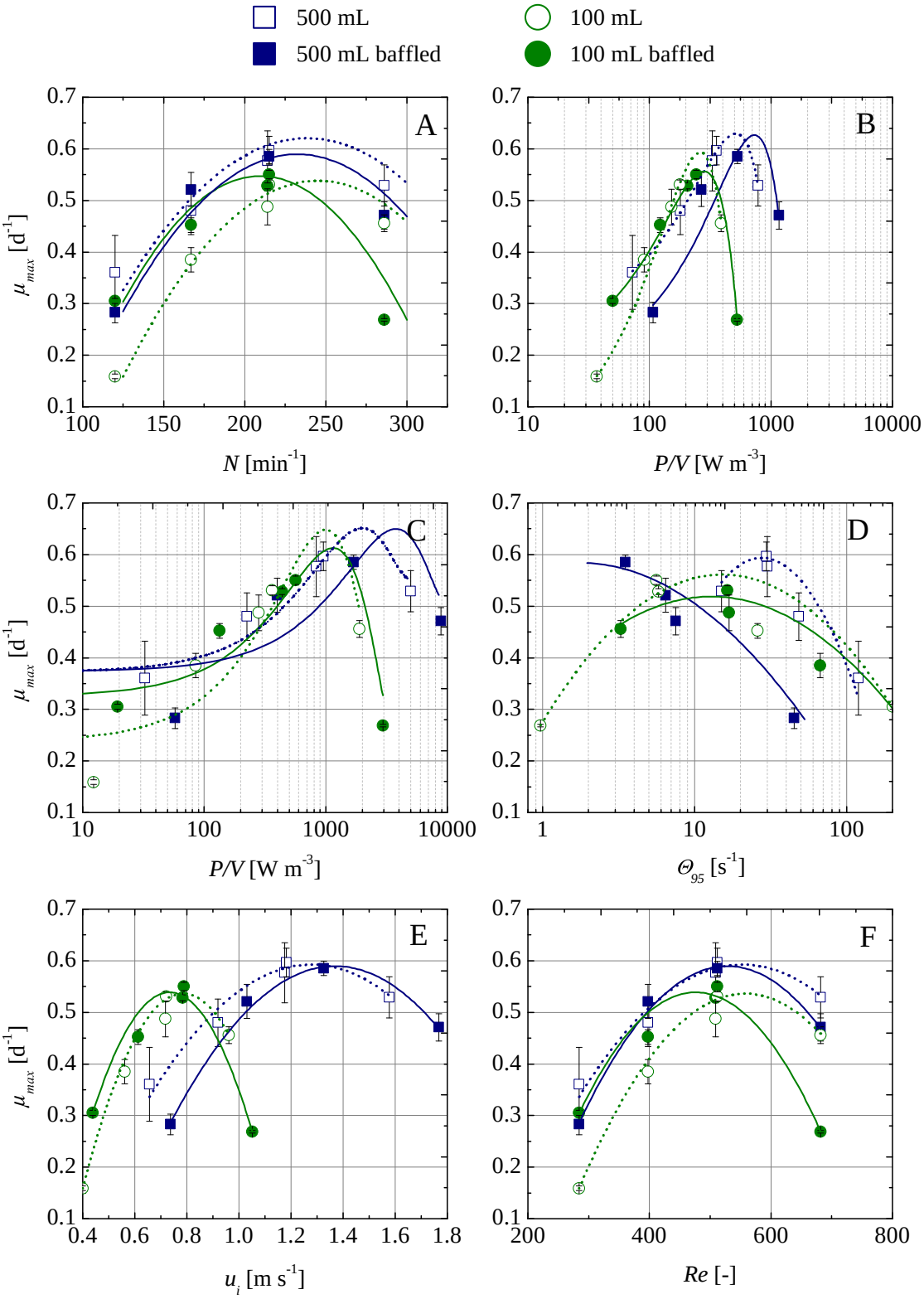

Figure 2.10: Dependency of μ_{max} on process comparability criteria during the cultivation of AGE1.HN cells in shake flasks. A: shaking velocity, B: power input according to [Büchs et al. (2000a), Büchs et al. (2000b)], C: power input according to [Kato et al. (1995)], D: mixing time at mixing degree of 95 %, E: maximum fluid velocity, F: Reynolds number according to [Kato et al. (1995)].

analyzed. The results will be shown and discussed later.

The dependency of μ_{max} on power input P/V can be seen in Figure 2.10.B with P/V determined by using the correlation by Büchs et al. [Büchs et al. (2000a), Büchs et al. (2000b)] and in Figure 2.10.C with the correlation based on Kato et al. [Kato et al. (1995)]. The x-axis in both graphs was set in logarithmic scale due to the number of data points at lower P/V values. The different correlations resulted in different P/V regions for maximum growth rates of AGE1.HN cells. Whereas it seems to be a common region for comparability of growth at lower P/V values, this comparison cannot be made at higher values. A steep increase in μ_{max} was observed for Kato's method at a P/V value of 200 - 400 $\mathrm{W\,m^{-3}}$, whereas according to Büchs' correlation this increase in μ_{max} can be found between 400 - 1000 $\mathrm{W\,m^{-3}}$. A slight drift of the curve fitting can be observed for the P/V of the baffled 500 mL shake flask, which appears to set the data out of the common trend. This might be only due to the fitting procedure and not due to a real deviation in the behavior of the culture. Even though the P/V results obtained with both methods are not comparable, the calculated values are still consistent with data reported in literature for the cultivation of mammalian cells in bioreactors [Smith and Greenfield (1992), Czermak (2008), Ma et al. (2003)].

According to the Phase number (Ph) proposed by Büchs et al., the 100 mL flasks operate in *in-phase* conditions for the N range studied, whereas all experiments performed in the 500 mL flasks operate in an *out-of-phase* regime ($Ph < 1.26$) (see Table 2.4). The reason for the calculation of lower Ph values in these flasks is the low shaking diameter (d_o) employed here during experimentation (see Equation 2.6), which is not covered by the procedure of Büchs et al. ($d_o > 1.25$). On the other hand, all cell culture experiments performed above $N = 120$ rpm are located in the range of efficient mixing proposed by Kato et al., which is $0.135Re^{-0.176} < Fr < 0.135Re^{0.186}$ (Re>1). This might speak for the good applicability of this procedure for the characterization of shake flasks at the studied conditions.

The dependency of μ_{max} on mixing time (Figure 2.10.D) shows a wide region for optimal growth. As for P/V, the x-axis is presented here in logarithmic form. The maximum values for μ_{max} are distributed within a range for Θ_{95} between 5 and 50 s, with a common region for maximum growth between 5 and 20 s for all flasks, excepting the baffled 500 mL flask, which shows a more significant reduction in μ_{max} above a mixing time of 10 seconds and a general offset of the fitting curve compared to

Table 2.4: Dependency of growth on process parameters during the cultivation of AGE1.HN in shake flasks.

Shake Flask	N [min^{-1}]	Np'^{a} [-]	P/V^{a} [$W\,m^{-3}$]	Np^{b} [-]	P/V^{b} [$W\,m^{-3}$]	Θ_{95} [s]	u_i [$m\,s^{-1}$]	Re^{a} [-]	${Re_f}^{a}$ [-]	Ph^{a} [-]	Re^{b} [-]	Fr^{b} [-]	$0.135 \cdot Re^{-0.176}$ [-]	$0.135 \cdot Re^{0.186}$ [-]	μ_{max} [d^{-1}]	s_μ [d^{-1}]
100 mL	119.5	0.327	36.9	0.059	12.3	443.6	0.40	11639	748	1.50	284	0.026	0.050	0.345	0.16	0.005
unbaffled	167.3	0.294	90.9	0.148	85.3	67.2	0.56	16295	1047	1.57	398	0.051	0.047	0.365	0.39	0.024
	214.0	0.273	151.9	0.290	281.0	16.9	0.72	20843	1881	1.69	509	0.083	0.045	0.380	0.49	0.034
	215.1	0.272	178.7	0.295	361.8	16.4	0.72	20950	1346	1.62	512	0.084	0.045	0.380	0.53	0.009
	286.8	0.250	388.8	0.650	1891.8	3.3	0.96	27934	1795	1.68	682	0.150	0.043	0.399	0.46	0.016
100 mL	119.5	0.309	49.8	0.059	19.3	200.9	0.44	13924	600	1.33	284	0.028	0.050	0.345	0.31	0.005
baffled	167.3	0.278	123.0	0.148	133.5	25.9	0.61	19493	841	1.40	398	0.055	0.047	0.365	0.45	0.014
	214.0	0.258	206.0	0.290	439.9	5.8	0.78	24934	1496	1.50	509	0.091	0.045	0.380	0.53	0.006
	215.1	0.258	242.4	0.295	566.3	5.6	0.79	25062	1081	1.44	512	0.092	0.045	0.380	0.55	0.008
	286.8	0.237	528.1	0.650	2961.2	1.0	1.05	33417	1441	1.50	682	0.163	0.043	0.399	0.27	0.002
500 mL	119.5	0.242	72.3	0.059	32.6	119.3	0.66	31328	2071	1.04	284	0.042	0.050	0.345	0.36	0.072
unbaffled	167.3	0.220	180.9	0.148	225.3	48.0	0.92	43859	2899	1.08	398	0.083	0.047	0.365	0.48	0.046
	214.0	0.205	328.4	0.290	835.1	30.0	1.18	56102	4349	1.13	509	0.136	0.045	0.380	0.58	0.058
	215.1	0.205	357.2	0.295	955.7	29.6	1.18	56390	3727	1.12	512	0.138	0.045	0.380	0.60	0.028
	286.8	0.189	783.4	0.650	4997.1	15.0	1.58	75187	4969	1.15	682	0.245	0.043	0.399	0.53	0.040
500 mL	119.5	0.226	106.9	0.059	45.1	52.8	0.74	39365	1567	0.90	284	0.048	0.050	0.345	0.28	0.020
baffled	167.3	0.206	267.0	0.148	398.7	6.4	1.03	55111	2193	0.94	398	0.093	0.047	0.365	0.52	0.033
	215.1	0.192	530.2	0.295	1691.4	3.5	1.33	70857	2820	0.96	512	0.154	0.045	0.380	0.59	0.014
	286.8	0.178	1164.2	0.650	8844.1	7.5	1.77	94475	3760	1.00	682	0.274	0.043	0.399	0.47	0.027

[a] Calculated according to Büchs et al. [Büchs et al. (2000a), Büchs et al. (2000b)].
[b] Calculated according to Kato et al. [Kato et al. (1995)].
N, shaking velocity; Np', modified power number; P/V, specific power input; Np, power number; Θ_{95}, mixing time; u_i, fluid velocity at flask wall; Re, Reynolds number; Re_f, liquid-film Reynolds number; Ph, phase boundary; Fr, Froude number; μ_{max}, specific growth rate; s_μ, estimated error of the slope.

the other flasks, with a maximum μ_{max} at 2.5 seconds. At this region, growth in the other flasks start to decrease. Some of the deviations during shake flask experiments are explained in the following.

During the shake flask experiments, attention was paid to the flow profile of the culture medium in the flasks, specially at both low and high shaking velocities such as in the range of $120 \geq N \geq 287$ rpm. In this rpm range, the culture in all flasks didn't move synchronously with the shaker; at 287 rpm for example, the culture in the baffled 500 mL flask was rocked, rather than agitated. This flow profile was impaired by the visually higher foam build-up at these conditions (foam-layer thickness of ca. 1 - 2 cm). As a result, the culture might have entered into an *out-of-phase* regime, having as a consequence an increase in mixing time and a decrease of the oxygen transport capacity to the cells.

According to the mixing time characteristic shown in Figure 2.11, there is in fact a slight increase of Θ_{95} in the baffled 500 mL flask at $N > 285$ rpm. Furthermore, foam formation during culture might have increased the real mixing time further compared to characterized data. If this is the case, the 500 mL baffled data in Figure 2.10.C might show a shift to the right and might fit better the common culture behavior of all flasks.

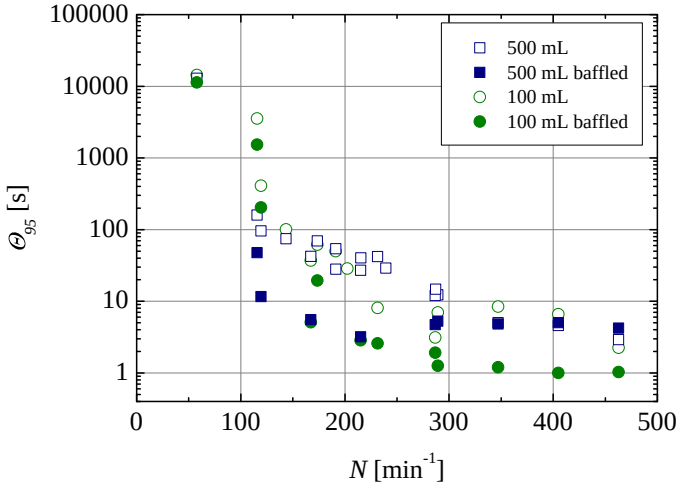

Figure 2.11: Mixing time characteristic Θ_{95} in baffled and unbaffled shake flasks.

For the maximum fluid velocity (u_i) clear separate process windows can be identified in Figure 2.10.E for the 100 mL and for the 500 mL flasks, with maximum growth rates at $u_i = 0.6$ - 1.0 m s^{-1} for both 100 mL flasks, and 0.8 - 1.6 m s^{-1} for both 500 mL

flasks. Although both curves overlap at a region between 0.6 and 1.2 $\mathrm{m\,s^{-1}}$, which is also common during the cultivation of mammalian cells in bioreactors, no common region for highest μ_{max} values can be identified for this parameter.

Finally, Figure 2.10.F shows the dependency of μ_{max} on Re. The Re numbers shown in Figure 2.10.F were calculated according to the correlation based on Kato et al. Since Re values depend on the shaking diameter of the machine (d_o), the dependency on μ_{max} shown in the Figure resembles its behavior shown in Figure 2.10.A, where N is the only remaining variable in Equation 2.10. The comparability of different shaking machines with this criterion has still to be verified. Maximum growth rates can be found for Reynolds numbers in the range of 400 - 600 for all flasks.

Analysis of the Oxygen Transport Capacity in Shake Flask Culture

Oxygen transfer in the shake flasks was assesed in order to exclude any possible limitation during culture. The oxygen transfer capacity of the shaken systems is presented in Figure 2.12 as a function of the volumetric oxygen transfer coefficient ($k_L a$) and the shaking velocity (N). A clear region for maximum oxygen transport in the flasks can be observed between 100 and 250 rpm for the baffled 500 mL, and for both 100 mL flasks. On the other hand, the $k_L a$ values in the unbaffled 500 mL shake flask always remain below $0.5\,\mathrm{h^{-1}}$.

In order to assess the capability of these flasks to supply cells with oxygen, a comparison of the culture dependent oxygen consumption (OUR) and the system dependent oxygen transfer (OTR) is presented in Figure 2.13.

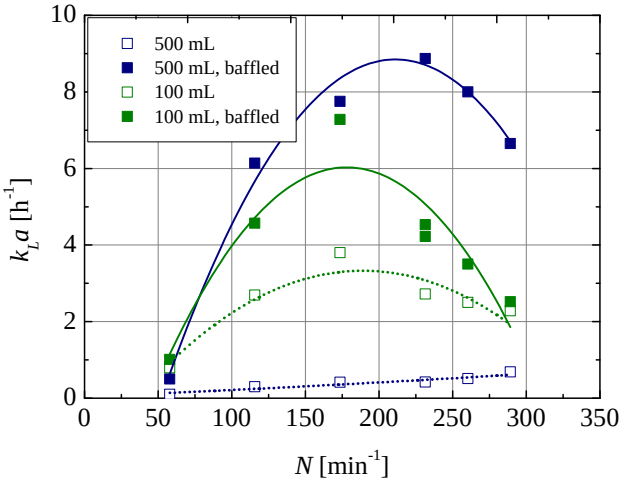

Figure 2.12: Volumetric oxygen transfer coefficient $k_L a$ in baffled and unbaffled shake flasks.

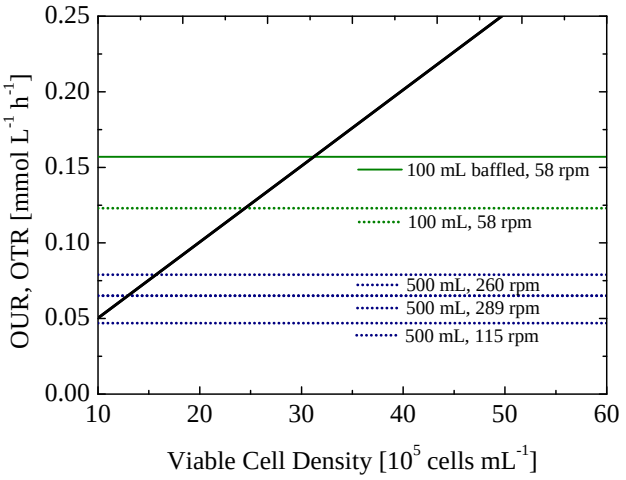

Figure 2.13: Oxygen uptake rate (OUR, black, bold line) and Oxygen tranfer rate (OTR, color lines) of AGE1.HN in shake flask culture.

Figure 2.13 shows the oxygen uptake rate (OUR) of AGE1.HN at different cell densities by assuming a cell-specific oxygen consumption rate of $q_{O_2} = 5.0313{\cdot}10^{-11}$ mmol cell^{-1} h^{-1}, and the oxygen transfer rate (OTR) of some of the flasks at different N values. The OTR lines shown in the Figure correspond to those lower OTR values which hinder culture growth above the corresponding cell density. It can be seen, that there are no real limiting conditions for μ_{max} calculation for the studied flasks but for the 500 mL unbaffled flask, which apparently cannot supply the necessary oxygen for allowing cell growth above $1.5{\cdot}10^6$ cells mL^{-1} at any of the conditions analyzed in this work. A common cell density of over $30{\cdot}10^5$ cells mL^{-1} cannot, according to the figure, be reached by cells growing in this flask. No critical conditions can be identified in Figure 2.13 for the other flasks used in this work, unless cultivation takes place at shaking values below 60 rpm.

Despite the low calculated OTR values for the unbaffled 500 mL shake flask, no growth limitation was observed during practice. In fact, this flask geometry allowed for the highest final cell densities with highest μ_{max} among all others. A possible explanation to this case might rely on the method used for $k_L a$ determination. The calculated $k_L a$ was intended to represent all resistances to oxygen transport from the incubator's atmosphere to the shake flask's liquid, which include the aluminium cap, the variable O_2 concentration in the flask's headspace, the CO_2 production by the cells, and the foam formation. The determination of the real influence of these variables is not a trivial task. In accordance with this, Mrotzek et al. [Mrotzek et al. (2001)] characterized the oxygen transfer resistance of aluminium caps in shake flasks

with no reproducible results due to strong fluctuation of the determined values.

During $k_L a$ measurements, the gassed N_2 into the flasks at the beginning of the experiment was not removed before recording the $MS_{O_2,t}$ data. The contained N_2 slowed the process of oxygen transfer down, and was intended to represent some of the resistances to oxygen transport in the flask. For a formal calculation of $k_L a$, however, $MS^*_{O_2}$ in Equation 2.26 was set constant. This fact reduces considerably the calculated $k_L a$ and therefore the resulting OTR values. In a more detailed OTR determination, the change of the oxygen concentration in the flask's headspace should be included. This would increase the value of the calculated oxygen transfer rates. After this, oxygen limitation might be excluded from the performed experiments. The reduction or increase in μ_{max} would therefore be solely a consequence of the process parameters used during the cultivations.

2.3.3 Process Parameters for Consistency in the Cultivation of AGE1.HN Cells in Bioreactors and Shake Flasks

The process windows defined through this work for the cultivation of AGE1.hn cells are shown in Table 2.5.

Table 2.5: Process parameters for the comparable cultivation of AGE1.HN cells in different shake flask and bioreactor systems.

Process Criterion	Units	Benchtop Bioreactor	Shake Flask
Power Input *(P/V)*	[$\mathrm{W\,m^{-3}}$]	-	200 - 400[a]
			400 - 1000[b]
Mixing Time (Θ_{95})	[s]	10 - 12	5 - 20
Maximum Fluid Velocity (u_i)	[$\mathrm{m\,s^{-1}}$]	0.7 - 1.0[c]	-
Maximum Reynolds Number (Re)	[-]	-	400 - 600[d]

[a] Values according to Figure 2.10.B

[b] Values according to Figure 2.10.C

[c] Impeller tip speed

[d] Values according to Figure 2.10.F

The values shown in the table represent the process parameter ranges, in which the standard deviation of μ_{max} between AGE1.HN cultures can be reduced from 0.060 to 0.016 $\mathrm{d^{-1}}$ for bioreactor culture, and from 0.12 to 0.027 $\mathrm{d^{-1}}$ for shake flask culture (see Figure 2.14). With this, $s_{\mu_{max}}$ was reduced in both systems to an average value of 25 % of its initial value at the beginning of this work and is less than 50 % of the value set for comparability at the beginning of this project ($s_{\mu_{max}} = 0.05\,\mathrm{d^{-1}}$).

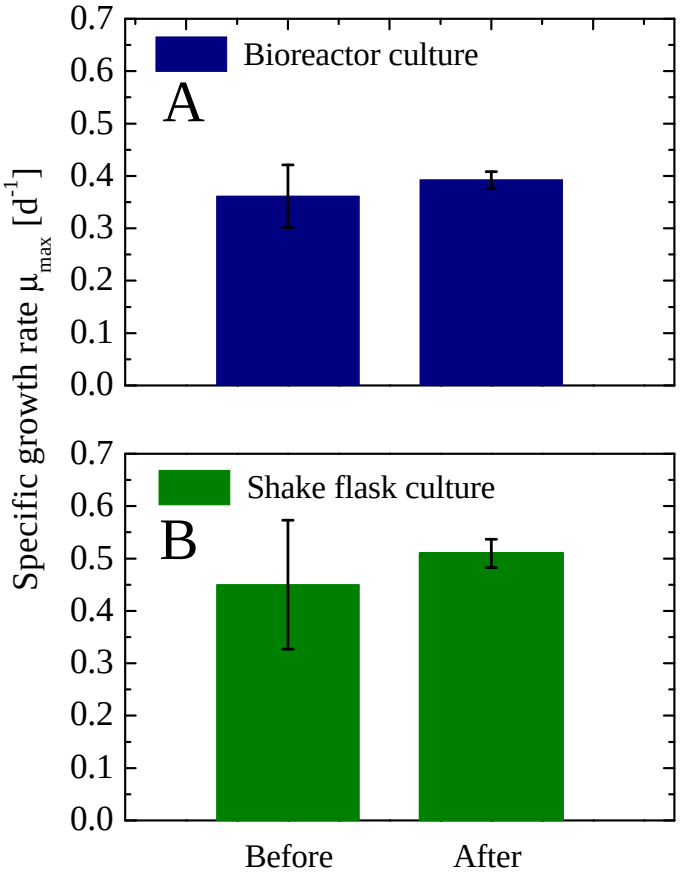

Figure 2.14: Average specific growth rate, μ_{max}, and standard deviation, $s_{\mu_{max}}$, of AGE1.HN culture runs before and after process characterization. A: Bioreactor runs with $\mu_{max} = 0.36\,\mathrm{d}^{-1}$ and $s_{\mu_{max}} = 0.06\,\mathrm{d}^{-1}$ (before), and $\mu_{max} = 0.39\,\mathrm{d}^{-1}$ and $s_{\mu_{max}} = 0.016\,\mathrm{d}^{-1}$ (after). B: Shake flask runs with $\mu_{max} = 0.45\,\mathrm{d}^{-1}$ and $s_{\mu_{max}} = 0.12\,\mathrm{d}^{-1}$ (before), and $\mu_{max} = 0.51\,\mathrm{d}^{-1}$ and $s_{\mu_{max}} = 0.027\,\mathrm{d}^{-1}$ (after).

These data allow for comparable results during the cultivation of the cell line and support the metabolic results obtained during culture in geometrically different systems. The choice of cultivation parameters for mammalian cells should, however, focus not only on one criterion but should put them together for analysis. This will allow to avoid misleading data when searching for consistency between cultivations.

2.4 Concluding Remarks

Criteria for standardized operation and process comparability were analyzed for the human industrial cell line AGE1.HN in different cultivation systems. They included four shake flasks and five benchtop bioreactors, all systems with geometric dissimilarities. Growth was compared within varied ranges for power input, mixing time, maximum fluid velocity and Reynolds number. Thus, common ranges for these process parameters were identified, at which a reduction in the standard deviation of the μ_{max} values in culture can be found. For benchtop bioreactors, no common P/V was found, which is mainly due to the differences related to the stirrer's designs. However, the values calculated in this work correspond very well to those reported in literature for the cultivation of mammalian cells. The mixing time as well as the impeller tip speed showed a high applicability as criteria for culture standardization. Especially for mixing time, a reduction of more than 70 % in the standard deviation of the average μ_{max} was demonstrated for the bioreactors studied.

In shake flask culture common values for P/V were identified for different shake flask sizes and geometries where cell growth was comparable. The P/V ranges for comparison depend on the calculation procedure employed. However, both calculated P/V ranges for common maximum growth correspond to data reported in literature for mammalian cell culture in bioreactors. As for mixing time, cell growth was maximum in a common region in both the shake flasks and in the bioreactors. This fact points to the applicability of Θ_{95} as criterion for comparability of growth in both systems.

This work can be used as a practical reference in laboratories as well as for process transfer during the cultivation of other mammalian cell lines, aimed at cell manufacturing or for the production of cell products. It is recommended for groups dealing with comparability studies, not to focus only on one criterion for process transfer but to perform a conscious analysis of the main parameters, which describe the culture dynamics in the employed vessels.

3 Synchronization Strategies for Cells Grown under Physiological Conditions

3.1 Theoretical Background

3.1.1 Cell Synchronization and its Relevance for Systems Biology

Mammalian cell expression has become the dominant recombinant-protein production strategy for clinical applications because of its capacity for post-translational modification and human protein-like molecular structure assembly [Zhu (2012)]. The high demand for these biopharmaceuticals has led to the development of large-scale manufacturing processes, with productivity improvements being many times achieved by optimization of bioreactor systems. However, more recently, the early steps of production, prior to bioreactor culture, have been presented as alternative areas where productivity enhancements can be achieved [Costa et al. (2010)]. Here, central metabolism of a cell line and the interaction of its dynamics during growth and product formation are main topics to be focused on to enhance the understanding of these processes and the knowledge about mammalian cell metabolism. For a comprehensive analysis of cellular metabolism, not only a qualitative determination of key molecules is necessary, but also their immediate quantification at the time they are produced. The determination of these components is the key to elucidate the complex quantitative relationships of mammalian cell metabolism. In this way research tools are available like metabolomics, for the analysis of small molecules participating in general metabolic reactions for maintenance, growth and normal function of the cell [Khoo and Al-Rubeai (2007)], genomics as the tool to determine gene sequences [Hu and Zeng (2012)], proteomics, which focuses on the elucidation of protein functions [Monti et al. (2009)], and glycomics, which studies the relationship of groups of glycans to a particular biological event [Cosgrave et al. (2011)].

Up to date, nearly 70 % of all therapeutically recombinant proteins are produced in CHO cells. With approximately 18 million cells per mililiter, end product titers up to 5 - 10 gram per liter can be reached in batch and fed-batch cultures [Moo-Young (2011)]. In order to further increase these current product titers and therefore decrease the scale of production, more efforts have to be done at cell line development and clone selection levels. A key task for this development in mammalian cell lines points to decoding the complex regulation of energy metabolism in cells. Furthermore, new strategies are needed to shift cells from the accelerated-growth phase to

a stable-production phase. Since product formation rates vary all over the cell cycle [Fogolín et al. (2004)], a systematic way to study populations of cell lines growing with synchrony is needed.

During the cell cycle (see Figure 3.1), the cell genome, organelles and macromolecules double their quantity to create two genetically identical daughter cells. These steps involve the two most important phases of the cell cycle, the S phase and the M phase. In the S phase (Synthesis), the chromosomes replicate. In the M phase (Mitosis), chromosome material is distributed to the new formed nuclei. Afterwards, the cytoplasm is divided (cytokinesis), resulting in the formation of the two daughter cells. For the time needed by the cell for synthesis of precursors, organelle division, cell growth etc. there are two Gap phases: the first one (G_1) between the Mitosis and the S phase, and the second one (G_2) between the S phase and the Mitosis phase. If the environmental growth conditions are not appropriate, cells in the G_1 phase will not move into the S phase, but will enter into a quiescent state, the G_0 phase, where they can remain for a long time. Only at appropriate growth conditions, cells will reach a point at the end of the G_1 phase (commitmet point or Start), at which they will commit to DNA synthesis and division, even if growth and division signals cease to exist [Alberts, B. et al (2011)].

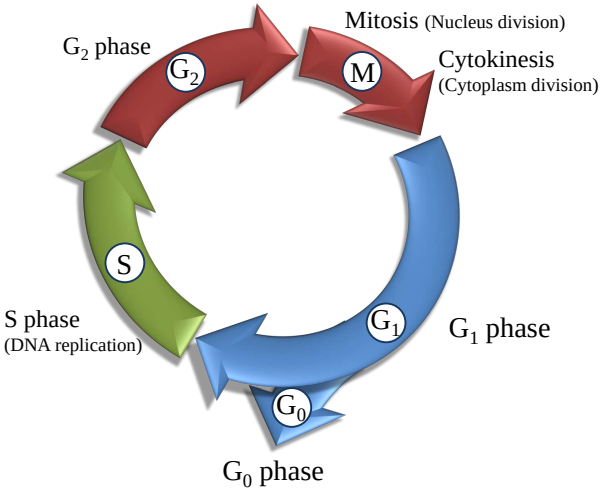

Figure 3.1: The four phases of the cell cycle. In most of the cells, the Gap phases G_1 and G_2 separate the S and M phases from each other. If environmental growth conditions are not appropriate, cells in the G_1 phase will not move into the S phase, but will enter into a quiescent condition, the G_0 phase.

Cell synchronization in the cell cycle represents an useful method to study the molecular interactions in cell cycle related metabolic pathways. There have been many attempts to synchronize cells and cell populations [Krishan et al. (1976), Enninga et al.

(1984), Keyomarsi et al. (1991), Knehr et al. (1995), Moore et al. (1997), Cooper (2002a), Fiore et al. (2002)]. Some of these attempts have however focused on arresting cell growth at a determined cell cycle phase and studying the consequences of growth arrest. Other authors have explained why many of the chosen methods for this purpose cannot be considered as successful [Spellman and Sherlock (2004), Cooper (1998), Cooper (2002b), Cooper (2003), Cooper (2006)]. Furthermore, the question of unperturbed cell growth after synchronization has not yet appeared during our definition of criteria for performing metabolic studies with synchronous cells.

The existing debate has somehow redefined the criteria to consider a cell population as being synchronized. These criteria are summarized as follows (modified from [Keyomarsi et al. (1991), Cooper and Shedden (2003)]):

Criteria for Synchrony of a Cell Population

1. Further unaffected cell growth after synchronization.
2. Minimal increase in cell number during the interdivision time.
3. Constant doubling time and equal to that of cells in exponential growth.
4. Narrow DNA distribution.
5. Narrow size distribution.

Therefore, a synchronization strategy for research on cell-cycle-dependent metabolism should consist of generating a homogeneous cell population within the same cell-cycle phase, with the same cell size, and with the capacity of further unaffected growth.

3.1.2 Synchronization Methods

Cell synchronization methods can be divided in two main groups: chemical and physical methods. Figure 3.2 shows some methods which have been used for synchronization of a whole cell population (whole culture methods) or a fraction of it (selective methods). These methods will be described in the following section.

Chemical Methods

These methods result mostly in a reversible blocking of cells at a certain growth phase by means of phased deprivation of a medium component (phased feeding) or addition of chemicals. Here, Colcemid or Nocodazole have been used for blocking cells in the M phase [Knehr et al. (1995), Boxberger (2007), Lindl and Gstraunthaler (2008)]; Aphidicolin, Hydroxyurea, Mimosine and Thymidine excess, for blocking

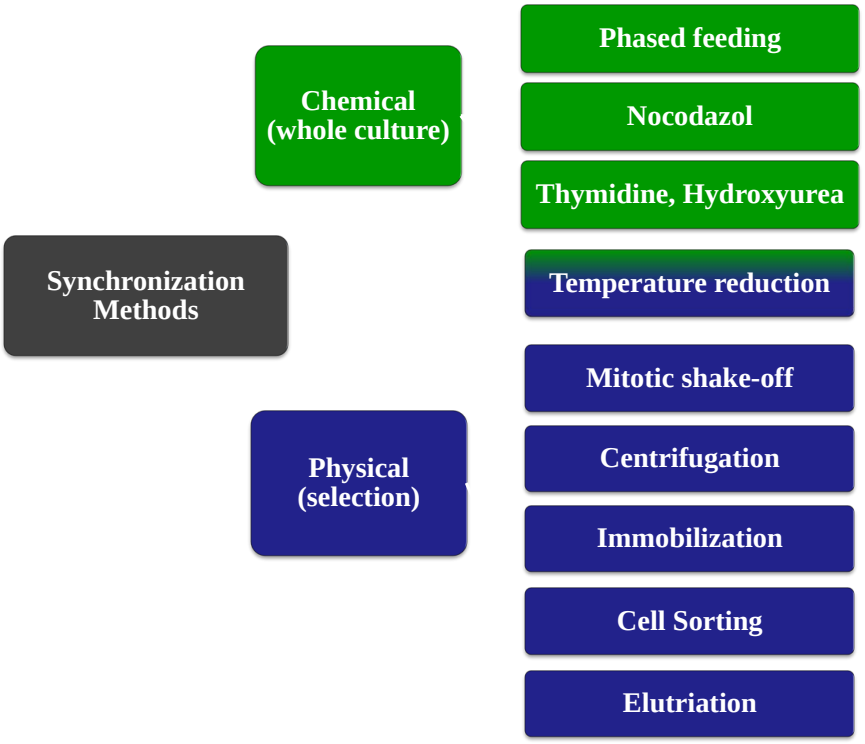

Figure 3.2: Chemical and physical methods for cell synchronization.

cells in the S phase [Knehr et al. (1995), Matherly (1989)]; serum or amino acid starvation, DMSO and Lovastatin for blocking cells in the G_1/G_0 phase [Fiore et al. (2002), Boxberger (2007)].

Depending on the selected chemical method, some of the mentioned criteria for synchronization of whole-cell populations might not be fulfilled, as the metabolic blocking is not always reversible in a short period of time. For a chemical, which acts during a specific phase of the cell cycle, the maximum theoretical reaction time for the blockade would account for almost the whole doubling time of the cell. Another disadvantage of the chemical methods is the difficulty to wash the chemicals off the culture, intracellularly and extracellularly. This includes more than one wash step and might lead to a longer lag-phase during restart of the culture. Depending on the chemical, some might induce cytotoxicity even at short exposure times [Matherly (1989)]. Important drawbacks of chemical methods that pursue cell synchronization in the G_1 phase such as starvation or inhibition have been very well described by Cooper, S. [Cooper (1998)] in a comprehensive so called *gedankenexperiment*.

Physical Methods

Temperature Reduction: A reduction in the cultivation temperature (30 - 34 °C) is used to arrest cells in the G_1/G_0 phase. It is also a way to increase product formation due to the resulting enrichment of cells within these phases after its reduction [Fogolín et al. (2004)]. According to the literature [Enninga et al. (1984), Cooper (2003), Vogt and Verma (1995), Boxberger (2007)], cells being in another cell cycle phase than G_1 at the moment of temperature reduction, will progress further through the cycle ($S \rightarrow G_2/M \rightarrow G_1$) to reach the G_1/G_0 phase. This method has been successfully tested by Enninga, I.C. [Enninga et al. (1984)] by arresting cell growth at 30 °C of human diploid fibroblasts VH-16 for 36 - 41 hours after 3 days of cultivation. A steep increase in [+3H]TdR (tritiated thymidine) incorporation determined the entrance of cells into the S phase after resumption of optimal growth conditions. After 25 hours incorporation of [+3H]TdR decreased to 16 % from its initial value, showing that the cells were already losing synchrony (see Figure 3.3).

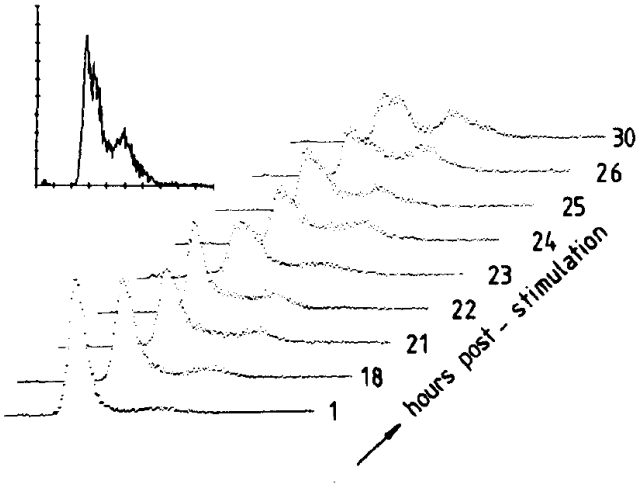

Figure 3.3: Variation of the DNA content distribution after temperature resumption of a 30 °C arrested cell population [Enninga et al. (1984)].

Moore et al. [Moore et al. (1997)] incubated CHO cells first for 48 hours and then tested two different temperature shifts (33 and 30 °C) for longer cultivation periods. On the third day, 87 % of the cells had entered the G_1/G_0 phase and accumulated in this phase up to 100 % at day 14 (see Figure 3.4). This high accumulation of cells in the G_1/G_0 phase after 14 days of culture points towards an accumulation of apoptotic cells more than to a real arrest of growth at the G_1 phase (see Figure 3.4). Some authors [Boxberger (2007), Lindl and Gstraunthaler (2008)] reported that, af-

ter a temperature reduction to 4 °C for 30 - 60 min (cold shock), cells would further divide with synchrony.

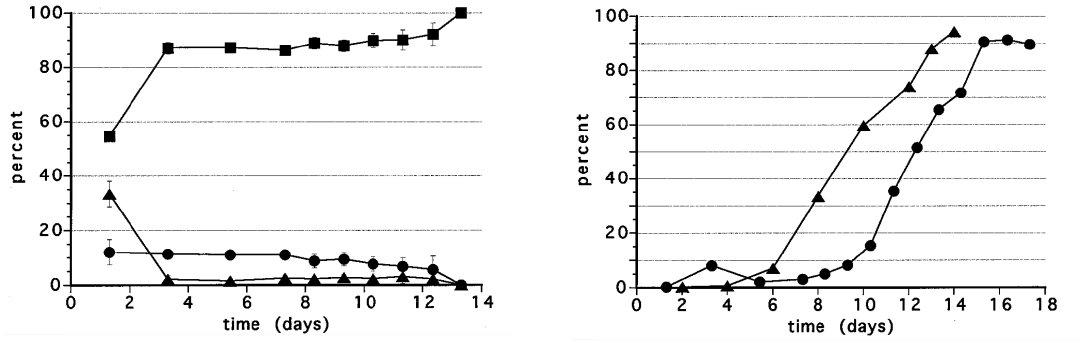

Figure 3.4: Left: Proportion of viable cells in each phase of the cell cycle; G_1/G_0 (■), S phase (▲), and G_2/M (●), on days 1 to 14, in a culture initiated at 37 °C and then temperature shifted to 30 °C after 48 hours. Right: Proportion of apoptotic cells as a percent of the total cell population from days 1 through 17. Cultures maintained at 37 °C (▲), and cultures which temperature was shifted to 30 °C after 48 hours (●). Source: Moore et al. [Moore et al. (1997)].

Mitotic-Shake-off: This method consists of detaching mitotic-dividing adherent cells from its surface while dividing in a T-Flask. The surface of the T-Flask is gently knocked to bring the young not-yet-attached cells into suspension. This method can be employed whenever anchorage dependent cells are used.

Gradient Centrifugation: Centrifugation in continuous and discontinuous gradients has been successfully used for separation of organelles [Britten and Roberts (1960)] or specific types of cells, which differ in their physical properties from the whole cell population [Rola-Pleszczynski and Churchill (1978), Holley (1988)]. The sedimentation velocity of a cell line in a gradient is, as well, defined by the Stocke's law (Equation 3.1), in which cell size and cell density are the parameters which will define the separation efficiency of the method. Furthermore, the density of the medium, ρ_m, can be varied in order to increase or decrease the sedimentation velocity of the cells. The easiest way to increase the density of the medium can be achieved by sucrose addition (see Figure 3.5, left). However, a sucrose solution that approaches the density of a cell will normally have elevated osmolalities. (Figure 3.5, right).

For this reason, high molecular polymers can be used for increasing the density of a solution without affecting its osmolality. Ficoll 400^{TM} is a highly branched polymer formed by the copolymerization of sucrose and epichlorohydrin [Amersham

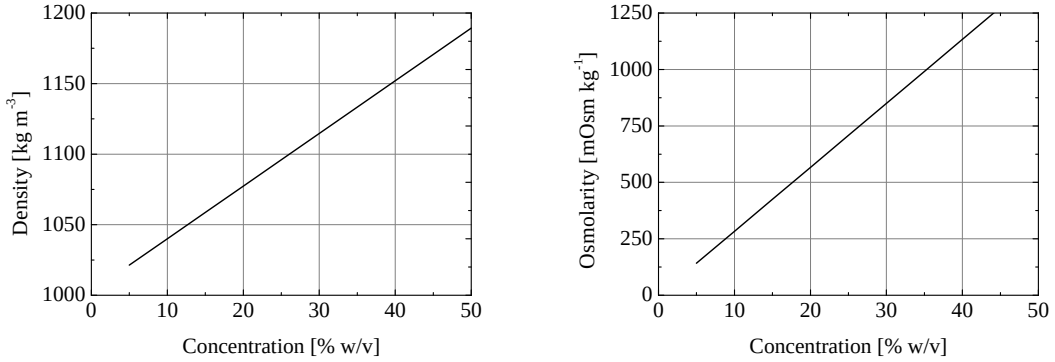

Figure 3.5: Density (left) and osmolality (right) values of sucrose solutions. Curve fittings of experimental data reported by [Rickwood et al. (1994)] and [Amersham Biosciences (2001)] at 5 °C; Left: $y = 3.7327x + 1002.7$, Right: $y = 1.02(x \cdot 10/360) \cdot 1000$.

Biosciences (2001)]. Addition of Ficoll to the centrifugation medium increases its density in a similar way as glucose does, but without affecting significantly its osmolality (left and right in Figure 3.6).

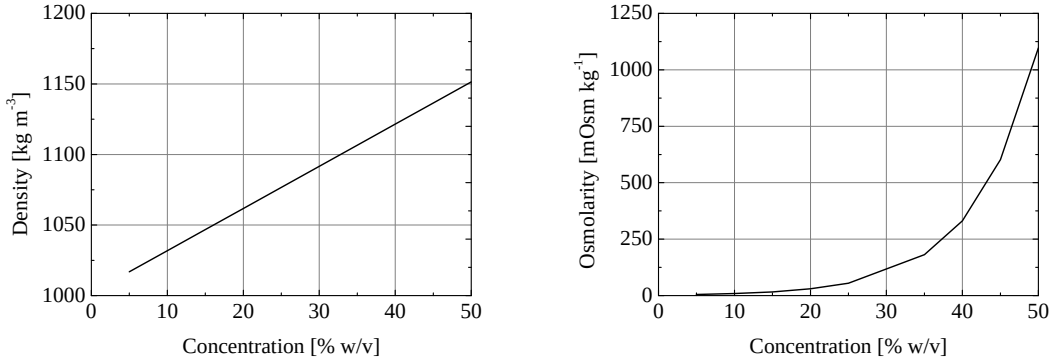

Figure 3.6: Density (left) and osmolarity (right) values of Ficoll solutions. Curve fittings of experimental data reported by Sharpe (1988) and Amersham Biosciences (2001) at 5 °C; Left: $y = 2.9908x + 1001.9$, Right: $y = 2.7318\ e^{0.1199} \cdot x$.

Membrane elution: This is an immobilization method consisting in the separation of newly born cells from their progenitors by a continuous flow of medium through a substrate, where the latters are attached and grow onto [Helmstetter and Cummings (1963), Cooper (2002a), Helmstetter et al. (2003)].

Growing cells are gently filtered onto a nitrocellulose membrane filter that has been treated previously with poly-D-lysine or concanavalin to allow cells to bind. After cell attachment, the filter is inverted, warm medium is pumped through the membrane, and the bound cells grow onto the surface of the filter. At cell division, one daughter cell remains attached to the membrane while the other daughter cell is eluted with

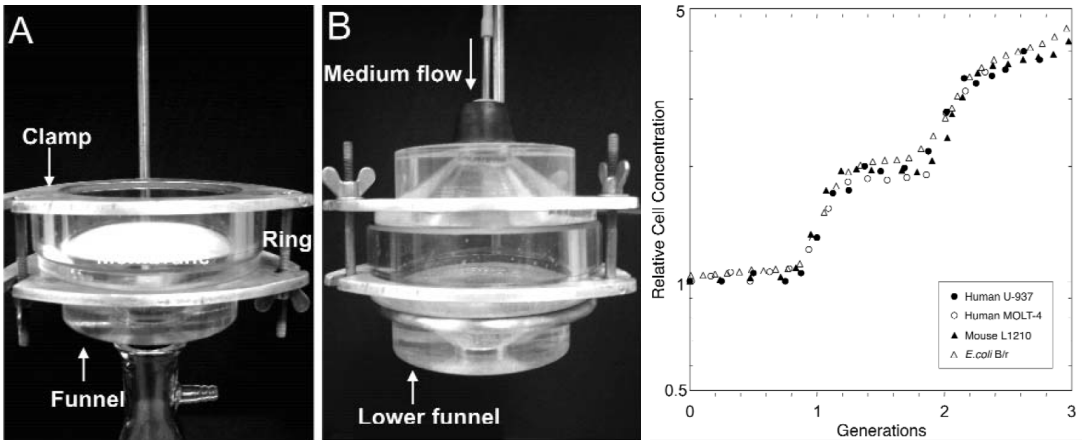

Figure 3.7: Membrane elution method. Left: Membrane filter holder as configured during attachment of cells (A) and during elution of newborn cells (B). Right: Synchronous growth of L1210, MOLT-4, U-937 and E.coli B/r. L1210. Source: Helmstetter et al. [Helmstetter et al. (2003)]

the medium. Eluted cells collected for a short time period, produce a culture with cells dividing synchronously and passing as a cohort through the sequential stages of the cell cycle. This procedure, also called the *eukaryotic baby machine*, is described in some publications [Cooper (2002a), Helmstetter et al. (2003)] as the only existing method that allows synchrony of a whole cell culture. A major drawback of this method for the synchronization of the AGE1.HN might be the tendency of the cell line to agglomerate in culture medium after relatively short time periods when no agitation is present (ca. 1 h). This fact would lead either to the formation of cell clumps in case cells are not well separated from each other on the membrane surface, or to an impossible separation of newly born cells from its progenitors.

Fluorescent-Activated Cell Sorting: Flow cytometry is a general method for rapidly analyzing large numbers of cells individually using light-scattering, fluorescence, and absorbance measurements. The power of this method lies both in the wide range of cellular parameters that can be determined and in the ability to obtain information on how these parameters are distributed in the cell population [Rieseberg et al. (2001)]. Cells or particles in suspension flow in a single file at uniform speeds (10^4 - 10^6 cells min^{-1}) through a laser light beam at which they interact individually. This yields, for each cell, a light scatter pattern which gives information about cell size, shape, density and surface morphology [Al-Rubeai and Emery (1993)]. In addition, flow cytometers can be combined with sorting units that offer the possibility of separating selected subpopulations. Most sorters are based on a sorting unit that breaks the cell stream into droplets. Before the droplets are formed, the cells

are electrically charged. The resulting droplets are deflected into a collection vessel by passage through an electric field and are collected depending on selected target parameters [Julius et al. (1972) Rieseberg et al. (2001)]. According to this principle, cell sorting can be performed based on the size of the cells. Since cell size and cell age are related [Jorgensen and Tyers (2004)], the size sorted subpopulations will show a higher degree in synchrony depending on the selectivity of the method. A possible disadvantage might be the low yield of cells (10^7 cells h^{-1}) [Miltenyi et al. (1990)], the possible cell damage during the sorting process, and the use of specific markers or dye solutions for labelling.

The *Magnetic-Activated Cell Sorting*, or *MACS*, can be used in a similar way to FACS for the separation of cells according to specific membrane markers. Cells are labelled with magnetic microparticles, which are covered with biodegradable polymers. Antibodies are then attached to the polymer surface of the particles. These antibodies attach afterwards to the specific receptors at the cell membrane. Unlabelled cells pass through a column, while labelled cells are retained. The retained cells can be easily eluted. This method has been proven to be successful in the separation of different cell subpopulations [Miltenyi et al. (1990)]. However, low yields and the possibly difficult detachment of the cell membrane markers when further growth is desired might be a disadvantage of this method.

Countercurrent Centrifugal Elutriation: This method combines two separation technologies, namely centrifugation, the process of sedimentation under the influence of a centrifugal force field, and counterflow elutriation, the process of separation by washing [Beckman Coulter (2007)]. Separation takes place in a rotor (see Figure 3.8) with a built-in funnel-shaped elutriation chamber (Figure 3.9).

Two opposite forces act on the cells in the chamber: centrifugal force (driving it away from the axis of rotation), and fluid velocity (driving it toward the axis of rotation, in counterflow). While the rotor is spinning in the centrifuge, a suspension of cells is pumped at a determined flow rate from outside the centrifuge into the rotor to the narrow end of the elutriation chamber. Cells move inside the chamber according to their sedimentation rates and to the point where equilibrium between the two opposite forces takes place. After increasing the flow velocity in the chamber (pump rate), small cells with low sedimentation rates move faster toward the axis of rotation (Figure 3.9). After crossing the elutriation boundary, cells will be dragged by the increasing flow velocity due to the narrowing chamber walls. These cells are washed out of the chamber into a collection vessel. Larger or denser cells

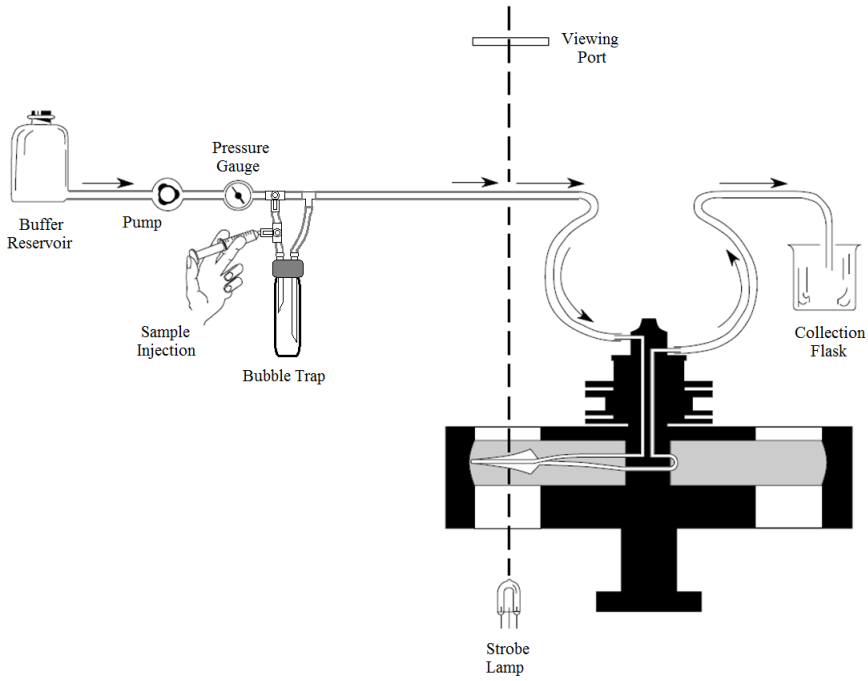

Figure 3.8: Counterflow centrifugal elutriation. Source: [Dorin (1994)]

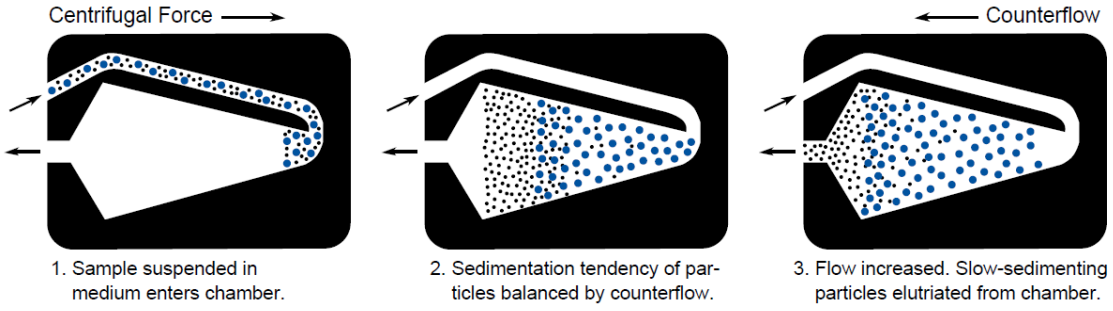

Figure 3.9: Cell separation during centrifugal elutriation. Source: [Dorin (1994)]

move through the chamber more slowly and reach a steady state somewhere else in the chamber at or before the elutriation boundary. By increasing the flow rate in gradual steps, successive fractions of increasingly large or dense cells can be washed out of the rotor and collected. Continued incremental increase of the flow rate will finally elutriate all cells from the chamber [Beckman Coulter (2007)]. The process of elutriation can be described by rearranging the Stocke's law for centrifugal gravity (see Equation 3.1). This equation expresses the settling velocities of small spherical particles in a fluid medium under influence of a centrifugal force:

$$V_{sG} = 2\frac{(\rho_p - \rho_m)R(\omega r_p)^2}{9\eta} \tag{3.1}$$

where V_{sG} is the settling velocity under centrifugal gravity, ρ_p the density of the cells, ρ_m the density of the medium, R the centrifugal radius, ω=$2\pi\frac{N}{60}$ the centrifugal velocity, r_p the particle radius, and η the medium viscosity.

In counterflow centrifugal elutriation, the forces that result in cell sedimentation in a radial direction are balanced by the velocity of fluid flowing in the opposite direction. The flow velocity at any point is equal to the flow rate (F), divided by the cross-sectional area at that point, A, (Equation 3.2).

$$V_{sG} = \frac{F}{A} \tag{3.2}$$

After this, cell separation will be influenced by following parameters:
a. The centrifugal force field in the elutriation chamber (g force).
b. The counterflow buffer stream in the elutriation chamber (counterflow velocity).
c. The size distribution of the cells in the mixture.
d. The geometry of the elutriation chamber.
e. The density of the cells and elutriation buffer.

Thus separation is the result of cells having different sedimentation velocities and being in a stationary state at different radial positions in the chamber. For ease of operation, the flow rate of the buffer and the velocity of the centrifuge have been correlated to a range of cell or particle diameters into a nomogram. The system settings can be taken out of it depending on the size of the cells to be elutriated

[Beckman Coulter (2007), Dorin (1994)].

In order to develop a protocol for cell synchronization in which cell metabolism would be minimally affected possible, this work focused only on physical methods. It was therefore the aim here to evaluate and implement a physical synchronization method which yields high numbers of synchronous AGE1.HN cells and that allows for further unperturbed growth during cultivation. Two methods were studied in this work: Temperature Reduction and Countercurrent Centrifugal Elutriation.

3.2 Materials and Methods

3.2.1 Preculture

AGE1.HN cells were precultured in 100 and 500 mL glass Erlenmeyer shake flasks (Duran Group GmbH, Germany) with working volumes of 50 and 200 mL, respectively as described in Section 2.2.2, p. 13. Cell counting and viability determination were performed by manual counting on a Neubauer Haemocytometer (Fuchs-Rosenthal).

3.2.2 Phosphate Buffered Saline, PBS

AGE1.HN cells aglommerate immediately in presence of Ca^{+2} and Mg^{+2}. For this reason, only Ca^{+2} and Mg^{+2}-free PBS was used in this work. After dilution of the components (see Table 3.1), the pH was brought to 7.3±0.1 with HCl or NaOH. Independently from the application PBS was always filtered with a pore size of 0.22 μm.

Table 3.1: Phosphate Buffered Saline formulation.

Component	[g L^{-1}]
NaCl	8.00
KCl	0.20
KH_2PO_4	0.20
$Na_2HPO_4 \cdot 7H_2O$	1.15

3.2.3 Temperature Reduction Experiments

A series of pre-experiments were carried out in shake flasks to initially analyze the effect of a temperature reduction on the cells. Cells in exponential growth were centrifuged (125 g, 5 min, Minicentrifuge, Heraeus, Germany), resuspended in fresh medium in three shake flasks ($15{\cdot}10^5$ cells mL^{-1}) and cultivated for additional 24 h. Afterwards, two of the three shake flasks were further cultivated at a reduced temperature. The third flask was used as a control (37 °C). Two temperatures were evaluated: 32 °C and 30 °C. The cell growth, cell-size distribution (Section 3.2.5, p. 57) and the percental distribution of the cells in each cell cycle phase (Section 3.2.6, p. 58) were analyzed to determine the degree of synchronization of the cells after temperature reduction. The results of these experiments were tested in a bioreactor under the assumption that cell enrichment within a specific cell-cycle phase might be incremented by the implementation of temperature reduction cycles during cultivation. Furthermore, bioreactor culture would allow for control of important culture parameters like pH and DO. Here, the bioreactor VSF2000 (see Section 2.2.4, p. 14) was inoculated with $10{\cdot}10^5$ cells mL^{-1}. The working volume was maintained at 1 L. The temperature shifts were controlled and took place 30 minutes after the setpoint was set.

Determination of Caspases as Apoptotic Indicators

Induction of apoptosis and activation of caspases can result from a variety of stimuli. Active caspases participate in a cascade of cleavage events that disable key homeostatic and repair enzymes in dying cells [Promega (2009)]. Caspase expression was studied as an indicator for apoptosis. Determination was performed with the Apo-One Homogeneous Caspase-3/7 Assay (Promega Corporation, USA). The determination was carried out as follows [Promega (2009)]:

1. Samples with certain cell numbers (10 000, 40 000 and 100 000 cells) were taken from the cultivation system, washed immediately with cold PBS (4 °C) and frozen in a constant volume of 100 μL at -80 °C.
2. The 100x concentrated substrate and buffer were thawed to room temperature and mixed by vortexing.
3. The substrate was diluted 1:100 with the buffer to obtain the desired volume of Apo-ONE Caspase-3/7 Reagent (e.g., 100 μL of 100X Substrate to 9.9 mL buffer). Reagents were stored in the dark, at 4 °C for up to 24 hours.
4. The blank was prepared with Apo-ONE Caspase-3/7 Reagent and cells that had

not experienced any temperature shift. The assay was carried out with Apo-ONE Caspase-3/7 Reagent and the treated cells.
5. The Apo-ONE Caspase-3/7 reagent was added to each well of a 96 multiwell plate which contained blank and assay samples. Mixing by pipetting was avoided due to bubble formation. Instead, mixing was performed using a plate shaker (400 rpm, 30 s, Titramax, Heidolph Instruments GmbH, Germany).
6. The samples were incubated for 18 hours at room temperature. The incubation time was selected according to the maximum time recommended by the manufacturer.
7. Fluorescence measurement was performed on a Fluorescent Plate Reader (Victor, Perkin Elmer Inc., USA). The optimal excitation wavelength for detection was 499 nm with emission maximum at a wavelength of 521 nm.

3.2.4 Countercurrent Centrifugal Elutriation

An Avanti Centrifuge with JE 5.0 Rotor was used for elutriation experiments (Beckman Coulter, USA). First, a cleaning procedure of the equipment was performed as described by the manufacturer [Beckman Coulter (2007)]. For equipment operation, setting of an elutriator and troubleshooting, detailed protocols can be found in literature [Balfavi (2008), Beckman Coulter (2007), Dorin (1994)]. The preparation consisted mainly of changing silicone tubings, disassembling and cleaning the elutriation chamber, and cleaning and greasing O-rings. A slight modification of the synchronization protocol presented by Balfavi was used in this work, which consisted in injecting the cells just before the elutriation chamber and not before the mixing and bubble-trap tube (see Figures 3.8 and 3.10). This was done in order to avoid long residence times of the cells in the tubing and bubble-trap tube before reaching the elutriation chamber. The procedure for elutriation employed in this work is described as follows:

Equipment Preparation and Desinfection
1. The silicon tubings for inlet and outlet were connected to the system. The tube inner diameter was chosen to be as small as possible to avoid void spaces and cell sedimentation at low pump rates, which was observed during initial experiments. In order to avoid microbial contamination, silicone components and fittings were sterilized in autoclave prior to work. Although the elutriation chamber can be autoclaved, desinfection was preferred.

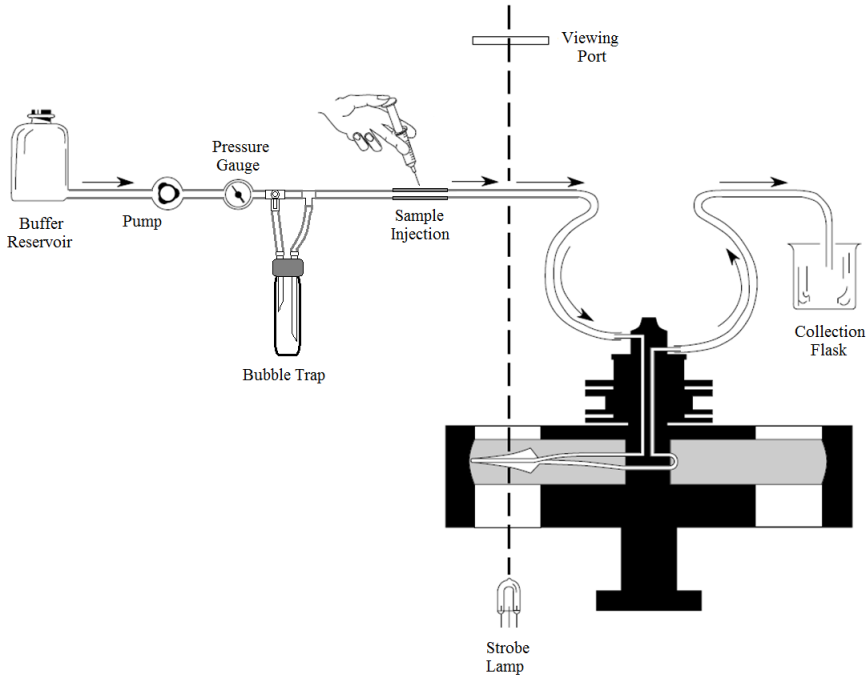

Figure 3.10: Elutriation process with injection of cells after bubble trap. Modified from [Dorin (1994), Balfavi (2008)]

2. A pulse free peristaltic pump was employed (8 rollers, medorex e.K., Germany). During previous elutriation experiments a very clear pulsing of the cell front in the elutriation chamber was observed while using a 2-roller peristaltic pump. This led to a reduction in synchrony of the collected fractions (discussed in Section 3.3.5, p. 79 in Results and Discussion).

3. The peristaltic pump was calibrated according to the tubing employed (TPE Pharmed®, Carl Roth, Germany).

4. After assembling of the system, the whole elutriation pathway (tubings, elutriation chamber) was desinfected with a 2 % v/v NaOCl solution (in ddH_2O, Carl Roth, Germany) for 30 min followed by 70 % ethanol for 2 h. After each cleaning step the system was rinsed with ca. 200 mL of sterile water or PBS.

5. A bottle containing enough PBS was connected to the inlet tubing. Ca. 2 L of PBS were needed for elutriating 10 fractions of a same population.

6. PBS was pumped through the system to eliminate all bubbles that might have remained inside. Shaking and turning the elutriation chamber up- and downwards might be necessary, since the presence of air in the system, especially inside the elutriation chamber, affects the elutriation process. The bubble trap must have a determined level of PBS for ensuring a bubble-free flow into the elutriator.

Elutriation

7. The peristaltic pump was set to its initial value according to the Rotor-Speed vs Flow-Rate nomogram or to the Flow Rate (F) value calculated from Equation 3.2. The centrifugation speed for elutriation was set constant for all experiments at 1800 rpm.

8. 3 - 5·10^6 cells were centrifuged (125 g, 5 min), resuspended in 3 - 5 mL PBS and drawn from the centrifuge tube into a sterile syringe.

9. The pump was turned off and the cell suspension was injected into the system through the silicon tubing. Unlike Balfavi [Balfavi (2008)] the cell suspension was not injected before the bubble trap (or sample mixing tube) in order to avoid long residence times of the cells before reaching the elutriation chamber.

10. After having finished injection of the cells the previously calibrated peristaltic pump was turned on.

11. Two parameters indicate the successful introduction of the cells to the system. First, the formation of a cell front at the elutriation boundary inside the separation chamber without significant loss of cells, identified in the waste bottle. Second, the absence of cell pellet at the radial farthest point of the separation chamber (chamber inlet).

12. After 1 minute the pump rate was increased in order to elute the first cell fraction. The intervals for increasing the pump rate during an elutriation process were set between 4 and 6 mL min^{-1}. This value depends on the desired cell number to be collected and on the expected synchrony degree. The smaller the increase of the pump rate, the higher will be the synchrony of the fraction, but the lower the cell number collected in the fraction tubes. The increase in the pump rate was done manually at around 2 - 3 mL min^{-2}.

13. At the point of fraction collection (tube outlet inside the clean bench) the height of the silicon tubing was kept as constant as possible in order to avoid variation in the pressure drop through the system. This would decrease the synchrony degree of the elutriated fractions.

14. After each increase of the pump rate 100 - 150 mL were collected in sterile plastic tubes.

15. A sample was taken from each fraction for cell count on the microscope, cell size measurement (see Section 3.2.5, p. 57) and cell cycle analysis (see Section 3.2.6, p. 58).

16. The fractions were centrifuged, resuspended in 10 - 20 mL culture medium, and kept on a rocking platform at room temperature to avoid cell sedimentation and agglomeration.

17. Before inoculation of a bioreactor, the cell mean diameter of the different fractions (see Section 3.2.5, p. 58) was determined as proof for a successful elutriation procedure.
18. After finishing an elutriation run, the agitation speed of the system was set to 0 rpm and the pump rate was increased to a maximum value of 80 - 100 mL min^{-1} for at least 1 minute to wash the remaining cells out of the elutriation chamber.
19. After use, the elutriator was desinfected as described above.

3.2.5 Cell Size Distribution

The determination of the cell size distribution of a cell population was performed in a particle counter (Z2, Beckman Coulter, USA) as it has been shown in literature to be a suitable method for cell size assessment [Anderson and Petersen (1967)]. In this equipment, the electrical resistance of a particle passing through a small aperture in a conductive liquid is measured and related to the size of the particle. The number of pulses relates to the particle count, while the amplitude of the electrical pulse depends on the particle's volume. Complete information about the principle and operation of this equipment can be found elsewhere [Beckman Coulter (1992-2002)].

Equipment Preparation, Calibration and Desinfection
1. Following settings were used for particle measurements: Capillary Aperture Diameter: 100 μm, Metered Volume: 0.5 mL, Repetitions: 3, Lower Particle Diameter: 6 μm, Higher Particle Diameter: 21 μm.
2. The system was calibrated with a calibration standard based on latex particles (Mean Particle Diameter: 10.37 μm, BS Partikel, Germany). The obtained calibration constant after every calibration remained in the range of 57.6 - 58.0 % of the capillar's aperture diameter (100 μm).
3. The equipment was cleaned by performing 3 measurements with the capillary tube submerged in hot (60±10 °C) 2 % NaOCl. After cleaning, the system was filled with fresh diluent (PBS).

Cell Size Measurement and Analysis
4. For measurement, 9.9 mL PBS and 0.1 mL of the cell suspension were pipetted into the cuvette. The cuvette was shaken by hand.
5. As far as this was possible, the measured data were transferred to a computer for further analysis via a serial port.
6. The cell (particle) count was normalized ($w_{i,norm}$) by dividing the cell count w_i

at each diameter $d_{p,i}$ by the total cell count (see Equation 3.3).

$$w_{i,norm} = \frac{w_i}{\sum w_i} \tag{3.3}$$

7. The normalized particle count data were smoothed by averaging every five immediately neighboring values in the data list.
8. From the smoothed data list, the maximum normalized-count value and its corresponding particle diameter were determined using the funtion "=MATCH()" (German "=VERGLEICH()") in Excel (Microsoft Corp, USA).

3.2.6 Analysis of the Cell Cycle

Cell Fixation
The procedure for cell fixation and PI staining was adapted from Riccardi and Nicoletti [Riccardi and Nicoletti (2006)]:
1. 1 - 2·10^6 cells were centrifuged (125 g, 5 min) in an Eppendorf tube and resuspended in 1 mL cold PBS (see Section 3.2.2, p. 52, for PBS preparation).
2. The suspension was centrifuged again (125 g, 5 min). The cell pellet was thoroughly resuspended in 288 μL PBS.
3. 712 μL ice cold 96 % ethanol were added to the sample followed by continuous pipetting to avoid the formation of cell agglomerates. After mixing, the sample was vortexed (ca. 600 rpm) for 10 seconds.
4. The samples were stored for maximum of 4 months at -20 °C.

Propidium Iodide Staining.
5. The sample tube was vortexed and then centrifuged at 400g for 5 minutes.
6. The cell pellet was washed once in 1.5 mL PBS.
7. After centrifugation (125 g, 5 min), the cells were thoroughly resuspended (pipetting + vortexing) in 480 μL PBS.
8. 10 μL RNAse (20 mg/mL, Invitrogen Cat.Nr.-12091-021, Lot.1004817) were added to the cell suspension. The samples were vortexed. For DNAse-free RNAse, put the RNAse containing tube into hot (almost boiling) water for 5 Minutes.
9. The cells were left for incubation for 30 minutes.
10. 10 μL propidium iodide solution (2 mg mL^{-1}, Carl Roth, Germany) were added after incubation. The samples were vortexed and stored in the dark for ca. 10 minutes until analysis.

Flow Cytometry.
In flow cytometry, light is directed to the sample and scattered in the forward direction, typically up to 20° offset from the laser beam's axis. This scattered light is collected by a lens known as the Forward Scatter Channel (FSC). The FSC intensity roughly equates to the particle's size and can also be used to distinguish between cellular debris and living cells. Light measured approximately at a 90° angle to the excitation line is called side scatter. The Side Scatter Channel (SSC) provides information about the granular content within a particle. Both FSC and SSC are unique for every particle. More information about flow cytometry can be found elsewhere [Rahman (2006), W.T. Shearer H.W. Schroeder A.J. Frew R.R. Rich and JR. (2008), Moo-Young (2011)].

11. The samples were analyzed by Flow Cytometry. Samples obtained from the temperature reduction experiments were analyzed in an Epics XL-MCL Flow Cytometer[7](Beckman Coulter, USA), Analysis Software: WinCycle (Phoenix Flow Systems, USA). All other samples were analyzed in a LSR II Flow Cytometer[8], Analysis Software: FACS Diva v6.13 (BD Biosciences, USA).
12. The region of the cell population of interest was gated. This means, that the

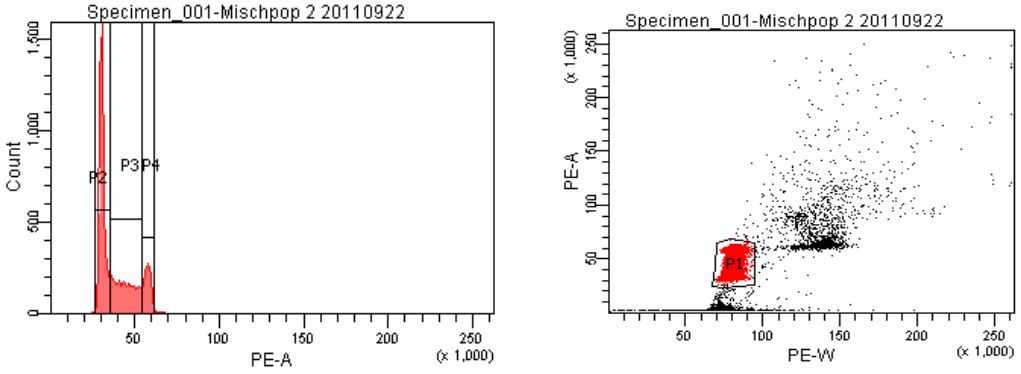

Figure 3.11: Left: Forward Scatter Channel (FSC) signal vs Particle Count (here PE-A vs Count), P2 = G_1 phase, P3 = S phase, P4 = G_2/M; Right: Side Scatter Channel (SSC) signal vs Forward Scatter Channel (FSC) signal (here PE-W vs PE-A). The red area represents the gated cell population. The black dots correspond to cell debris (bottom) and agglomerates (right). Analysis Software: FACS Diva v6.13 (BD Biosciences, USA).

[7]with kind support from D. Landgrebe, C. Kasper and T. Scheper, Institute for Technical Chemistry (TCI), Leibniz University Hannover, Hannover, Germany.
[8]with kind support from A. Carambia, J. Herkel and A. Lohse at University Medical Center Hamburg-Eppendorf, Hamburg, Germany.

region of analysis was delimited only for cells, excluding debris and agglomerates. A non-synchronous cell population was used for this purpose. Two main diagrams were needed: one displaying the signal of forward scatter channel (FSC) of the sample against the particle count (see Figure 3.11, left); the second displaying the signal of the side scatter channel (SSC) against FSC (see Figure 3.11, right). The former diagram speaks for the count and the intensity (or size) of the propidium iodide stained cells. The latter correlates the intensity of the particles (size) to its form. This gate was not modified within an experiment, unless the cell number in the sample had varied significantly. A variation of the cell number in the sample leads to a signal displacement, which has to be corrected by redefining the region of analysis.

3.2.7 High Cell Density Culture

A dialysis bioreactor (Bioengineering AG, Switzerland) was used for culture scale-up with synchronous cells. This bioreactor consists of an inner chamber (culture chamber) and an outer chamber (dialysis chamber), both displayed in Figure 3.12. The culture chamber is built-in inside the dialysis chamber and is separated from the medium by a transparent non-porous dialysis membrane made of regenerated cellulose (Cuprophan, cut-off = 10 kDa) which is at the same time the culture chamber's wall. Toxic metabolites of low molecular weight can be removed from the culture chamber through the dialysis membrane. Cells and high-molecular-weight products are retained inside the culture chamber. Hence, the use of a dialysis process allows for a longer exponential cell growth as well as for high cell density and higher productivity during cultivation [Märkl et al. (1989), Pörtner and Märkl (1998)].

The culture chamber of the dialysis bioreactor is geometrically similar to the bioreator VSF2000 (6-RT) described in Section 2.2.4, p. 14. For this reason, the culture conditions in the inner chamber were set according to the process windows for comparability obtained in the last chapter ($N = 210\,\mathrm{rpm}$). pH and DO measurements were done in both chambers, but actuator response for both parameters (base addition and aeration) took place only in the outer chamber. DO control in the culture chamber was done by means of a cascade controller actuating in the outer chamber ($N = 300\text{ - }1300\,\mathrm{rpm} \longleftrightarrow \mathrm{Air} = 5\text{ - }240\,\mathrm{mL\,min^{-1}} \longleftrightarrow \mathrm{Air/O_2}$ ratio).
The dialysis process prevents the culture from reaching substrate limiting values in a relatively short time period, as it happens commonly in batch culture. In this way, dialysis culture was employed to study the number of synchronous divisions of the cultured subpopulation.

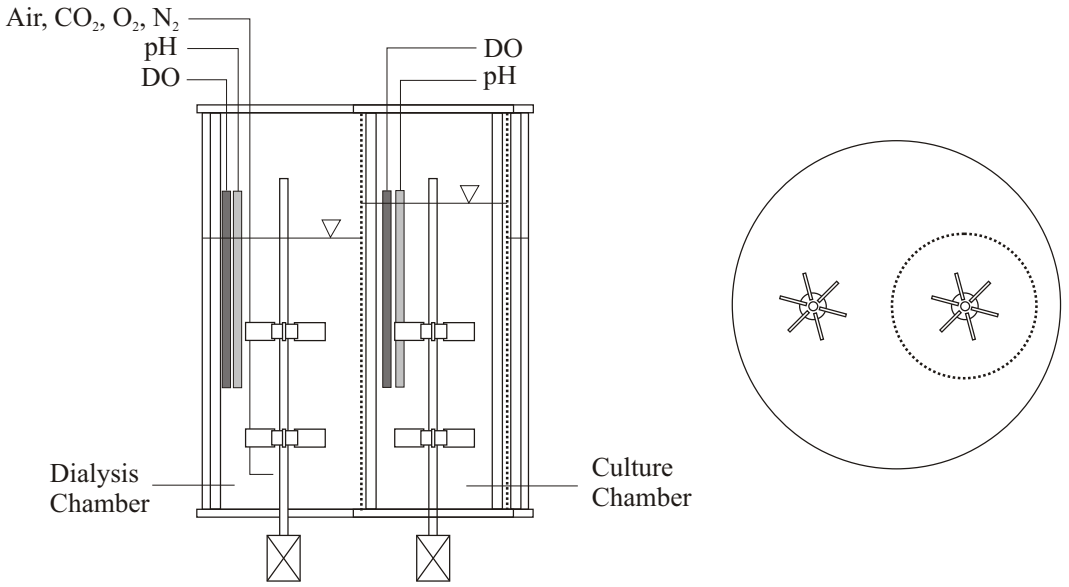

Figure 3.12: Dialysis Bioreactor (Bioengineering AG, Switzerland). The culture chamber is built-in inside the dialysis chamber and is separated from the medium by a transparent non-porous dialysis membrane which is at the same time the culture chamber's wall. Toxic metabolites of low molecular weight can be removed from the culture chamber through the dialysis membrane. Cells and high-molecular-weight products are retained inside the culture chamber. This allows for a longer exponential cell growth as well as for high cell density and higher productivity during cultivation (Modified from [Pörtner and Märkl (1998)].)

For the inoculation of this system elutriation cycles were performed. Immediately after each elutriation, cell subpopulations were centrifuged and resuspended in fresh culture medium. The tubes with the resuspended cells were put onto a rocking platform at room temperature (ca. 22 °C) for keeping cells in suspension with low growth rates until inoculation.

The range of pump rates used for collection of determined subpopulations was set depending on the number of cells to be collected. In case of the dialysis bioreactor, a wider pump velocity range was used in order to reach the desired cell number for inoculation (800 mL, $9{\cdot}10^5$ cells mL^{-1}).

3.2.8 In-situ Microscopy

Cell count was further assessed in one experiment with an *in situ* microscope system (ISM)[9]. The system (see Figure 3.13) consists of two autoclavable tubes with lenses at the tip; one tube has a smaller diameter and can be placed inside the other one. In doing so, the remaining small space between both lenses forms a chamber. At chamber's height, two tube ports for connection of pump tubing allow for culture inlet and outlet. Culture conveyance to the microscope and back into the bioreactor is done by a peristaltic pump (here 10 mL min^{-1}). O-rings between all components keep sterility in the chamber during culture flow. A digital camera (XCD-SX 910, Sony, Japan) with a large objective is mounted into the inner tube. The separation between lenses can be adjusted and calibrated with a motor integrated in the system, and the object can be focused by a second motor to which the camera is attached. A high intensity light-emitting diode (LED) is used as a light source, which is set beneath the microscope lens. Images can be taken at user-defined intervals and be analyzed afterwards by an image analysis software. A detailed description of this system and its applications can be found elsewhere [Prediger et al. (2011)].

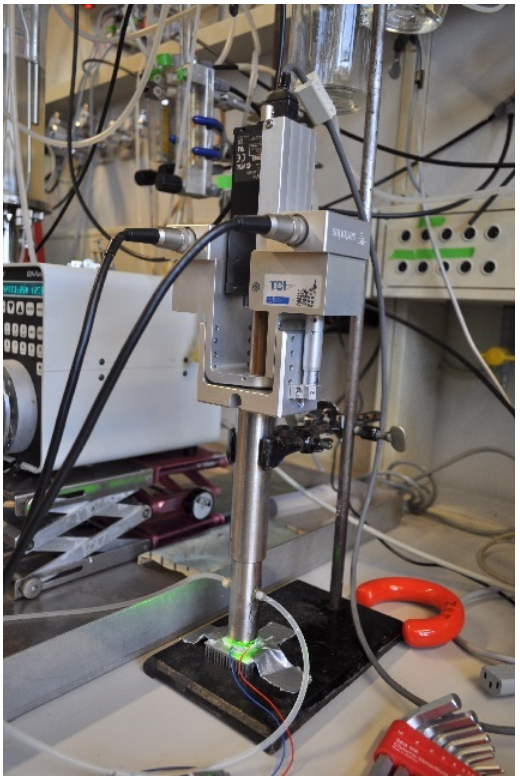

Figure 3.13: In-situ microscope for continuous culture monitoring of cell density.

[9]kindly supplied by A. Babitzky and T. Scheper, Institute of Technical Chemistry, Leibniz University Hanover, Hanover, Germany.

3.3 Results and Discussion

3.3.1 Temperature Reduction in Shake Flasks

All cultures were run in parallel with a 24 h preculture at 37 °C, after which the temperature was reduced to 30 and 32 °C, respectively with corresponding references at 37 °C. Figure 3.14 shows the growth curves of six different shake flasks. The left side of the column (A, B, C) shows the experiments carried out at 32 °C while the right side (D, E, F) represents those carried at 30 °C.

Both control shake flasks (A and D) showed normal exponential growth during further cultivation after splitting, whereas there is a clear reduction in the growth rate of the cells in the flasks cultivated at lower temperatures. One of the flasks (B) remained at 32 °C for 142 h and showed no effect on cell viability, even after a 2:3 split of the cells. This dilution of the culture was performed so as to avoid reaching the end of exponential growth (set for these experiments at a maximum of $35{\cdot}10^5$ cells mL^{-1}), and not because of any other limiting values (e.g. Glc, Gln). Only after resetting the temperature of the flask to 37 °C, the viability did fall drastically to 70 %.

A similar case was observed for the flasks at 30 °C (E and F), in which almost no cell growth was observed at this temperature. In both flasks, the viability dropped after both medium exchange and temperature resumption. Sampling was performed in a more frequent manner from shake flask F so as to observe any possible synchronous growth. In this flask, the cell density remained constant during the first hours after resumption to 37 °C, which is to be expected after synchronization in the G_1 phase. However, no cell division was observed after more than 72 hours (common doubling time of AGE1.HN cells $t_d = 40$ h).

Thus, in general, the growth curves didn't point to a synchronous growth of the cell populations; on the other hand, variations in the size distribution and in the DNA content of the cells can be observed (see Figures 3.15 and 3.16 respectively). Compared to the reference flasks, the size distribution of the cell population shows a dynamic behavior after temperature reduction. All flask experiments performed at 30 °C showed a slight displacement of the cell diameter 20 hours after the temperature reduction (Figure 3.15.E, F). This displacement increased further to almost 2 μm from ca. 14 to 16 μm after 100 h of treatment (black symbols). Especially in flask F

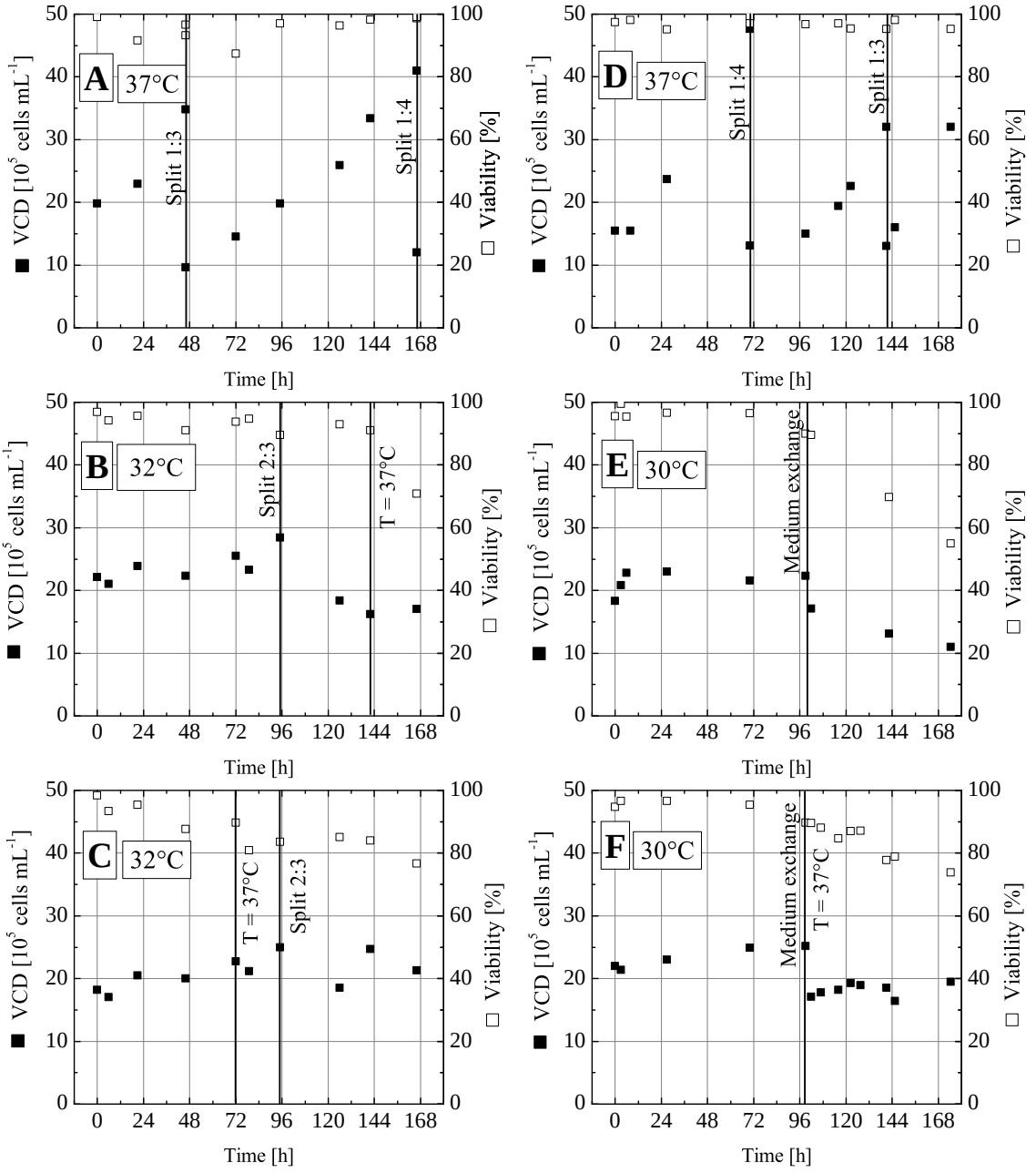

Figure 3.14: Growth of AGE1.HN cells in shake flasks after temperature reduction. A, D: reference flasks at 37 °C; B, C: 32 °C; E, F: 30 °C.

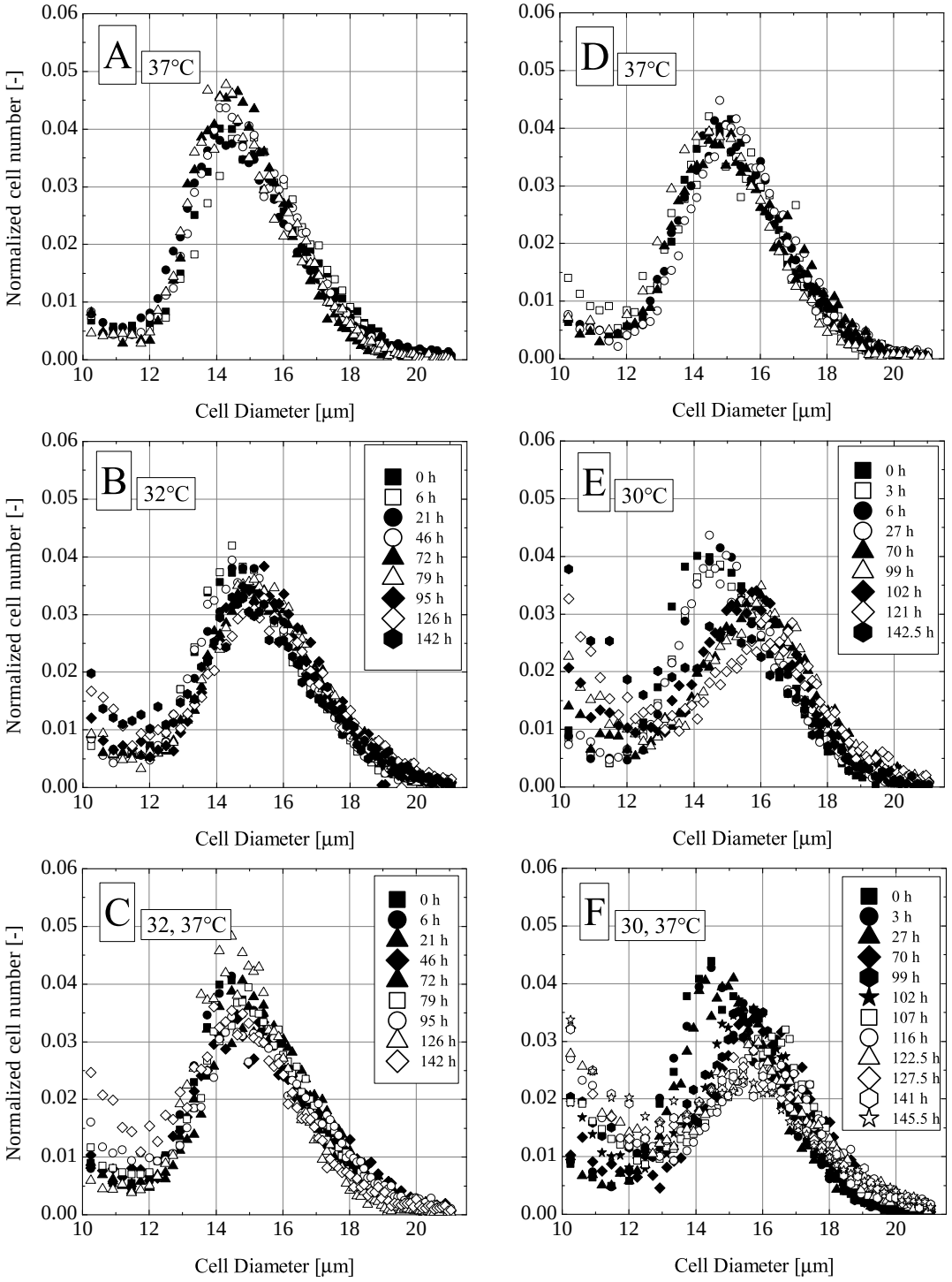

Figure 3.15: Mean cell size distribution curves in the temperature reduction experiments in shake flasks. A, D: reference flasks at 37 °C; B, C: 32 °C; E, F: 30 °C. Black and white symbols are used here undistinguishly. In flasks C and F, the black symbols belong to the reduced temperature period, whereas white symbols represent data after resetting temperature to 37 °C.

(Figure 3.15.F), a reduction in the normalized cell number can be seen at $d_{p,i} = 16\,\mu$m and a simultaneous increase in the normalized cell number at $d_{p,i} = 10\,\mu$m after resetting the temperature to 37 °C. This would point to the division of one part of the cell population, which was only slightly observed in the manual cell countings (see Figure 3.14.F). The increase in the cell diameter of the cell population after temperature reduction might support Enninga et al.'s statement about cell growth at lower temperatures. At the moment of temperature reduction, cells in the G_1 phase will be arrested. On the other hand, those cells which have left the G_1 phase will continue through the whole cell cycle until they divide [Enninga et al. (1984)]. This increase of the normalized cell number in Figure 3.15.F might be, thus, the sum of newly divided cells and cell debris originated during cell disruption after viability decreases.

As expected, the reduction of the cultivation temperature had a clear effect on the distribution of the cell cycle phases in the cell population [Enninga et al. (1984), Moore et al. (1997)]. While the cell cycle phase distribution of a heterogeneous exponential growing AGE1.HN cell population presents an average distribution of $G_1 = 55$ - $60\,\%$, $S = 30$ - $35\,\%$ and $G_{2/M} = 10$ - $15\,\%$, these values changed after temperature reduction, as shown in Figure 3.16. In this Figure the S phase is presented as the indicator for accumulation of cells after temperature reduction, which might not match cell accumulation data in the G_1 phase as reported by Enninga et al. and Moore et al. [Enninga et al. (1984), Moore et al. (1997)]. This analysis of the DNA distribution result might lie in the algorithm employed for cell cycle analysis (Synchronization Module, Wincycle, DB Biosciences), which considered the accumulation of cells at the end of G_1 as a part of the S phase. Knowing this, the results can be further used for indication of cell arrest and accumulation.

According to our results a maximum of 50 - 60 % of the cells will accumulate in the S phase after 72 hours when the temperature is reduced to 32 °C, while 80 % of the cells will accumulate in this phase after 100 hours, when the temperature is reduced to 30 °C. This increase of 50 % synchrony is congruent with the maximum accumulation of cells in the G_1 phase reported by Moore et al., where the percentage of cells in G_1 phase varied from 50 to 90 % after 4 days at 30 °C.

3.3.2 Temperature Reduction Cycles in Bioreactor

The results of the shake flask experiments (Section 3.3.1, p. 63) pointed to the feasibility of cell enrichment in the S phase using short temperature reduction periods

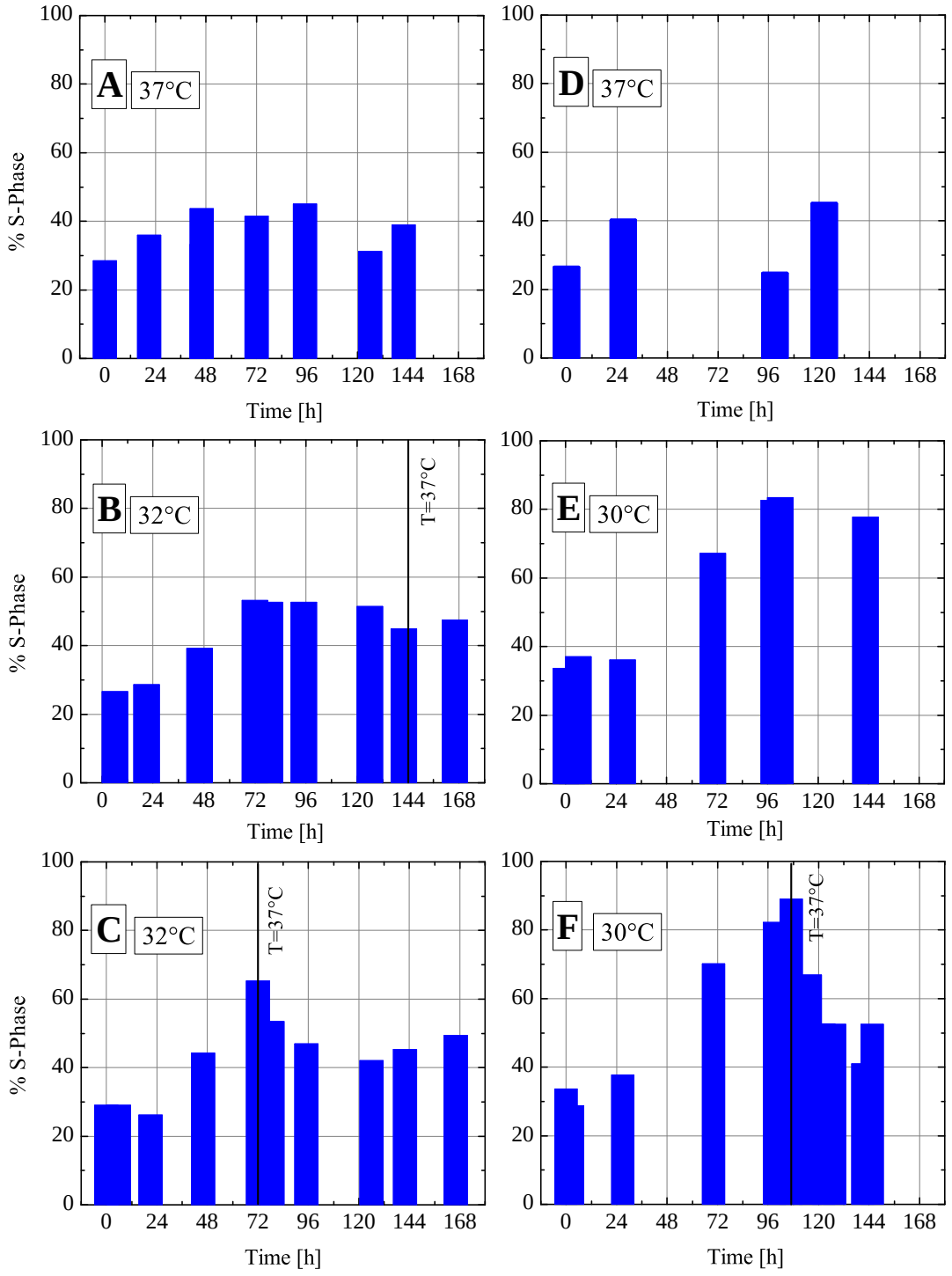

Figure 3.16: Fraction of cells in the S phase after temperature reduction. A, D: reference flasks at 37 °C; B, C: 32 °C; E, F: 30 °C.

between 48 - 72 h. Longer periods, however, might cause reduction in cell viability after temperature resumption (37 °C). Hence, temperature reduction cycles during culture in bioreactor (VSF2000) were planed at 30 °C in order to keep cell growth at a minimum value, while achieving a rapid accumulation of cells in the S phase. The cell growth curve and the distributions of cell cycle phases and mean cell diameter are shown in Figure 3.17.

During the first temperature reduction cycle of 48 hours, cell growth was clearly slowed down (Figure 3.17.A). Accumulation of cells in the S phase can be observed, coupled with a large increase in the mean cell diameter (Figure 3.17.B, C), as observed during shake flask experiments. After resetting the temperature to 37 °C, cells grew with a growth rate of $\mu = 0.55$ d^{-1} (Coulter data) and $\mu = 0.48$ d^{-1} (manual count). These values are higher than the expected μ_{max} value for bioreactors under previously used conditions (0.43 d^{-1})[10]. This increased growth rate might have taken place due to the cells in the G_2/M phase, who may have commited to cell division at the time of temperature shift. Probably, cells continued this process at a very low rate, until the temperature was reset to 37 °C. The steep increase of the mean cell diameter X_{w_i} during temperature reduction might confirm this finding (see Figure 3.17.C). Afterwards the culture remained for a very short period (ca. 18 h) at 37 °C, until it was split and a new temperature reduction cycle was started.

During this second period at 30 °C, cell growth didn't seem to be arrested, shown by an increase in cell density. There is again a slight increase in the percentage of S as well as of G_2/M cells, and an increase of the mean cell diameter of cells in culture. These changes are more noticeable at the end of this cycle (ca. 60 h at 30 °C), where the percentage of S phase cells is further reduced and cells accumulate in the G_2/M phase (20 % accumulation) coupled with an increase in mean cell diameter in ca. 0.5 μm. Due to the cell density reached at this point, the culture was splited at 1:2, since at a cell density of ca. $25{\cdot}10^5$ cells mL^{-1} a complete doubling of the cell population might not be possible; this means, that in case of synchrony no complete division could have been observed.

The third temperature reduction cycle was carried out at 28 °C. This temperature reduced culture growth to a minimum. Furthermore, the accumulation of cells in the S phase as well as the change in X_w of the cell population took place in a slower

[10] this is a common μ_{max} value in the VSF2000 bioreactor with a 4-pitch-blade turbine according to the results presented in Section 2.3.1, p. 26.

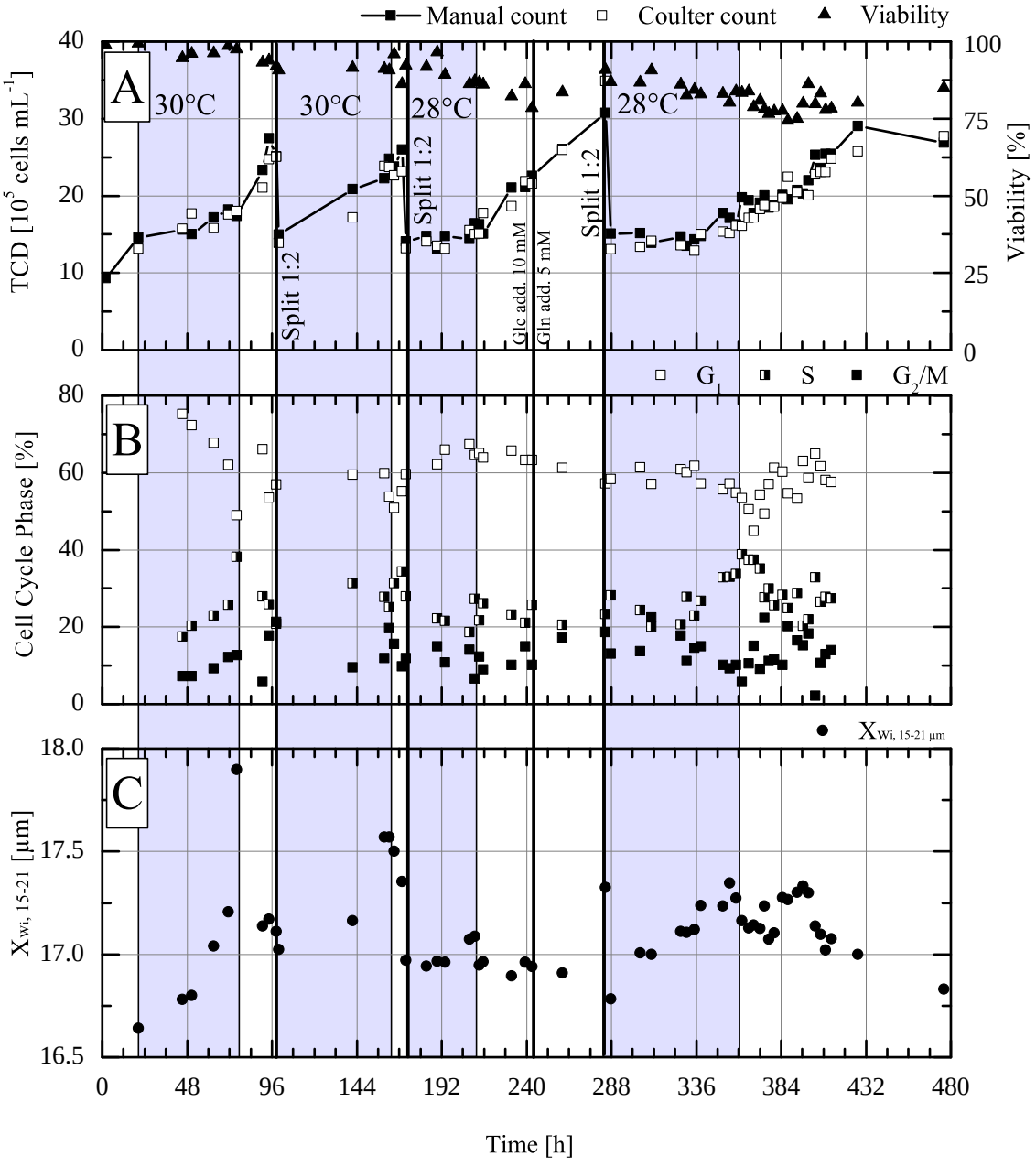

Figure 3.17: Cell growth (A), cell cycle phase (B) and cell size (C) distributions of AGE1.HN cells during temperature reduction cycles in bioreactor culture. The light-blue backgrounds represent the temperature reduction cycles. The bold lines indicate the dilution (split) of the culture or addition of nutrients.

manner. Due to a decrease in the culture viability, this cycle was stopped and the temperature was reset to 37 °C. At the moment of temperature resumption, cells grew almost normally in the bioreactor. However, viability had dropped to values around 85 % during temperature reduction and remained at this level for the next 30 h at 37 °C. After 240 h of culture, glucose and glutamine (10 mM and 5 mM respectively) were added to the culture to avoid limitations of these two components during the growth phase of the cells. The culture was split in a 1:2 ratio after 40 h and the last temperature reduction cycle was started. This cycle lasted ca. 50 hours. As the temperature was reset to 37 °C, an abrupt decrease of the culture viability took place during the next 24 h.

Further cell growth with recovery of the culture viability took place with no further visible signs of synchrony in culture according to the cell counts, which were performed every 4 hours. However, an accumulation of the cells in the S phase until 40 % and an increase in X_w of 0.75 μm could be reached during this last cycle.

3.3.3 Determination of Caspases as Apoptosis Indicators

Temperature reduction might be due to the easiness of the method, a suitable possibility for enrichment of a whole cell culture in a specific phase of the cell cycle. However, temperature reduction might inactivate or activate other metabolic pathways and gene expression, like caspase expression, which might bring noise into further metabolic studies performed with the cells.

During shake flasks experiments as well as during bioreactor culture, the viability of the cultures dropped after temperature resumption during all treatments, but not before. In order to assess for the possibility of caspase expression as indicator of cellular apoptosis, a second bioreactor cultivation was carried out at 28 °C. Sampling was performed once per day for caspase determination. Figure 3.18 shows the increase in the fluorescence intensity of the samples versus time at 28 °C as an indicator for caspase expression.

According to the figure, the reason for the decrease in viability of the cultures might be the immediate expression of caspases after temperature reduction. This experiment might also show, that other cell metabolic pathways can be affected during temperature reduction experiments, as it might happen during the treatment of the culture with chemicals.

The reduction in temperature during cultivation has proved to be a successful way to enrich cells in a determined phase of the cell cycle. As a whole-culture method for cell synchronization, temperature reduction can account for high yields of synchronous cells depending on the scale of the culture system. However, sufficient synchrony yields can only be achieved by longer periods at reduced temperature or by means of repeated temperature cycles, which might affect cell viability and induce cell death. This method would be applicable while studying temperature dependent reactions, which occur in production cell lines at the time of temperature shift for monoclonal antibody production.

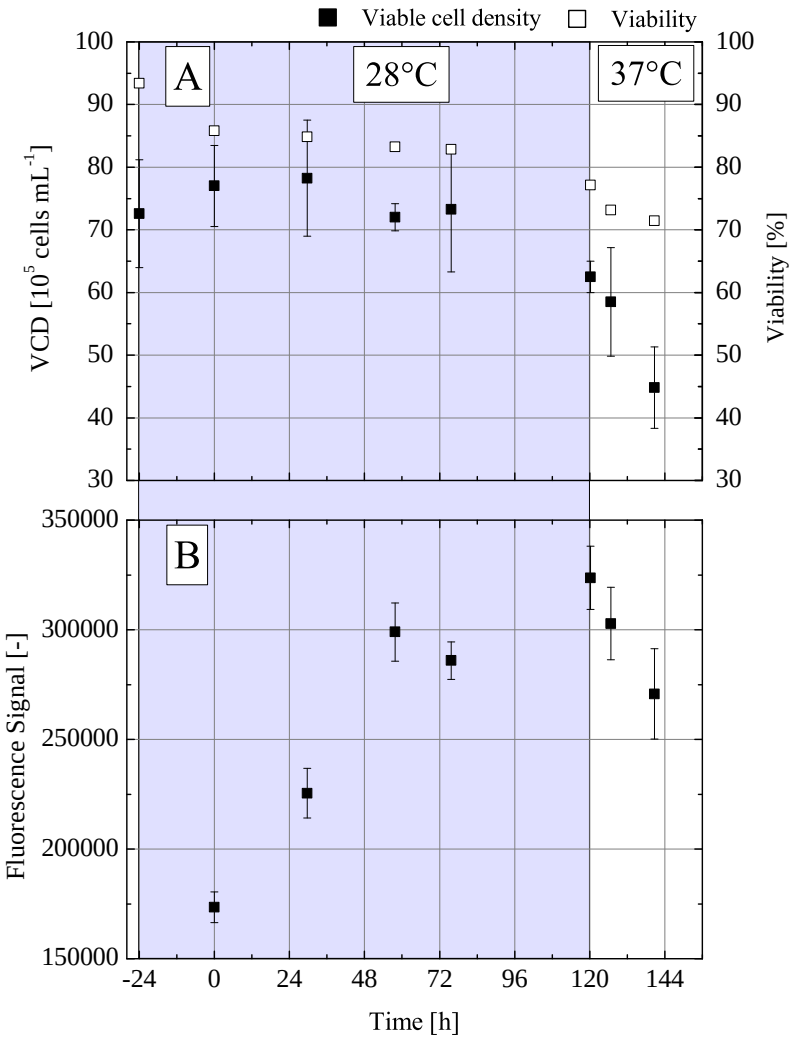

Figure 3.18: A: Viable cell density and viability during bioreactor cultivation of AGE1.HN cells at reduced temperature. The light-blue background indicates temperature reduction to 28 °C. B: Fluorescence signal of bioreactor samples for caspase determination as indicator for apoptosis.

3.3.4 Countercurrent Centrifugal Elutriation

A first elutriation experiment was carried out[11] with an initial cell number of $5{\cdot}10^8$ cells. Cells were centrifuged, resuspended in PBS and introduced via a syringe into the elutriator's silicone tubing (see Figure 3.10). The rotation speed used was 1800 rpm. The initial pump rate was set to $4\,\mathrm{mL\,min^{-1}}$. Around 100 mL cell suspension were collected after every increase of the pump rate. A total of 9 subpopulations was collected. As a first indicator of synchrony in these subpopulations, the cell size distribution was immediately assessed. The results are shown in Figure 3.19. Due to the similarity in their mean cell diameter, subpopulations 4 and 5 were poured together for further experiments and will be shown in the results as subpopulation 4,5. Table 3.2 summarizes the characteristics of the subpopulations collected during the first elutriation experiment. A very clear variation in the distribution of

Table 3.2: Cell cycle phases and cell size distribution of the subpopulations obtained from a first elutriation experiment.

Subpopulation[a]	G_1 [%]	S [%]	G_2/M [%]	Cells collected [10^6 cells]	X_w [μm]	s_w [μm]
Async. pop.	65.8	19.0	15.2	500.0	14.65	1.71
1	78.4	7.1	14.5	30.1	13.93	1.88
2	83.4	10.5	6.1	48.7	14.80	1.73
3	80.6	11.9	7.5	49.0	15.17	1.80
4,5	66.8	25.5	7.7	44.4	15.26	1.82
6	54.3	35.1	10.7	46.2	15.46	1.90
7	26.9	50.6	22.5	57.0	15.73	2.06
8	7.4	26.2	66.3	56.9	15.61	2.29
9	22.9	25.3	51.8	38.0	15.58	2.37

[a] The pump rate was set in this experiment according to experience values with a non-calibrated pump. For this reason, no indication of the pump rate was done.

the cell cycle phases and of the mean cell diameter (X_w) can be seen compared to an asynchronous cell population (first row, Async. pop.), where the first elutriated subpopulations correspond to those with smaller X_w and therefore, with the higher percentage values in G_1. As the subpopulation number increases, the percentage values of the S and G_2/M phases become more relevant. The higher these values are, the higher are their expected X_w. Visual differences in mean cell diameter of the subpopulations are depicted in Figure 3.19, whereas Table 3.2 shows as well the standard deviation (s_w) during the calculation of X_w. The s_w values are high and speak for a low selectivity of the cells during experimentation. The reasons for low

[11] with kind support of R. Hass. Clinic for Gynecology and Obstetrics, Hannover Medical School, Hannover, Germany

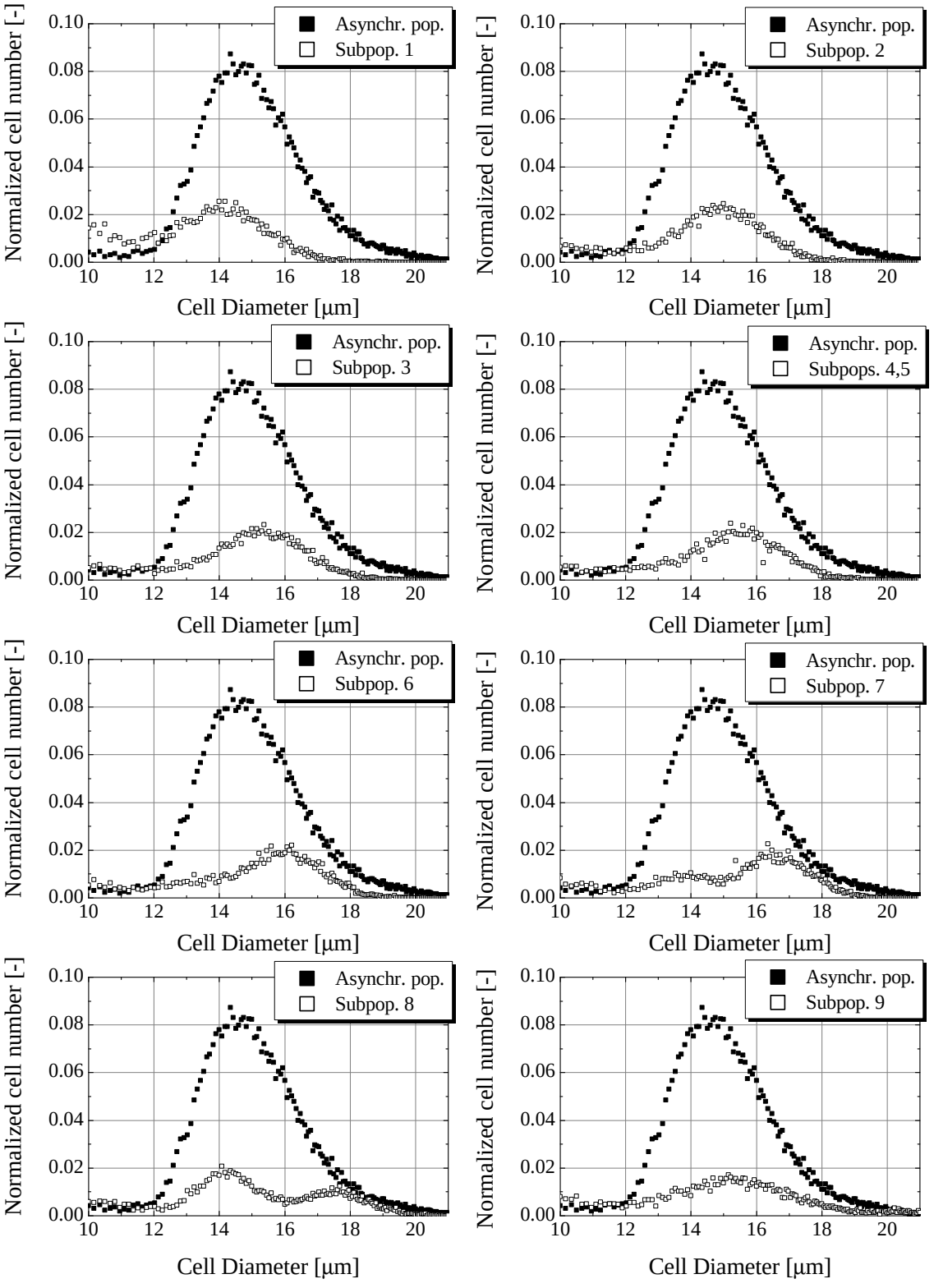

Figure 3.19: Cell size distribution of AGE1.HN subpopulations after a first elutriation experiment.

selectivity and the corresponding troubleshooting are discussed later.

The 8 subpopulations were further cultivated in shaken systems (500 mL, 100 mL shake flasks or 50 mL plastic tube with filter cap). The size and volume of the culture flask depended on the number of cells contained in the subpopulation. The growth curves are depicted in Figure 3.20. The first cell count value (t = 0 h) corresponds to the calculated inoculation cell density value after sampling of the subpopulation during elutriation. After the second sample (t = 13 h), the cell density was lower in almost all flasks. This might be due to a deviation in the counting procedure after elutration and to the time cells were exposed to different conditions. Due to this fact, the initial cell density didn't allow for immediate exponential growth in most flasks and cells entered into a longer lag-phase. This was not the case for the subpopulations 7 and 8, where the cells divided after 48 h and again after 96 h. The increase of the doubling time (ca. 48 h) in contrast to the common doubling time of AGE1.HN in exponential growth ($t_d = 40$ h) might be explained by the intermittent sampling (every 4 - 6 hours) performed during the experiment, which might have led to repeated temperature reduction in the flasks.

The cell size as well as the cell cycle phase distributions of the subpopulations during cultivation are shown in Figures 3.21 und 3.22. Due to the low volume of culture flasks 1, 6, 7 and 9, it was not possible to assess their DNA content for each sample. For this reason, only four representative cultures are displayed in Figure 3.22. The distribution of the DNA content is presented with colors and in a stacked way to make the interpretation of the experimental data easier.

During synchronous growth, an oscillating behavior of the phases should be observed. Widest regions for each phase (color) represent those time points, at which a higher percentage of cells traverse through the corresponding phase. It is interesting to observe, that despite of the low growth of subpopulations 2, 3 and 4,5 (Figure 3.20), the oscillating behavior of their cell cycle phases can be clearly observed, displaying highest G_1 peaks every 48 hours. The curves of those subpopulations with high initial G_1 values (subpops. 2, 3, 4,5) show an almost identical time course, whereas the time course of subpopulation 8 (high initial G_2/M value) shows a time shift of ca. 24 h compared to the others. This shift represents the difference in the age between cell populations.

Summarizing, Figure 3.23 shows the viable cell count, the total particle count (Z2

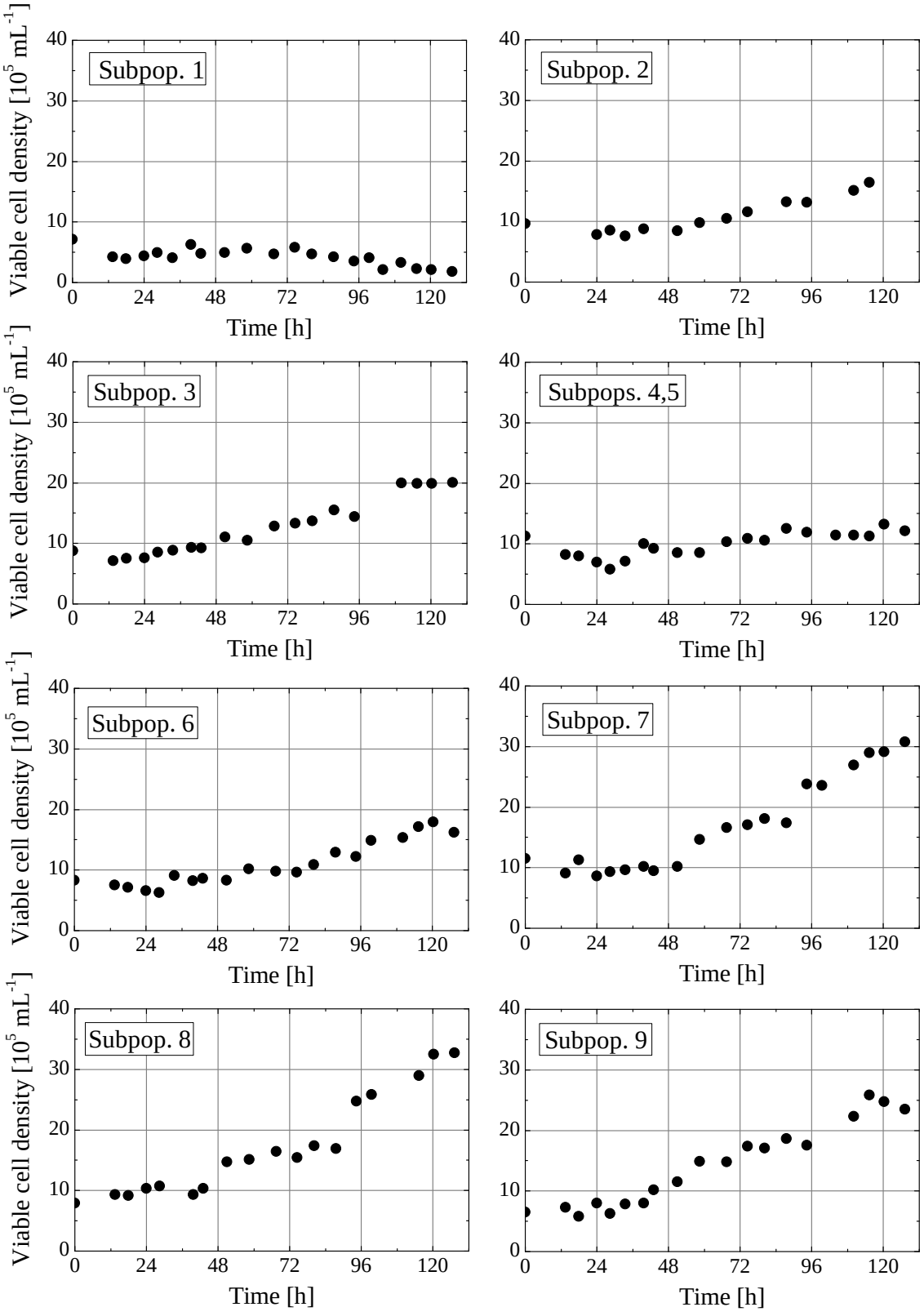

Figure 3.20: Growth curves of synchronous subpopulations in shake flask culture (first elutriation experiment).

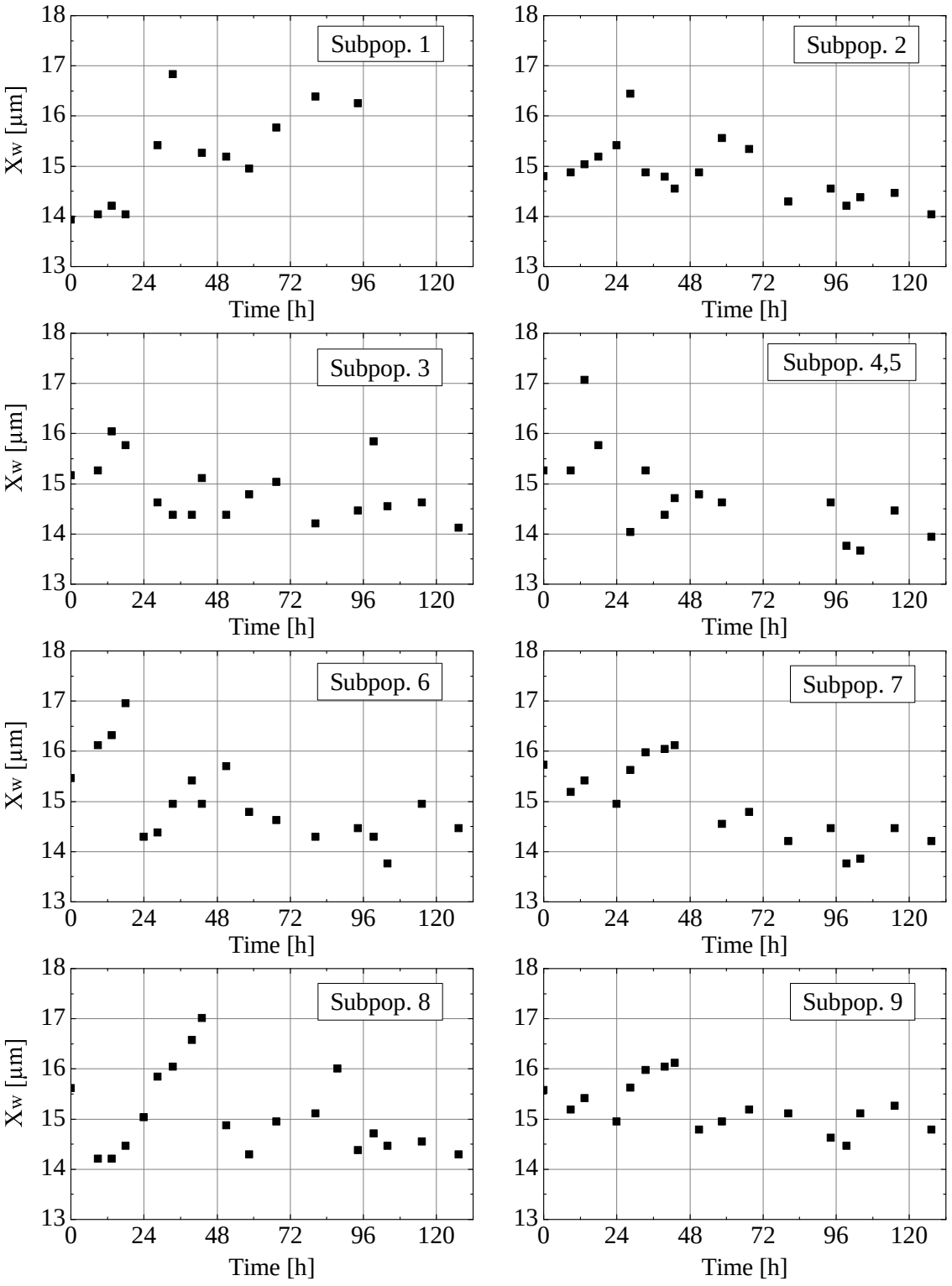

Figure 3.21: Cell size distribution of the subpopulations during cultivation (first elutriation experiment).

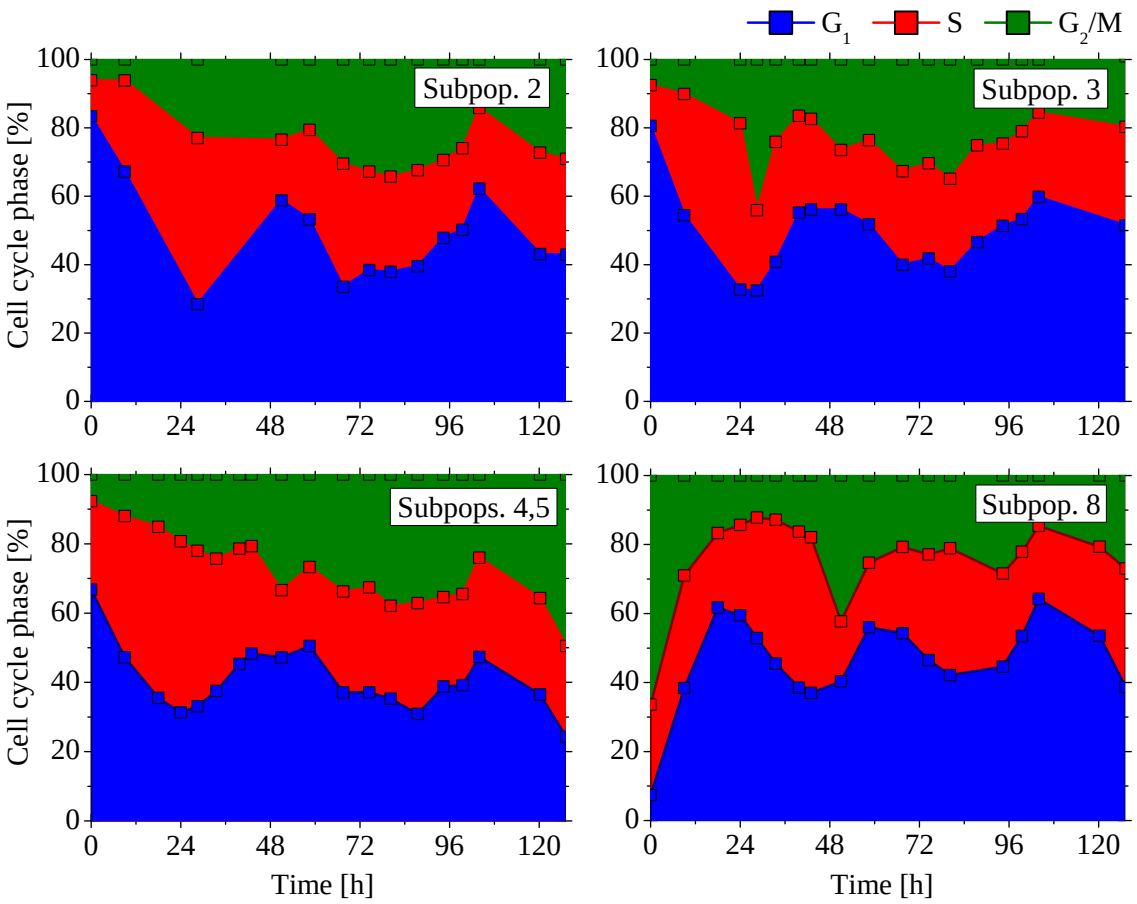

Figure 3.22: Stacked representation of the cell cycle phase distribution during the cultivation of elutriated AGE1.HN cell subpopulations (first elutriation experiment).

Particle counter), the cell cycle phase, and the cell size distributions of subpopulation 8 during the cultivation. Here, the cell size distribution curve is also presented in color. According to the cell cycle phase distribution, most cells (G_2/M, green) were dividing at the time of inoculation ($G_2/M = 66.3\,\%$). This might be the reason for the slightly higher cell count after inoculation compared to those subpopulations with higher G_1 percentages.

After inoculation, the mean cell diameter (X_w) shows its highest value, since a high percentage of cells are still in the G_2/M phase. After ca. 12 h most cells in the G_2/M phase have already divided. At this moment, the fraction of cells in the G_1 phase reaches a maximum, and the mean cell size of the population is consequently reduced to its minimum. Afterwards, X_w doesn't seem to change for the next 12 h, until an abrupt increase in its value is observed (culture time = 29 h). This represents the beginning of the S phase (DNA synthesis), which ends at a culture time of ca. 48 h. Then, within a short time, cells commit again into the G_2/M phase and

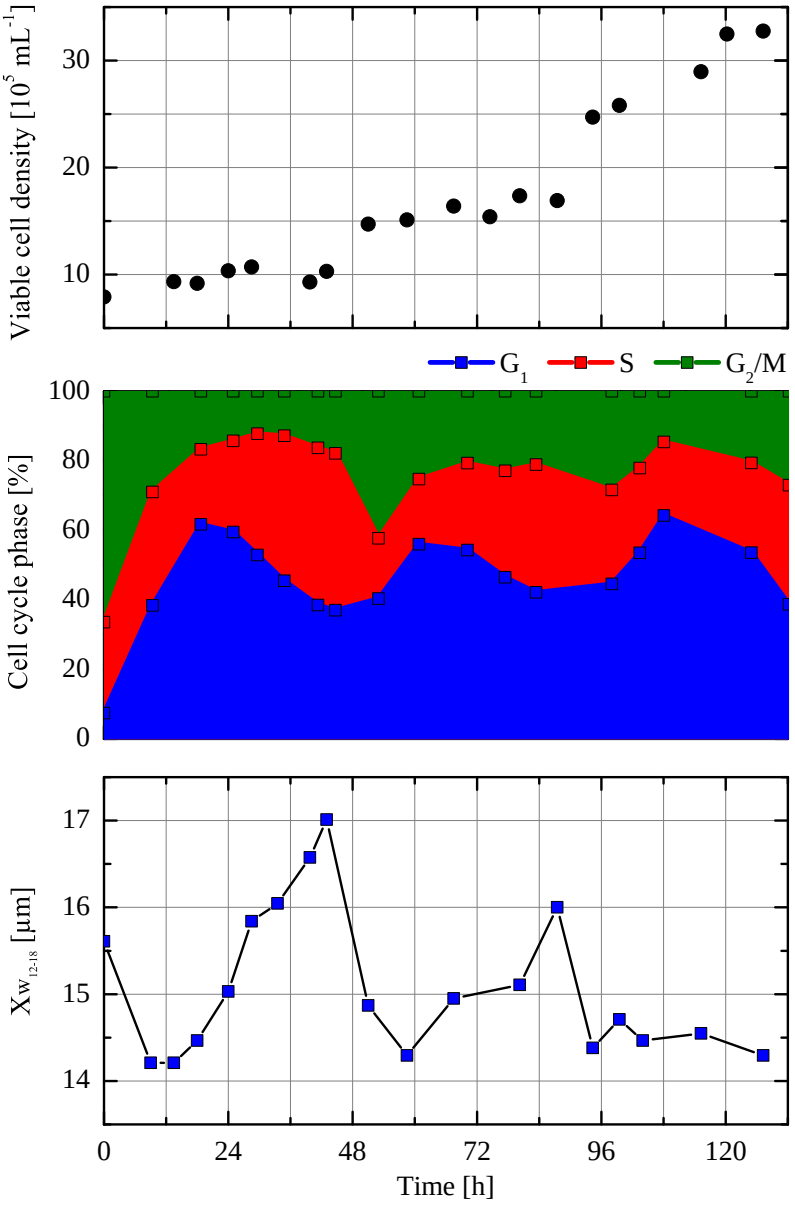

Figure 3.23: Viable cell density, cell cycle dynamics and mean diameter of subpopulation 8 during growth (first elutriation experiment).

divide. Cell division is finished at a culture time of ca. 60 h. The next cell division in this culture flask was detected after 94 h. At this point the oscillation of the cell cycle phases can still be clearly seen, whereas the change in the cell size distribution begins to flaten as cells lose their synchrony after every division.

3.3.5 Separation Quality during Centrifugal Elutriation

During the countercurrent centrifugal elutriation, the synchrony of a subpopulation of cells depends mainly on two parameters:

1. *The pump and its operation:* Inside the elutriation chamber, a front of cells with similar size is formed at the elutriation boundary. The formation of this front and its quality (homogeneity in cell size) is affected by the pump type and its operation. During the first elutriation experiment, a peristaltic pump with a two-roller head was used. The use of 2 rollers led to the pulsation of the fluid in the chamber. This was clearly observed during the elutriation process and might have been the reason for the double-peaked cell size distributions observed in the first experiment.The effect of pulsating liquid inside the chamber increases even more when tubing with large inner diameter is used, which in turn is due to the increased quantity of liquid that is intermittently pulsed through the chamber. This problem can be reduced by using a pulse-free pump with a higher roller number, and also by the using tubing with a smaller inner diameter.

Another phenomenon, which limits the selectivity of cell separation is the presence of jet streaming and turbulence inside the elutriation chamber. This phenomenon has been well described by Lutz et al. [Lutz et al. (1992)] for a non-rotating system, and is depicted by Figure 3.24 for the rotating system used in this work. This flow profile inside the chamber is due to the design of the chamber and its side inlet. Other chamber designs with a modified buffer inlet have been proposed, which might have the capacity to avoid this phenomenon [Lutz et al. (1992)].

2. *The cell size distribution and its correlation to DNA-content:* Depending on the quality of a cell line in culture, the size of cells of the same age might remain quite homogeneous. However, cells that have experienced unfavorable culture conditions will show differences in its inner and outer morphology (e.g. apoptotic bodies, non-defined borders, giant cells, etc.). This will be reflected in the selectivity of the separation.

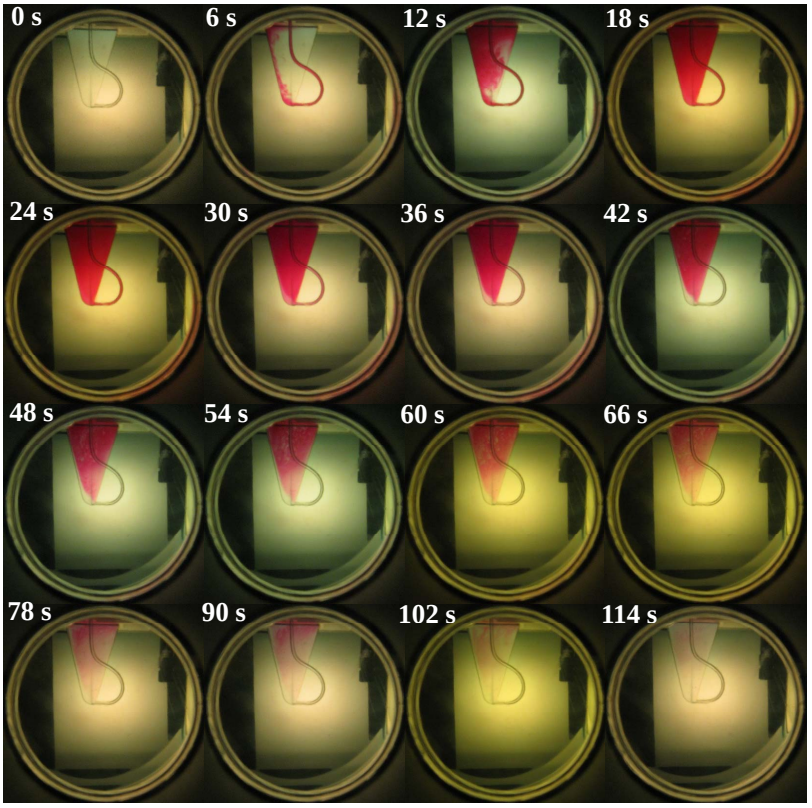

Figure 3.24: Flow profile in the elutriation chamber during operation of the elutriation system. The buffer was switched at time t = 0 s by a phenol red solution. Pictures were taken with a digital camera (Powershot S5IS, Canon, Japan).

If the differences within a cell population are minimized with good handling practices, good synchrony in culture can be achieved by choosing a group of cells from the cell population, which shows marked differences to their counterparts, which are some hours younger or older. A rapid change in cell characteristics occurs mainly during the S and G_2/M phases, where the size of a cell increases faster than in the G_1 phase, due to the replication of the genetic material and further cell division.

The average duration of the cell cycle of an AGE1.HN cell in this work is $\bar{t_d} = 40\,\mathrm{h}$. According to the cell cycle analysis, the distribution of cells within the cell cycle in an asynchronous population is $\bar{G_1} = 57.5\,\%$, $\bar{S} = 32.5\,\%$ and $\bar{G_2/M} = 10\,\%$. Considering that the size of a cell varies minimally during the G_1 phase, then the cell cycle dependent growth of an AGE1.HN cell would be less relevant during the first 23 h of the cell cycle (57.5 %·40 h = 23 h). During the next 17 hours, the AGE1.HN cell would double its genetic material (S phase: 13 h) and will finally commit to cell division (G_2/M: 4 h).

The percentage of cells within a cell cycle phase, or the so called Synchrony Degree, has been used to define the quality of a synchronization process. According to Table 3.2, subpopulation 2 displays the highest synchrony degree in the G_1 phase among the other subpopulations, since 83.4 % of the cell population is distributed within the G_1 phase. However, if the age of the cells is considered within the cell cycle, then 83.4 % of the whole cell population might be distributed within an age range of 23 h. On the other hand, in subpopulation 8 (Table 3.2), the age differences of 66.3 % of the cells might be distributed within a maximum of only 4 h.

If the duration of the cell cycle phase is introduced into the calculation for the enrichment of cells in a subpopulation, the synchrony degree of a cell subpopulation can be divided by the percentage of cells in the same cell cycle phase within the parental asynchronous population (see Equation 3.4).

$$Y_{\text{sync}} = \frac{N_{\Omega}}{N_{\Omega,\text{par}}} \tag{3.4}$$

The resulting dimensionless coefficient represents the enrichment factor of a specific subpopulation. Subpopulations 2 ($G_1 = 83.4\,\%$) and 8 ($G_2/M = 66.3\,\%$) from the first elutriation experiment (see Table 3.2) would show enrichment factors of $Y_{G_1} = 83.4/65.8 = 1.27$ and $Y_{G_2/M} = 66.3/15.2 = 4.36$ respectively. In this way, a cell subpopulation with a high percentage of cells in the G_1 phase might not grow with a higher synchrony than a counterpart with a lower percent of synchrony in the S or G_2/M phases.

3.3.6 Reproducibility during Centrifugal Elutriation

A new elutriation experiment was carried out[12] considering the points discussed above. This time, pulsation was minimized by using a peristaltic pump with an 8-roller head (medorex e.K., Germany), and by reducing the inner diameter of the tubing ($d_i = 2$ mm, Carl Roth, Germany). The time needed for varying the pump rate after collection of every subpopulation was decreased to around 2 - 3 mL min^{-2} (for the first experiment it was done within 10 s, independent of the pump rate), so as to avoid cross-mixing of different-sized cells at the elutriation boundary (see

[12]this work was performed at the Department of Internal Medicine, University Medical Center Hamburg-Eppendorf, Hamburg, Germany, with kind support of A. Carambia, J. Herkel and A. Lohse.

Figure 3.19). Furthermore, the initial cell number used for elutriation was reduced from 5.0 to $3.5 \cdot 10^8$ compared to the first experiment, since the former number has been reported as the maximum cell number which can be introduced to the elutriation chamber, before clumping occurs in a more relevant way.
The results of the elutriation experiment are shown in Table 3.3. As for the first

Table 3.3: Cell cycle phases and cell size distribution of the subpopulations obtained after optimization of the elutriation procedure.

Subpopulation	Pump rate [mL min^{-1}]	G_1 [%]	S [%]	G_2/M [%]	Cells collected [10^6 cells]	X_w [μm]	s_w [μm]
Async. pop.	-	65.4	23.6	11.0	350.0	14.23	1.74
1	14	93.4	4.8	1.6	12.0	13.35	1.87
2	18	94.9	4.1	0.9	36.9	13.49	1.18
3	22	89.7	8.1	2.1	37.5	13.74	1.12
4	26	75.6	19.0	5.0	29.1	14.13	1.22
5	30	57.6	32.4	9.8	22.8	14.49	1.24
6	35	16.3	53.2	30.3	25.2	14.98	1.28
7	41	6.4	42.1	51.2	17.7	15.48	1.29
8	47	6.4	17.9	75.2	12.3	15.78	1.58
6-2	35	26.6	51.1	22.1	14.4	14.69	1.42
7-2	41	10.3	40.1	49.5	13.5	15.54	1.30
8-2	47	5.7	25.5	68.5	7.2	15.89	1.71

experiment, the percentage values of the cell cycle phases change with the subpopulation number. Figure 3.25 shows the cell size distribution of the 8 elutriated subpopulations. No clear visual indication of cross-mixing (double-peaked cell size distribution curves) of cells can be observed in the Figure 3.25 as observed during the first elutriation experiment. This is also reflected in the standard deviation values as shown in Table 3.3, where s_w was reduced by approximately 22 % of its average value during the first elutriation experiment.

Due to the lower number of cells in the S or G_2/M phases compared to the G_1 phase (see Table 3.3), the inoculation of a bioreactor system with cells in these phases might consider the performance of elutriation cycles. Considering this, the reproducibility of an elutriation experiment was tested by repeating the elutriation of the last three subpopulations in Table 3.3 with the higher percentage values in the S and G_2/M phases (subpopulations 6, 7, 8). The cell cycle phase distribution and mean cell diameter values of these three new subpopulations (6_2, 7_2, 8_2) are shown in the last three rows of Table 3.3. The normalized cell size distribution of the subpopulations is shown in Figure 3.26.

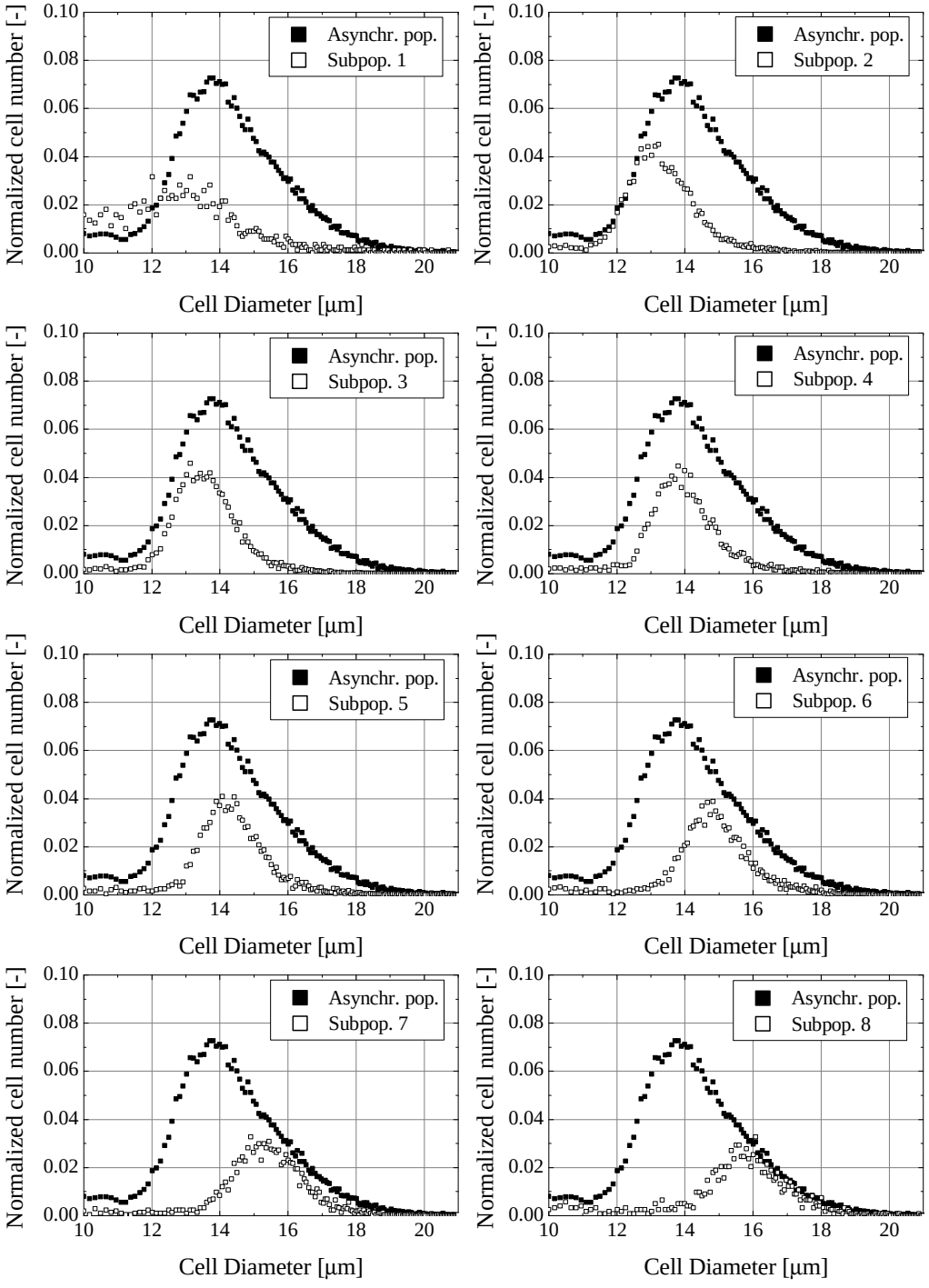

Figure 3.25: Cell size distribution of subpopulations after optimization of the elutriation procedure.

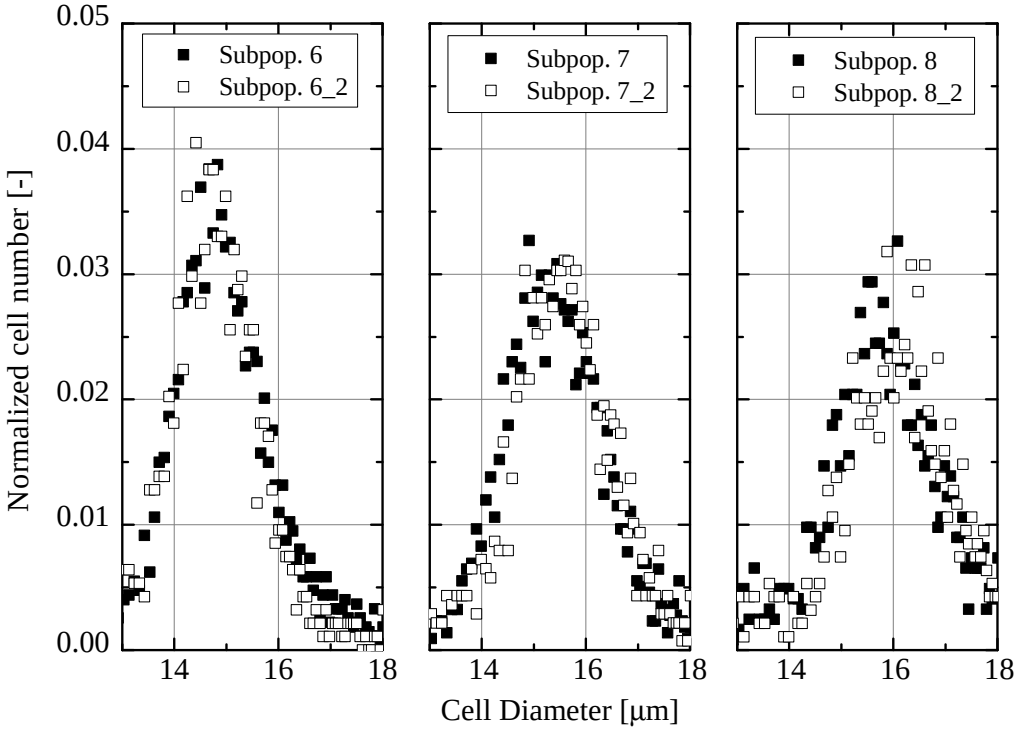

Figure 3.26: Reproducibility in the generation of cell subpopulations in centrifugal elutriation.

3.3.7 Dialysis Culture of Synchronous AGE1.HN Cells

A total of 17 elutriations were performed in order to elutriate $7.2{\cdot}10^8$ cells with the characteristics of the last three subpopulations of Table 3.3 for an initial cell density of $9{\cdot}10^5$ cells mL^{-1} in 800 mL. The preculture consisted of nine 500 mL shake flasks with 180 mL culture each, with cells growing exponentially at around $30 - 40{\cdot}10^5$ cells mL^{-1}. Figure 3.27 depicts the integrated system for the dialysis culture of synchronous cells with continuous in-situ monitoring of the cell density through in-situ microscopy.

Figure 3.28 shows the results of the dialysis culture of the synchronized cells. Although the cultivation lasted 155 hours, the results are presented for 120 hours of culture, where synchronous growth could be observed clearly. During this period, 3 synchronous divisions took place; the first at the time of inoculation and during the first 12 hours, the second at around 36 hours of culture and the third after 66 hours. During these three synchronous divisions cells showed specific growth rates of $\mu_{max} = 1.12$, 1.46 and 0.97 d^{-1} with standard deviations of $\mathrm{s}_\mu = 0.45$, 0.45 and 0.11 d^{-1} respectively (calculated from manual cell count).

In comparison to the growth curve shown in Figure 3.20 for subpopulations 7 and

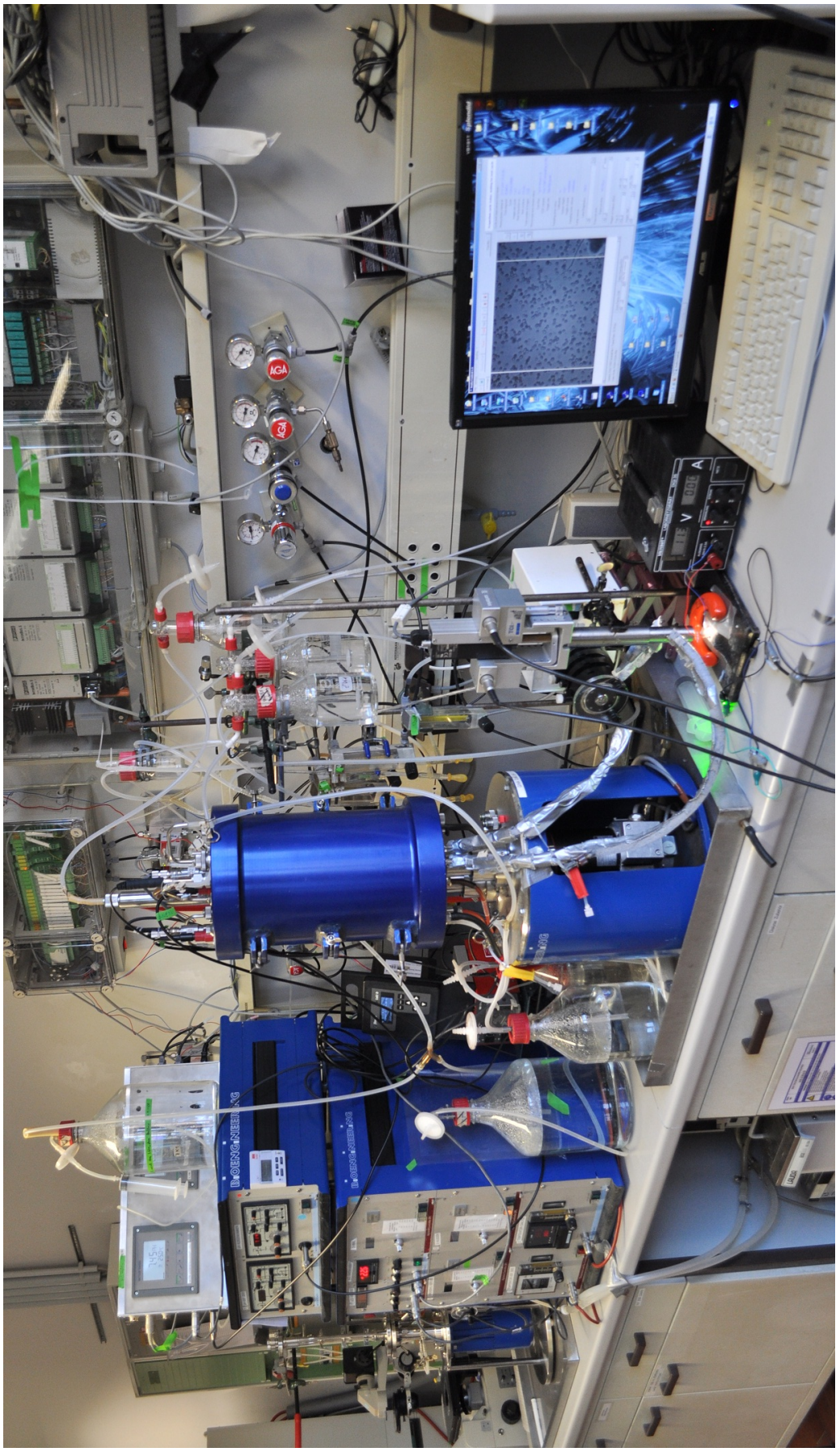

Figure 3.27: Experimental setup for the dialysis culture of synchronous cells. Left: dialysis bioreactor and control unit. Middle: in-situ microscope. Right: in-situ microscope's control software.

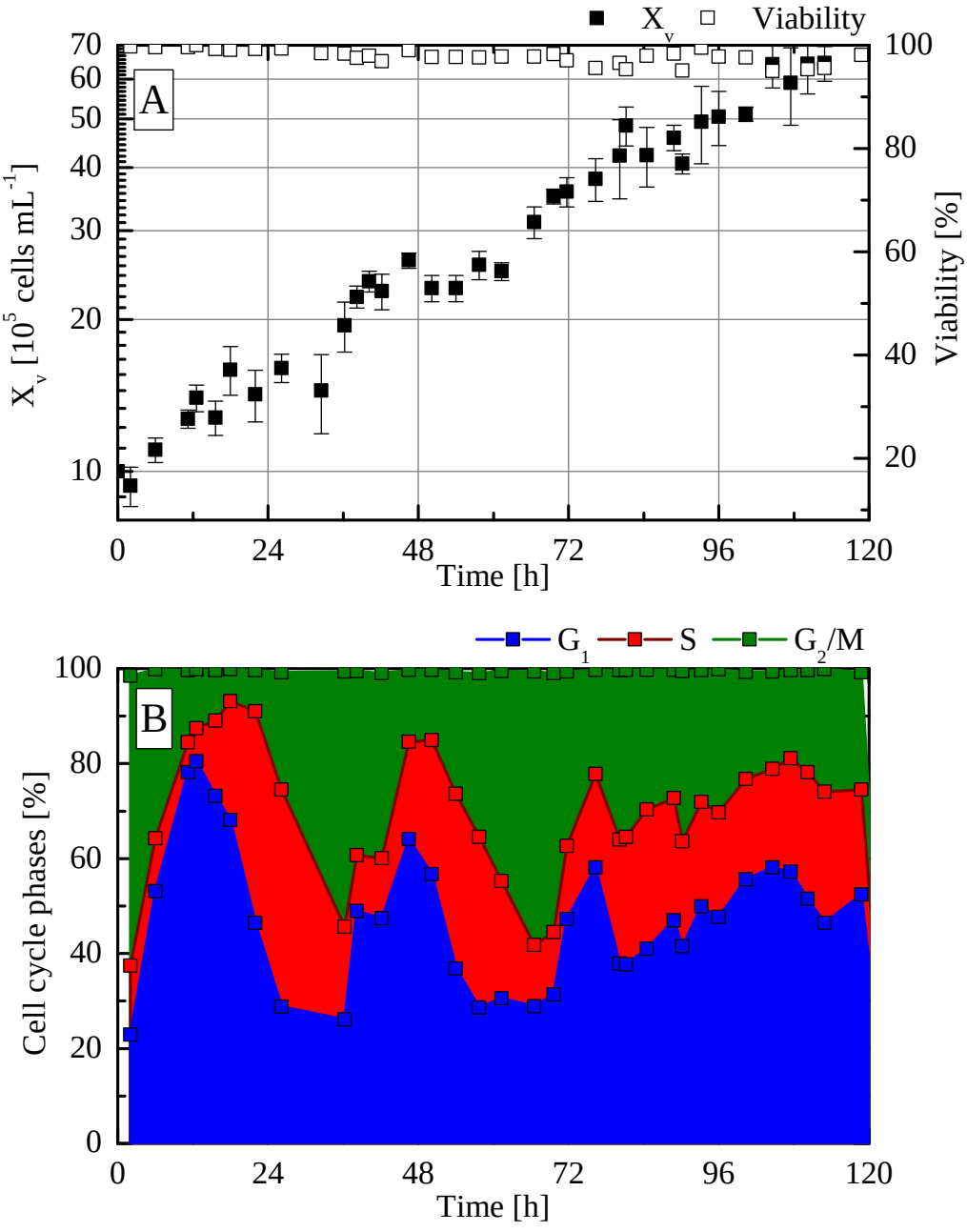

Figure 3.28: Synchronous growth of AGE1.HN cells in a dialysis bioreactor. The cultured cells were elutriated with a high synchrony in the G_2/M phase. A: viable cell density, B: percentage values of the cell cycle phase distribution.

8, where the observed synchronous divisions took place every 48 hours, synchronous division in this experiment can be observed every 30 hours. This can be explained by the fact that the subpopulations used for inoculation of this bioreactor belonged to both S and G_2/M phases. The collection of cells in both phases was needed in order to reach the desired cell number for inoculation. Therefore, the pump range employed (see Table 3.3) was changed from 35 - 50 mL min^{-1} to 30 - 55 mL min^{-1}. This new pump rate range led to the collection of cell subpopulations with a higher percentage of S phase cells than G_2/M cells (subpopulation 6 in Table 3.3). Hence, the age differences of the collected subpopulations was broadened due to a cross-mixing with younger cells. The doubling time ($t_d = 40$ h) of the cells remained constant, which indicates unperturbed growth of the cells inside the dialysis bioreactor.
For comparison purposes, the synchrony coefficients for the G_2/M phase ($Y_{G_2/M}$, Equation 3.4) are shown Table 3.4 for four different subpopulations. The first subpopulation (1) corresponds to subpopulation 8 from the first elutriation experiment (Table 3.2); the second value (2) belongs to subpopulation 8 from the optimized elutriation experiment (Table 3.3); the third value (3) was calculated for the inoculum of the dialysis bioreactor according to the original inoculation plan; and the last value (4) represents the calculated enrichment factor for the bioreactor's inoculum after modification of the pump rate range (including subpopulations 6, 7 and 8 from Table 3.3). As shown in Table 3.4, the calculated synchrony coefficient for the

Table 3.4: $Y_{G_2/M}$ of four AGE1.HN subpopulations elutriated in the G_2/M.

Experiment	$Y_{G_2/M}$
1	4.36
2	6.83
3	5.54
4	4.24

dialysis experiment (4.24) was not as high as expected (5.54). The use of a larger pump rate range reduced the synchrony coefficient and broadened the differences in age of the cells used for inoculation. Thus, the average time needed by the cells to divide during dialysis culture accounts for up to 12 h (first two divisions), whereas cells from subpopulation 8 in Figure 3.20 needed only 7.5 h.

The fact that the elutriation procedure lasted around 10 hours might also have played an important role. The elutriated subpopulations were kept in suspension at room temperature (ca. 22 °C). The reason for choosing room temperature for cell storage until inoculation was to keep growth at a minimum level without inducing

cold shock to the cells (4 °C). A complete arrest of cell growth during this time was not further asessed.

Due to the closely spaced intervals for sampling, the oscillations of the cell cycle phases and their time offset during cell growth can be well recognized. According to the cell cycle analysis of the first sample, the culture was started with an initial percentage value of 60 % of cells in the G_2/M. At least four G_1 peaks can be identified, whereas the fourth peak is almost not noticeable in the growth curve. After a culture time of 120 h, almost cell growth developed asynchronous and continued growing exponentially.

3.3.8 Synchronous Culture of a CHO-K1 Cell Line

The feasibility of the elutriation process to generate and synchronous culture of AGE1.HN cells was tested for a second industrial production cell line CHO-K1[13]. This second elutriation procedure considered the inoculation of a smaller batch bioreactor (Vario1000, see Section 2.2.4, p. 14, $N = 300$ rpm). The bioreactor was inoculated with $4{\cdot}10^5$ cells mL^{-1} ($V_w = 250$ mL) with a high synchrony in the S phase. Table 3.5 shows the results of the elutriation procedure which was carried out prior to culture. The aimed subpopulations for this experiment were subpopulations 5 and 6 in Table 3.5, with a synchrony degree in the S phase of 53.3 % and a synchrony coefficient of $Y_S = 1.79$. The pump rate range employed was as shown in Table 3.5, 34 - 42 mL min^{-1} for these subpopulations. Five elutriation cycles were necessary to achieve the needed initial inoculum cell number.

For this experiment the in-situ microscope was used. A two-roller pump (Watson Marlow, USA), and a wide pump silicon tubing ($d_i = 5$ mm) were used for liquid conveyance to the microscope so as to reduce the volume specific contact area during peristalsis. Furthermore, possible temperature oscillations in the flow pathway to the in-situ microscope were solved by setting the microscope into an incubator. After these slight modifications, both cell size distribution analysis and use of the in-situ microscope for cell count were possible. Figure 3.29 displays the results of the cultivation. Compared to the manual count shown in Figure 3.29.A (only three samples during the first 12 h of culture), the in-situ microscope show counting results in closer intervals (Figure 3.29.B) and allowed as well for a more precise detection

[13]kindly provided by T. Noll, Bielefeld University, Bielefeld, Germany, for the project SysCompart.

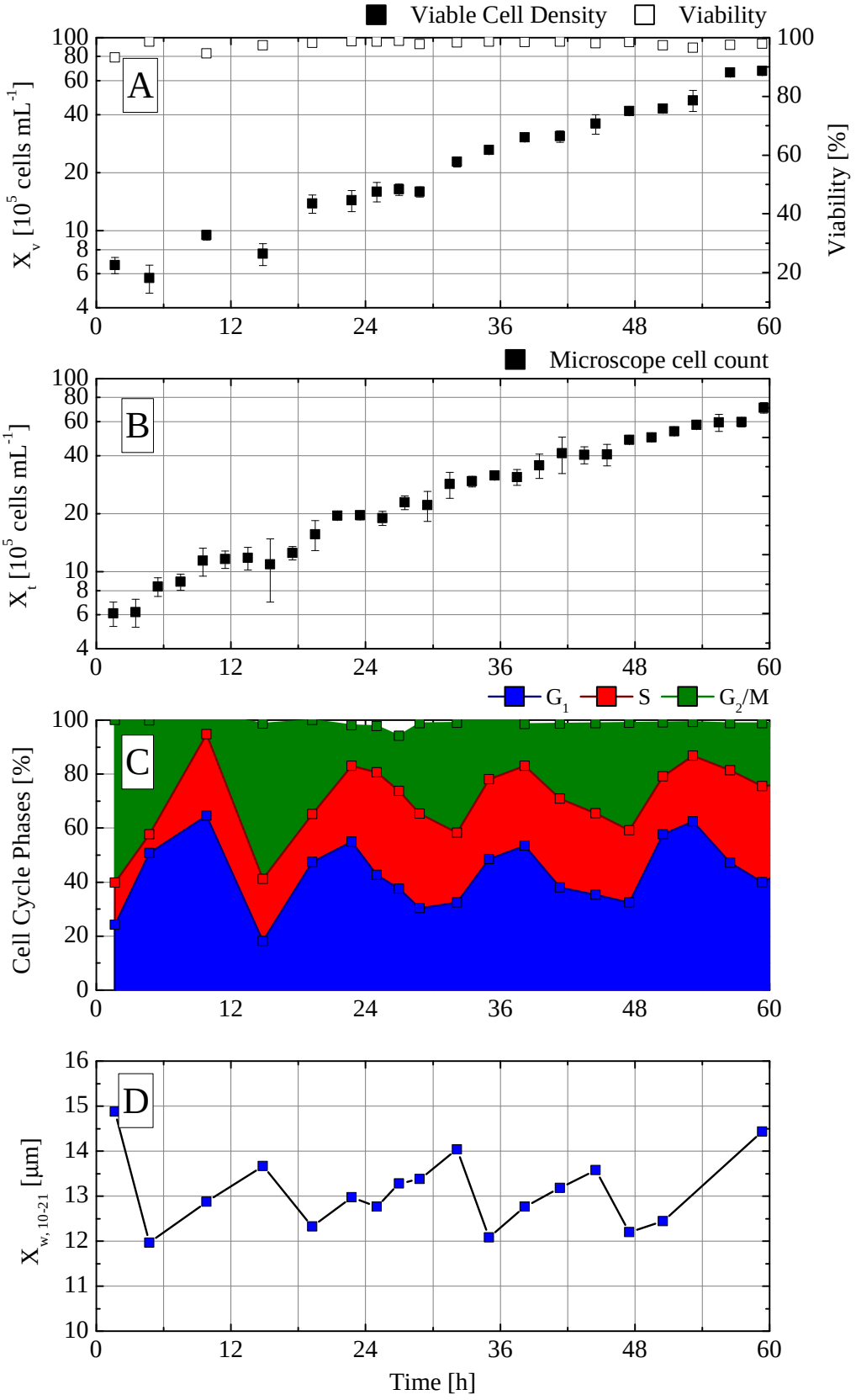

Figure 3.29: Batch synchronous growth of CHO cells in a benchtop bioreactor. A: viable cell density (manual count), B: in-situ microscope count, C: cell cycle phases distribution, D: cell size distribution.

Table 3.5: Cell cycle phases and cell size distribution of the subpopulations after elutriation of a CHO-K1 cell line.

Fraction	Pump rate [mL min^{-1}]	G_1 [%]	S [%]	G_2/M [%]	Cells collected [10^6 cells]	X_w [μm]	s_w [μm]
Async. pop.	-	48.0	29.7	21.6	380	13.24	1.38
1	22	83	10.7	6.3	0.81	11.41	1.15
2	26	92.3	6.3	1.3	3.40	11.86	1.33
3	30	72.4	23.7	3.7	1.95	12.07	1.55
4	34	34.3	51.3	14.2	16.98	12.65	1.13
5	38	13.4	56.9	29.5	26.32	13.16	1.19
6	42	8.3	42.1	49.5	8.52	13.83	1.29
7	46	6.1	24.6	68.7	6.30	14.03	1.50
8	50	6.2	13.3	78.9	2.64	14.21	1.77

of cell division.

Again, three to four synchronous divisions can be observed in both growth curves depicted in Figure 3.29.A, B. Cell division occurs according to the diagram every 15 - 16 h. This indicates an unperturbed cell growth according to the doubling time for this CHO-K1 in continuous culture ($\bar{t}_d = 16 \pm 2.6$ h, data not shown). Figure 3.29.C shows a very high percentage of cells in the G_2/M phase at the beginning of the cultivation. These cells might have been entering the G_2/M phase after inoculation, since first observable cell division took place almost 5 hours after inoculation, which corresponds, at least, to the duration of the G_2/M phase of the CHO-K1 cell population in Table 3.5 ($\%G_2/M \cdot \bar{t}_d = (21.6)(16\,\text{h})/100 = 3.5\,\text{h}$).

During the cultivation, very similar peak heights can be observed in the cell cycle phase distribution, where even after 50 h in culture, no loss of synchrony can be seen (see Figure 3.29.C). The mean cell size of the synchronous population (Figure 3.29.D) shows a time course, which correlates inversely with the G_1 peaks of the cell cycle phase distribution diagram (Figure 3.29.C). Thus, maximum values in the G_1 phase show the time points for which the cell size of the population reaches its minimum value (after division) and viceversa. Taking into consideration, that the change in cell size of a cell population is more significant during the S and the G_2/M phases, the time course of the mean cell diameter X_w should resemble a saw-tooth, where a slow increase of X_w takes place during the G_1 phase, then the increase will be faster in the S and G_2/M phases, until an abrupt decrease in X_w will take place after cell division.

3.4 Concluding Remarks

In this work, strategies for synchronization of the human industrial cell line AGE1.HN were evaluated and implemented. The reduction of the cultivation temperature showed that cell enrichment within the G_1 phase was possible to reach up to 80 % synchrony. However, accumulation does not happen immediately but requires more than 3 days at the studied temperatures for reaching high synchrony values. After temperature resumption, the cell viability decreased, indicating metabolism hindrances. Temperature reduction cycles in the bioreactor cultures were proposed to shorten temperature reduction intervals. These cycles led to a redistribution of the cell cycle phases in the cell population, but did not increase the synchrony degree of the whole culture compared to experiments in shake flasks.

The countercurrent centrifugal elutriation allowed for reproducible and scalable cell synchronization of AGE1.HN cells with high synchrony degrees, up to 95 % in G_1, 53 % in S and 75 % in the G_2/M phases. Subpopulations with high synchrony degrees can be obtained from an asynchronous population within a short time. These subpopulations can be further cultivated and sampled to generate data on cell cycle dependent metabolism. A parameter called *enrichment factor* was proposed, which can be used as a criterion for synchrony of a cell subpopulation in addition to the normally used synchrony degree. This factor relates the synchrony degree of a cell subpopulation to the percentage of cells in the same cell cycle phase in an asynchronous population. In this way, the age dependent change in the cell size is included for synchrony determination.

After assessing the reproducibility of elutriation results, the process was scaled up successfully for inoculation of a dialysis bioreactor, where synchronous unperturbed growth was observed at least for 3 cell divisions. A very clear oscillation of the cell cycle phases was observed during synchronous growth.

Furthermore, this strategy was applied for the synchronization and further culture of a CHO-K1 production cell line with good results. The quantity of information generated through the use of an in-situ microscope and the determination of the mean cell diameter of the population during cultivation makes this strategy powerful for research purposes on cell cycle dependent metabolism and its population dynamics.

4 DoE Evaluation of Fed-Batch Culture Strategies

4.1 Theoretical Background

4.1.1 The Fed-Batch Culture Mode

During the design of new biotechnological processes the choice of the culture system as well as its operation mode play a decisive role [Hass and Pörtner (2011)]. Stirred tank systems and production modes like Batch, Fed-batch, Chemostat and Perfusion have been well established for the production of biologics. Among these modes the fed-batch approach has become a leading technology in production of biologics based on animal cell culture [Whitford (2006)].

During fed-batch culture a substrate feeding is started during the exponential growth phase, prolonging growth by avoiding the culture to enter into the stationary phase. In this way growth continues until it is again limited by the absence of substrate or inhibited by excess accumulation of product. The supplementation of nutrients is done by external feeding and therefore there is a need to carefully select the initial feed concentration and the feed rate. Usually the inlet substrate feed is kept as concentrated as possible so that a minimum addition is needed to enhance substrate availability in the bioreactor. This minimizes as well unnecessary dilution in order to optimally use the entire bioreactor volume for prolonged product formation [Srivastava and Gupta (2011), Hass and Pörtner (2011), Xie and Zhou (2006)]. Therefore cell culture in fed-batch operation increases the duration of the exponential growth phase while minimizing cell death. Since most of the products built by cells are growth related, the final product titer can be also increased by fed-batch culture [Hass and Pörtner (2011), Xie and Zhou (2006)].

Neither complex technology nor complete modification of bioreactors and equipments is required for establishing a fed-batch process, except for a feed tank and a pump. Additional advantages of fed-batch culture include ease of process validation and characterization [Whitford (2006)]; other advantages relate to the controlled growth of cells, avoidance of excessive nutrients at the beginning of a cultivation, easiness to be adapted to the uptake of a specific metabolite, and light dilution, but not removal of inhibitory metabolites. The impossibility of removing toxic metabolites leads to its accumulation and many times to the end of the process. This feature becomes relevant at those processes in cell culture, where toxic metabolites reach in-

hibiting concentrations (e.g ammonium) even before substrate has been completely consumed. Most advanced large-scale fed-batch optimization in cell culture has been performed for proteins, especially monoclonal antibody (MAb) based pharmaceuticals.

4.1.2 Process Development with Fed-Batch Culture

Efficient fed-batch culture strategies have been systematically developed in parallel with intensive cell line and culture medium development to achieve a lower manufacturing cost of goods and higher product purities [Whitford (2006)]. Process development and optimization in fed-batch culture is carried out considering two main aspects: medium improvement (batch and fed-batch) and the fed-batch control strategy (time/rate of administration).

Medium Improvement
In general, salt-free nutrient concentrates are fed at rates required to prevent nutrient depletion/accumulation, so that the nutritional and biochemical parameters including osmolarity, carbon dioxide and other by-product concentrations can be maintained within levels suitable to promote cell growth or minimize cell death for product expression. Design of culture media and nutrient feeding solutions is principally based on stoichiometric nutritional analysis [Xie and Zhou (2006)]. In order to optimize the feeding medium, small scale experiments can be performed on culture plates or culture tubes [Jordan and Jenkins (2007)], in which a broad range of parameters including nutrient concentrations and start of feed can be evaluated. However, the low culture volume used in culture plates impairs sampling over long cultivation periods (5 - 10 days). Thorough optimization in culture tubes requires space in the incubator. Furthermore, the feed solution can generally only be added batchwise. This is not representative for those strategies which consider a constant feed inlet and might lead to temporarily high substrate concentrations in culture, with undesirable effects on cell metabolism (e.g. overflow metabolism).

The Fed-Batch Control Strategy
In addition to feed medium design, the method of feed delivery is another important consideration than can greatly affect the performance of a fed-batch process. A common control goal for fed-batch cultures is to maintain one or more key nutrients within an acceptable range of concentration. Ideally, the uptake or production rate of a reference compound can be used to establish a feedback loop that determines

how much medium should be added. This can be implemented using complex on-line measurements paired with an automated feeding system, or using very simple off-line measurements followed by manual feeding. Measured variables in cell culture processes typically include the concentrations of glucose, lactate, glutamine, and cell density. Concentrations of other amino acids can also be used as a reference to establish an optimum fed-batch process [Wlaschin and Hu (2006)].

The control strategy defines in which way a previously designed feed can be added to the culture. Some feeding strategies described in literature consider substrate addition at low concentration, constant, linear, or exponential addition of nutrient feeding, pseudo-steady state of product or substrate [Srivastava and Gupta (2011), Wlaschin and Hu (2006)], or more sophisticated strategies like the adaptive, model based OLFO (Open-Loop-Feedback-Optimal) strategy [Frahm et al. (2005)]. The right choice of a feeding strategy will depend mostly on cell metabolism and on the sensitivity to limitation and/or inhibition.

4.1.3 The Need of Tools for the Evaluation of Fed-Batch Strategies

With the help of mathematical simulation, the effect of parameters such as substrate set-point concentrations, feeding time-step patterns, and concentration of feeding solutions, etc., can be studied in order to know how variables should be adapted to elicit a desired response. Insights gained from modeling can guide in the adjustment of a process, eliminating unnecessary rounds of characterization. Finally, comparing actual experimental results with model predictions helps improve the models over time [Sercinoglu (2011)].

Depending on the cell line and the culture mode, different mathematical models can be employed and adapted to the cell-specific kinetics. The choice of a model for process simulation depends on the purpose of simulation, the growth phases to be simulated (whole growth curve, exponential growth) and the goal after simulation.

For a detailed description of regulation mechanisms of cell lines, kinetic models which regard the interaction of different factors are needed [Zeng and Deckwer (1995), Frahm et al. (2005)]. The more factors the model includes, the higher will be its complexity and accuracy. However, in most of the cases only small data sets regarding culture are available. The use of models with a higher complexity is in this way still very limited. Furthermore, data generation of specific metabolites includes

complex analytics, which is mostly not available in every laboratory.

Unstructured and unsegregated models have been the common type of models used in mammalian cell culture as they include fewer parameters than structured models and are therefore easier to construct [Augusto et al. (2007), Engasser et al. (1998), Jang and Barford (2000)]. After determination of a short number of kinetic parameters, this kind of models can be used for simple prediction of growth, uptake and production kinetics. In this way, if a simple model fulfills the requirements of growth prediction of a cell line in batch culture, it can be used for prediction on other culture modes like fed-batch. The results of this *in-silico* experimentation might help the user to evaluate different feeding strategies before performing experimentation in the laboratory.

Still, the whole task of both *in-silico* and experimental evaluation and implementation of feeding strategies might become a long lasting task. Furthermore, performance of experiments is most of the times expensive, due to the working capacity and quantity of culture medium used for this task, and time consuming, depending on the cultivation capacities of the experimentation laboratory. When a tool for evaluation of fed-batch strategies is combined with Design of Experiments (DoE), an extraction of a maximum amount of information from experiments conducted for process development can be carried out while spending a minimum amount of resources [Mandenius and Brundin (2008)].

In this work, a procedure for *in-silico* and experimental evaluation of fed-batch strategies was conceived and implemented. A tool for *in-silico* evaluation of fed-batch strategies was developed, in which kinetic models have been programed for describing batch and fed-batch growth of mammalian cells. The models can be selected, modified, or even written new and saved into the software. Systematic *in-silico* experimentation is possible through DoE. As a proof of design, the computer evaluation of feeding strategy parameters for the human production cell line AGE1.HN was planed by a full factorial design on two levels. The obtained results were reproduced in the laboratory by carrying out fed-batch experiments in a bench-top bioreactor.

4.2 Materials and Methods

4.2.1 Preculture, Shake Flask and Bioreactor Experiments

Preculture as well as shake flask experiments were performed with the AGE1.HN cell line as indicated previously (Section 2.2.2, p. 13). Shake flask experiments for kinetic parameter determination were carried out in 500 mL glass shake flasks (DIN 12385, Schott Duran, Wertheim am Main, Germany) with a working volume of 200 mL. The pH value of the cultures was measured externally (CG 822, Schott AG, Mainz, Germany) during sampling. A scheduled reduction of the CO_2 partial pressure in the incubator's atmosphere was followed as described in Section 2.2.2, p. 13.

Bioreactor experimentation was carried out in a benchtop bioreactor (VSF2000, Bioengineering, Switzerland, 6-RT, see Section 2.2.4, p. 14, $N = 240\,\mathrm{rpm}$). A third impeller was mounted onto the stirrer shaft in order to allow for efficient mixing during volume increase due to feeding. Furthermore a precise peristaltic pump (Model TL, medorex, e.K.) with corresponding tubing (TPE Pharmed®, Carl Roth, Germany), and a 500 mL flask containing the feed medium were used.

4.2.2 Batch and Fed-Batch Medium

To date there is no commercially available formulation of a feed medium for AGE1.HN; for this reason bioreactor *batch* and *fed-batch* media were designed from a basis formula.

For shake flask experiments, variation of the initial concentrations of glucose and glutamine was possible by using a glucose, galactose and glutamine-free formulation of the culture medium (42-MAX-UB, Teutotell AG, Bielefeld, Germany). Glucose and Glutamine were added as a powder to avoid medium dilution (D-Glucose: Merck, Germany; L-Glutamine: Difco Laboratories GmbH, Germany). D-Galactose (Merck, Germany) was added proportionally to glucose at a 12:1 molar ratio (Glc:Gal). For experiments with initial lactate or ammonia concentrations, ammonium chloride and sodium lactate (Merck, Germany) were used.

For batch culture, a low-salt medium formulation of the 42-MAX-UB (Teutocell AG, Bielefeld, Germany) with an initial osmolality of 205±5 mOsm kg^{-1} was supplemented with 10 mM D-Glucose, the corresponding D-Lactose, and 2 mM L-Glutamine.

Fed-batch media were formulated according to the experimental design. The increase in medium osmolality was calculated afterwards with equation 4.1:

$$osmol/kg = \rho_m \sum_i \varphi_i n_i C_i \tag{4.1}$$

where
$\rho_m =$ medium density [$\mathrm{kg\,m^{-3}}$]
$\varphi =$ osmotic coefficient [-]
$n =$ number of penetrating ions, solutes or particles into which a molecule dissociates.
$C =$ mol concentration of the solute [$\mathrm{mol\,m^{-3}}$]

The medium density was considered for calculations as 1000 $\mathrm{kg\,m^{-3}}$. The difference in medium osmolality between a normal batch medium ($\approx$ 280 mOsm $\mathrm{kg^{-1}}$) and the resulting formulations was compensated by NaCl addition ($\varphi_{NaCl} = 0.93$). Generally, NaCl addition was not necessary after osmolality calculation of feed media.

4.2.3 Analytics

Glucose, glutamine and lactate concentrations were measured in a YSI analyzer (Model 7100, Yellow Springs Instruments). Ammonium concentration was measured using a photometric test by Merck (no. 11752, Merck eK, Darmstadt, Germany). Cell counting and viability determination were performed by manual counting on a Neubauer Haemocytometer (Fuchs-Rosenthal).

4.2.4 Data Treatment

Experimentally obtained data from shake flask culture were smoothed by using the Asymmetric Logistic Equations (ALE) proposed by Acosta et al. [Acosta et al. (2007)] for mammalian cells, which yielded a better fit of the data obtained in this work. The ALEs used are shown as follows for viable and dead cell concentrations (Equation: 4.2) and for glucose, lactate, glutamine and ammonium concentrations

(Equation 4.3):

$$X(t) = a{+}b{\cdot}exp\left(-\frac{t+dln(e)-c}{d}\right)\left(1+exp\left(-\frac{t+dln(e)-c}{d}\right)\right)^{-e-1} e^{-e}(e{+}1)^{e+1} \tag{4.2}$$

$$C(t) = f + \frac{g}{\left(1+exp\left(-\frac{t-iln\left(2^{1/j}-1\right)-h}{i}\right)\right)^{j}} \tag{4.3}$$

In some cases the ALEs didn't give a satisfactory fit. This was the case for the death phase of culture and the observed lactate uptake. For this parts of data, polynomials of either second or first order were used additionally [Sercinoglu (2011)].

4.2.5 Calculation of Kinetic Variables

The characteristic kinetic variables were calculated according to the following equations for batch culture [Sercinoglu (2011)]:

Apparent specific growth rate:

$$\mu_{app} = \frac{1}{X_v}\frac{dX_v}{dt} \tag{4.4}$$

Death rate:

$$k_d = \frac{1}{X_v}\frac{dX_d}{dt} \tag{4.5}$$

Specific growth rate:

$$\mu = \mu_{app} + k_d \tag{4.6}$$

Glucose uptake rate:

$$q_{glc} = -\frac{1}{X_v}\frac{dC_{glc}}{dt} \tag{4.7}$$

Glutamine uptake rate:

$$q_{gln} = -\frac{1}{X_v}\left(\frac{dC_{gln}}{dt} + K_{d,gln}C_{gln}\right) \tag{4.8}$$

Lactate production rate:

$$q_{lac} = \frac{1}{X_v}\frac{dC_{lac}}{dt} \tag{4.9}$$

Ammonium production rate:

$$q_{amm} = \frac{1}{X_v}\left(\frac{dC_{amm}}{dt} - K_{d,gln}C_{gln}\right) \tag{4.10}$$

where $K_{d,gln}$ is the first order decomposition rate of glutamine in the medium which was assumed to be $0.0023\,h^{-1}$ [Ozturk and Palsson (1990)].

For simplification, only mean values of the smoothed data between each real sampling point were used to calculated the specific rates. The differentials in the above equations were thus, discretized. For example, the apparent specific growth rate between the timepoints t_{n+1} and t_n was calculated as:

$$\mu_{app} = \frac{1}{(X_{v,n+1} + X_{v,n})/2}\frac{X_{v,n+1} - X_{v,n}}{t_{n+1} - t_n} \tag{4.11}$$

4.2.6 Bioreactor Model for a Fed-batch Process

The dynamic bioreactor model for the fed-batch process is presented as follows:

$$\frac{dX_v}{dt} = (\mu - k_d)X_v - \frac{F}{V}X_v \tag{4.12}$$

$$\frac{dX_d}{dt} = k_d X_v - \frac{F}{V}X_v \tag{4.13}$$

$$\frac{dX_t}{dt} = \mu X_v - \frac{F}{V} X_t \tag{4.14}$$

$$\frac{dC_{glc}}{dt} = -q_{glc} X_v - \frac{F}{V} C_{glc} + \frac{F}{V} C_{glc,feed} \tag{4.15}$$

$$\frac{dC_{gln}}{dt} = -q_{gln} X_v - K_{d,gln} C_{gln} - \frac{F}{V} C_{gln} + \frac{F}{V} C_{gln,feed} \tag{4.16}$$

$$\frac{dC_{amm}}{dt} = q_{amm} X_v + K_{d,gln} C_{gln} - \frac{F}{V} C_{amm} \tag{4.17}$$

$$\frac{dV}{dt} = F \tag{4.18}$$

4.2.7 Software Development

The software was developed to provide the following functions:

• Define a dynamic model of a bioprocess (an ODE system)

• Simulate batch processes at different initial conditions

• Simulate fed-batch processes for different strategies and control parameters

• Analyze batch and fed-batch control parameters according to a pattern defined in an experimental design

During its development, the mentioned functions were implemented within three modules, named (1) bioprocess simulation, (2) fed-batch control on the simulated process and (3) analysis of the process via DoE [Sercinoglu (2011)]. Programming was done using MATLAB. During an initial development of the tool, two feed strategies were implemented: a simple constant or linearly increasing feed-rate strategy without any sampling (feedback) from the process, and a pulse feeding strategy,

which gives the culture a *bolus* feed depending on time or substrate concentration in the bioreactor.

4.2.8 Use of DoE during Simulation

A general two-level full factorial design was used for the analysis of fed-batch control parameters. Randomization, replication and blocking are considered by the Matlab's DoE module during design creation. Using full factorial designs reduces the number of experiments, so that further experimentation in the lab can be carried out in a more efficient manner.

4.3 Results

4.3.1 Determination of Kinetic Parameters for Modelling

The specific growth rate was considered to follow a kinetic based on that proposed by Monod [Monod (1949)]. Alternatives, like the attribution of growth inhibition to unknown, not-yet-identified autoinhibitor (autocrine) components, have been already validated for a hybridoma cell line in continuous culture [Zeng et al. (1998a)]. However, since the identity of this component is still unclear, an underlying assumption behind model formulation is a constant specific production rate for the autoinhibitor. In order to keep the strategy developed in this work as simple as possible, this approach was not considered for the description of the culture kinetics.

The model selected for simulation of fed-batch culture includes only four metabolites in its structure. Glucose and glutamine were assumed to be the major growth-limiting components of the medium, whereas lactate and ammonium were taken as the major growth-inhibiting metabolites. A series of 4 shake flask experiments was used for kinetic parameter estimation. The four experiments considered both low and high concentrations of each component. The experimental design for the determination of kinetic parameters can be seen in Table 4.1. The initial concentrations of the four components in Table 4.1 were chosen according to their specific uptake rates (data not shown) in order to avoid parallel limitation (Glc and Gln) or inhibition (Lac, Amm) during culture. It has been observed that lactate concentrations until 30 mM doesn't slow down the growth of AGE1.HN cells. At a lactate concentration of 30 mM, metabolic shift took place with the consequent lactate consumption as long as the pH value in culture was above 7.0. Due to this behavior, it was no

Table 4.1: Concentration of the metabolites used in the experimental design for determination of kinetic parameters

Experiment	Glucose [mM]	Glutamine [mM]	Lactate [mM]	Ammonium [mM]
1	10	5	0	0
2	30	2	0	0
3	30	5	30	0
4	30	5	0	2

possible to determine K_{lac} from shake flask experiments. For this reason, lactate inhibition was not considered in the growth model for simulation.

A more clear inhibition was observed for ammonia, which reached a final concentration of 7 - 8 mM, in batch cultures, for experiments performed in our laboratory as well as for experiments performed by our project partners. For this reason, ammonia was considered for the construction of the model as the only inhibiting component during culture. The formulations of μ and k_d including ammonium as the main toxic metabolite are shown by Equations 4.19 and 4.20.

$$\mu = \mu_{max} \frac{K_{amm} + C_{amm}}{K_{amm}} \frac{C_{glc}}{C_{glc} + K_{glc}} \frac{C_{gln}}{C_{gln} + K_{gln}} \tag{4.19}$$

$$k_d = k_{d,max} \frac{K_{d,\mu}}{K_{d,\mu} + \mu} \frac{C_{amm}}{K_{d,amm} + C_{amm}} \tag{4.20}$$

Equation 4.20 considers growth inhibition exerted by ammonium accumulation independently of substrate sufficiency.

In order to account for the dependency of the glucose uptake rate on the specific growth rate, a maintainance energy model with wide acceptance [Pirt (October 1965)] was considered for specific glucose consumption (see Equation 4.21) [Sercinoglu (2011)].

$$q_{glc} = \frac{1}{Y_{X/glc}} \mu + m_{glc} \tag{4.21}$$

The increase in uptake rate due to excess glutamine concentrations [Zeng and Deck-

wer (1995)] is included in the formulation for the glutamine uptake rate (Equation 4.23):

$$q_{gln} = \begin{cases} \frac{\mu}{Y_{X/gln}} + \Delta q_{gln}^{max} \frac{C_{gln} - C_{gln,thres}}{C_{gln} - C_{gln,thres} + K_{gln}^{gln}} & \mathrm{C}_{gln} > \mathrm{C}_{gln,thres} \\ \\ \frac{\mu}{Y_{X/gln}} & \mathrm{C}_{gln} \leq C_{gln,thres} \end{cases} \tag{4.22}$$

Although consumption of other amino acids can significantly contribute to ammonium production [Zeng et al. (1998b)], its build-up was related only to glutamine uptake by means of a yield constant ($\mathrm{Y}_{amm/gln}$):

$$q_{amm} = Y_{amm/gln} \cdot q_{gln} \tag{4.23}$$

The values after parameter estimation from shake flask culture are given in Table 4.2. These values were firstly used after calculation to simulate a bioreactor batch culture. Simulated and experimental data are shown in Figure 4.1.

Table 4.2: Kinetic parameters for AGE1.HN cells determined from shake flask cultures [Sercinoglu (2011)].

Parameter	Value	Parameter	Value
μ_{max}	$0.025\,\mathrm{h}^{-1}$	$\mathrm{Y}_{X/gln}$	$3{\cdot}10^{9}$ cell mmol^{-1}
$\mathrm{k}_{d,max}$	$0.003\,\mathrm{h}^{-1}$	$\mathrm{Y}_{X/glc}$	$0.9{\cdot}10^{8}$ cell mmol^{-1}
K_{glc}	0.08 mM	m_{glc}	$5.82{\cdot}10^{-12}$ mmol cell^{-1} h^{-1}
K_{gln}	0.02 mM	$\mathrm{Y}_{amm/gln}$	0.7 mol mol^{-1}
K_{amm}	2 mM	$\mathrm{K}_{d,\mu}$	$0.0003\,\mathrm{h}^{-1}$
Δq_{gln}^{max}	$4.4{\cdot}10^{-11}$ cell mmol^{-1}	C_{gln}^{thres}	0.5 mM
K_{gln}^{gln}	2 mM	$\mathrm{K}_{d,amm}$	2 mM

4.3.2 Verification of Kinetic Parameters obtained from Shake Flask Culture for Simulation of Bioreactor Data

Data shown in Table 4.2 were set into the model for simulation of bioreactor cultures. Simulation and experimental results are shown in Figure 4.1. The results obtained from simulation show a very good concordance to the experimental results obtained after bioreactor culture, despite of the use of a relatively simple model for simulation.

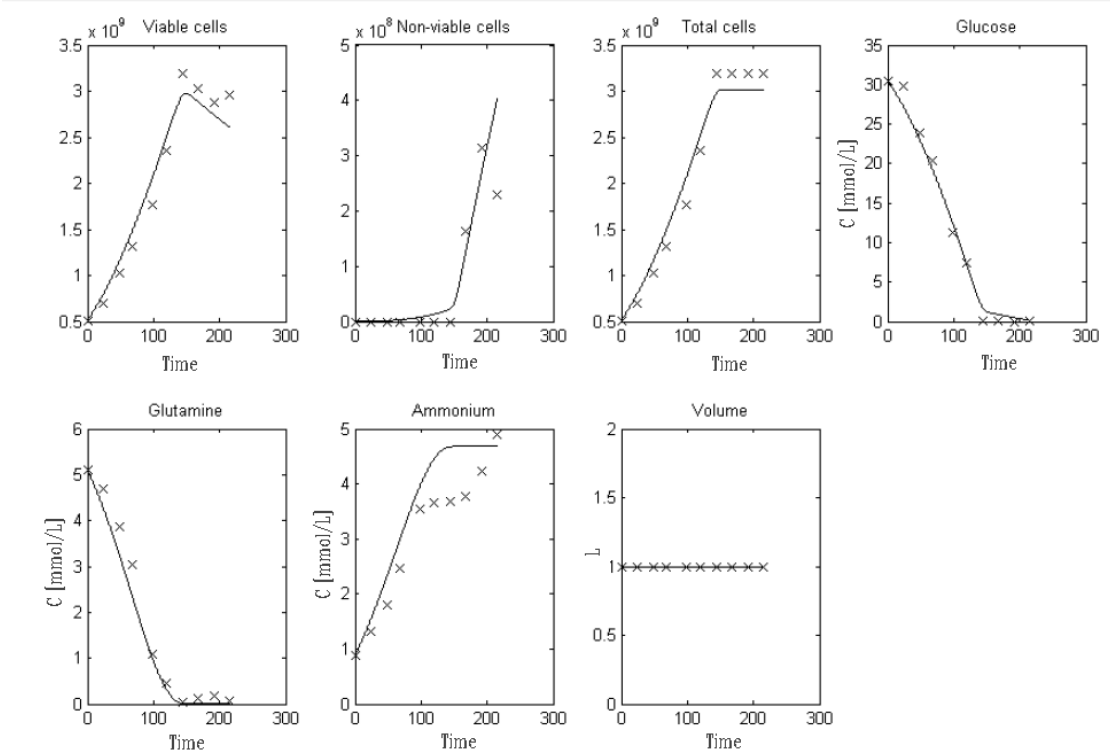

Figure 4.1: Comparison of simulated data (lines) to experimental data obtained from batch culture in a bioreactor (x). Kinetic parameters for simulation were obtained from shake flask experiments.

4.3.3 Analysis and Evaluation of a Linear Constant Fed-Batch Strategy

The designed fed-batch culture was simulated firstly with the fed-batch analyzer. A full factorial design was used to evaluate the effect of the initial glucose and glutamine concentrations in the feed for a constant linear feeding strategy. This easy-to-evaluate strategy was used as a proof of concept for the evaluation of the developed tool.

The factor levels are shown in Table 4.3. Both extreme values for Glc and Gln concentrations in the feed were selected in a way so as to generate a clear response window for the influence of these components on the maximum viable cell density. The dependency of X_v on $C_{glc,feed}$ and $C_{gln,feed}$ is shown in Figure 4.2. Maximum *in silico* viable cell densities in the range of 4.6 - 5.4·10^9cells L^{-1} can be reached with a constant linear feeding profile according to the results matrix generated by the fed-batch analyzer, whereas a clear reduction of the final viable cell density can be observed for those *in silico* experiments carried out with $C_{glc,feed} < 100$ mM and $C_{gln,feed} \leq 2$ mM. Values above these will, according to the software tool, yield max-

Table 4.3: Factor levels for evaluation of a constant feed rate strategy. $F_{const} = 0.00347\ \mathrm{L\,h^{-1}}$, Feed start: 24 h, $V_{max} = 1.5$ L.

Level	$C_{glc,feed}$ [mM]	$C_{gln,feed}$ [mM]
1	15	2
2	60	8
3	105	14
4	150	20
5	195	26
6	240	32

imum values for X_v.

Four fed-batch experiments were carried out in the laboratory for validation of the

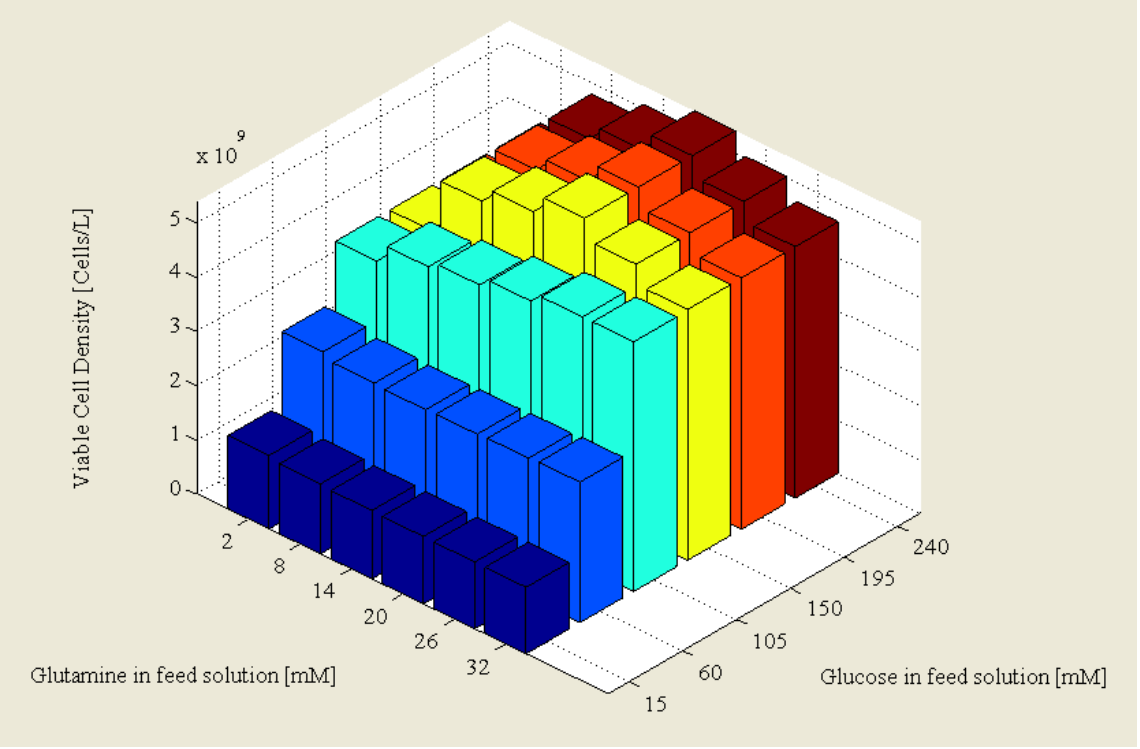

Figure 4.2: Influence of $C_{glc,feed}$ and $C_{gln,feed}$ on the final cell density $X_{v,t=168h}$ of AGE1.HN cells in fed-batch culture. $F_{const} = 0.00347\ \mathrm{L\,h^{-1}}$, Feed start: 24 h and $V_{max} = 1.5$ L.

results from the fed-batch analyzer. The fed-batch experimental plan is shown in Table 4.4. The experiments were carried consecutively in the laboratory with initial conditions ($X_{v,0}$, $C_{glc,0}$, $C_{gln,0}$, $C_{glc,feed}$, $C_{gln,feed}$) as close as possible to the planed values.

Table 4.4: Fed-batch experiments performed in a 1 L benchtop bioreactor. $F_{const} = 0.00347$ L h^{-1}, Feed start: 24 h, $V_{max} = 1.5$ L.

Fed-batch Experiment	$C_{glc,feed}$ [mM]	$C_{gln,feed}$ [mM]
1	60	8
2	105	32
3	195	20
4	240	14

Table 4.5 summarizes the predicted and the experimental values for the viable cell density X_v, at culture time t = 7 days. The experimental values for cell density at t = 7 d, $X_{v,exp}$ increase along with C_{glc} as expected according to the simulated values shown in Figure 4.2. Substrate depletion was only observed in the Fed-batch experiment with $C_{glc,feed} = 60$ mM and $C_{gln,feed} = 8$ mM (Fed-batch 1). In the other experiments no substrate depletion or clear inhibition was observed.

The average relative error of the simulated values compared to the experimental values is 17.7 %. This value is not high considering the use of a simple model which includes a low number of kinetic parameters. Furthermore, the fact that the kinetic parameters are determined from shake flask culture experiments makes the implementation of this strategy easier. The relative errors shown in Table 4.5 for Fed-batch experiments move from negative into positive values parallel to the consecutive experiment number. Lower relative errors in fed-batch culture might point to those experiments, in which culture conditions are more similar to the conditions in shake flask culture for kinetic parameter determination.

The reason for choosing a simple feeding profile in this work had to do with the characteristics of the process studied. The simplified batch and fed-batch media described in Section 4.2.1, p. 97, were created by simple supplementation of a normal batch medium without glucose and glutamine. This batch medium (42-MAX-UB) was designed stoichiometrically to be supplemented with 30 mM glucose and 5 mM glutamine. Thus, the maximum cell density, which can be reached in a fed-batch process here is equal to the maximum cell number reached in batch culture with initial values of Glc = 30 mM and Gln = 5 mM. A common maximum X_v of AGE1.HN in batch culture lies around 4.5 - 5·10^9 cells L^{-1} after 5 - 6 days in culture (inoc. X_v = 1· 10^9 cells L^{-1}). Knowing this, the proposed fed-batch might reach experimentally the same X_v value under optimal conditions. The process duration was fixed to a maximum of 7 days, with feed-start 24 hours after inoculation. Accordingly, the feed

Table 4.5: Batch and Fed-batch experiments performed in a 1 L benchtop bioreactor. For Batch $V_w = 1$ L, for Fed-batch $F_{const} = 0.00347$ L h^{-1}, Feed start: 24 h, $V_{max} = 1.5$ L.

Experiment	$C_{glc,feed}$ [mM]	$C_{gln,feed}$ [mM]	$X_{v,sim}$ [10^9 cells L^{-1}]	$X_{v,exp}$ [10^9 cells L^{-1}]	$s_{X_{v,exp}}$ [10^9 cells L^{-1}]	$(X_{v,exp}\text{-}X_{v,sim})/X_{v,exp}$ [%]
Batch	30	5	1.77	2.04	0.38	13.2
Fed-batch 1	60	8	3.44	2.68	0.39	-28.4
Fed-batch 2	105	32	3.91	4.61	0.11	15.2
Fed-batch 3	195	20	4.12	4.37	0.23	5.7
Fed-batch 4	240	14	4.20	5.65	0.28	25.7

500 mL was divided into 6 days resulting in a linear feeding profile of 0.00347 $L\,h^{-1}$. The end of the fed-batch process was defined by reaching the maximum bioreactor volume (1.5 L) after 7 days of culture.

Only in this way, experimentally possible limitations were made to depend only on glucose or glutamine concentrations, but not on other nutrients, for which there is no metabolic information (e.g. amino acids). Although it would be worthy to study longer fed-batch periods, this shall be performed with a real feed medium. Other parameters such as the influence of the feed-rate or the begin-of-feed on the culture could also be included in a full factorial design for process evaluation when using a special feed formulation.

Furthermore, considering practical work, there might be clear differences in cell growth between shake flask and bioreactor culture. This differences may be taken into account to avoid misleading data and erroneous introduction of model kinetic parameters obtained from shake flasks, which cannot describe the bioreactor cultures. In an ideal case, the user has access to process windows for comparability of growth of the used cell line for the cultivation systems in study.

The challenge for a constant-linear feeding strategy was to keep the substrate concentration within an optimum range so that the cell viability remains high until the end of the process. Since the growth of cells is not taken into account by this strategy, a too low rate may cause substrate limitation. On the other hand too high substrate concentrations may result in viability loss or slow-down of growth due to excessive metabolite production. The aim of this work was to find the combination of control parameters which would yield the maximum amount of cells without leading to substrate limitation or excessive metabolite accumulation.

4.4 Concluding Remarks

A method for evaluation of feeding strategies during fed-batch culture was presented. First, a tool for the evaluation of feeding profiles was developed. This tool allows the user for loading or creating new growth models depending on the complexity of the process.

A simple kinetic model was used for simulation of growth and uptake rates of AGE1.HN cells. The kinetic parameters for model fitting were obtained from shake flask cultures.

After the development of a simple fed-batch medium from a basic batch medium, a constant linear feeding strategy was tested in the laboratory with a previous *in silico* experimental design. This type of substrate feeding was rather simple to implement as it involved only proper selection of the initial substrate concentrations and turning on of the pump to ensure constant rate of feeding during a time interval.

Four fed-batch experiments were performed in a benchtop bioreactor for confirmation of the results. An average relative error of 17 % between simulated and experimental values for the final cell density in the bioreactor was calculated. This value can be considered low, due to the simplicity of the model used, which considered a low number of kinetic parameters for process simulation. With this method a simple and easy-to-implement evaluation strategy for feeding profiles during fed-batch culture has been established, which allows for the reduction in the number of experiments during the evaluation of feeding strategies in mammalian cell culture.

5 Summary and Outlook

In this work, three process strategies were developed and implemented for the characterization of the novel human industrial cell line AGE1.HN.

The growth dependency of AGE1.HN cells on process parameters was experimentally verified for geometrically different bioreactors and shake flasks. Process windows were identified for both systems which allow for comparable cell growth and serve as a basis for ensuring lab-to-lab consistency of the results generated from different cultivation systems. This strategy can be implemented when data generation should be performed in cultivation systems with important geometric differences and for the transfer of process parameters between working groups. Current work in the chemical and pharmaceutical industry points to the need of comparability assessments during the production of biologics after changes in the production process [Lubiniecki et al. (2011)]. Further work with suspendable cell lines should regard the dependency of cell growth on the process parameters of the cultivation system. Furthermore, the influence of the hydrodynamics in the cultivation system on other parameters of cell metabolism may be considered in more detail.

A synchronization strategy for suspendable cell lines in a common phase of the cell cycle was presented. The highest yield of synchronous AGE1.HN cells was achieved by using the method of countercurrent centrifugal elutriation. This physical method proved to be reproducible and scalable for the obtention of synchronous cell subpopulations. Synchrony was reflected in the cell growth curves, as well as in the cell size and cell cycle distributions over time. This method can be applied to other suspendable cell lines for further characterization of cell cycle dependent metabolism. Specially, areas of study like energetic metabolism and process efficiency during product formation in mammalian cell culture can be more precisely analyzed, since a more detailed quantitative description of their kinetics is still needed for modelling. Acquired knowledge on this topic would undoubtedly lead to an increase in the efficiency of industrial processes and the consequent reduction of culture volume in production bioreactors.

Finally, a systematic evaluation of fed-batch strategies was proposed, which is based on the use of a simple kinetic model. The experimental validation of this strategy showed a good applicability of the method in order to reduce the number of experiments to discretize among feeding strategies in mammalian cell culture. This

strategy opens the possibility to a faster and easier evaluation of feeding strategies with a further reduction in the complexity and the time needed for their evaluation. Further work should consider the implementation of new growth kinetic models as well as new feeding profiles. In this way, the capacity of the tool can be extended and adapted to the needs of either academic or industrial users.

References

M. L. Acosta, A. Sánchez, F. García, A. Contreras, and E. Molina. Analysis of kinetic, stoichiometry and regulation of glucose and glutamine metabolism in hybridoma batch cultures using logistic equations. *Cytotechnology*, 54(3):189–200, 2007.

M. Al-Rubeai and A. N. Emery. Flow cytometry in cell culture. *Bio/Technology*, 11:572–579, 1993.

M. Al-Rubeai, R. P. Singh, M. H. Goldman, and A. N. Emery. Death mechanisms of animal cells in conditions of intensive agitation. *Biotechnology and Bioengineering*, 45(6):463–472, 1995. ISSN 1097-0290. doi: 10.1002/bit.260450602.

A. Amanullah, B. Buckland, and A. Nienow. Mixing in the fermentation and cell culture industries. In E. L. Paul, V. A. Atiemo-Obeng, and S. M. Kresta, editors, *Handbook of Industrial Mixing*, pages 1071–1170. Wiley-Interscience, Hoboken and N.J, 2004. ISBN 0-471-26919-0.

Amersham Biosciences. Ficoll pm 70, ficoll pm 400, 2001. URL `https://somapps.med.upenn.edu/pbr/portal/immune/Ficoll_info.pdf`.

E. Anderson and D. Petersen. Cell growth and division. ii. experimental studies of cell volume distributions in mammalian suspension cultures. *Biophysical Journal*, 7:353–364, 1967.

E. F. Augusto, M. F. Barral, and R. A. Piccoli. Mathematical models for growth and product synthesis in animal cell culture. In *Animal cell technology from biopharmaceuticals to gene therapy*. Taylor & Francis, New York [u.a], 2007.

G. Balfavi. Cell cycle synchronization of animal cells and nuclei by centrifugal elutriation. *Nature Protocols*, 3(4):663–673, 2008.

R. Bates and P. L. C. R. Fondy. An examination of some geometric parameters of impeller power. *IEC Process Design and Development*, 2(4):310–314, 1963.

Beckman Coulter. Z-series: User manual 9914591-d, 1992-2002. URL `http://www.coulterflow.com/bciflow/documents/instruments/Z%20series/ZSeries%20Op%20Manual%20%289914591D%29.pdf`.

Beckman Coulter. The je-5.0 elutriation system: for use with avanti j-20xp series, j-26xp series and j6-mi centrifuges, 2007.

V. Blanchard, X. Liu, S. Eigel, M. Kaup, S. Rieck, S. Janciauskiene, V. Sandig, U. Marx, P. Walden, R. Tauber, and M. Berger. N-glycosylation and biological activity of recombinant human alpha1-antitrypsin expressed in a novel human neuronal cell line. *Biotechnology and Bioengineering*, 108(9):2118–2128, 2011. ISSN 1097-0290. doi: 10.1002/bit.23158.

H. J. Boxberger. *Leitfaden für die Zell- und Gewebekultur: Einführung in Grundlagen und Techniken*. Wiley-VCH, Weinheim, 2007. ISBN 3527314687.

R. Britten and R. Roberts. High-resolution density gradient sedimentation analysis. *Science*, 131, 1960.

J. Büchs, U. Maier, C. Milbradt, and B. Zoels. Power consumption in shaking flasks on rotary shaking machines: I. Power consumption measurement in unbaffled flasks at low liquid viscosity. *Biotechnology and Bioengineering*, 68(6):589–593, 2000a. ISSN 1097-0290.

J. Büchs, U. Maier, C. Milbradt, and B. Zoels. Power consumption in shaking flasks on rotary shaking machines: II. Nondimensional description of specific power consumption and flow regimes in unbaffled flasks at elevated liquid viscosity. *Biotechnology and Bioengineering*, 68(6):594–601, 2000b. ISSN 1097-0290.

Y. Chisti. Hydrodynamic damage to animal cells. *Critical Reviews in Biotechnology*, 21(2):67–110, 2001. ISSN 0738-8551. doi: 10.1080/20013891081692.

M. W. Chudacek. Impeller power numbers and impeller flow numbers in profiled bottom tanks. *Ind. Eng. Chem. Process Des. Dev.*, 24:858–867, 1985.

S. Cooper. Mammalian cells are not synchronized in G1-phase by starvation or inhibition: considerations of the fundamental concept of G1-phase synchronization. *Cell Proliferation*, 31:9–16, 1998.

S. Cooper. Minimally disturbed, multicycle, and reproducible synchrony using a eukaryotic "baby machine". *BioEssays : news and reviews in molecular, cellular and developmental biology*, 24(6):499–501, 2002a. ISSN 0265-9247. doi: 10.1002/bies.10108.

S. Cooper. Reappraisal of G1-phase arrest and synchronization by lovastatin. *Cell biology international*, 26(8):715–727, 2002b. ISSN 1065-6995.

S. Cooper. Rethinking synchronization of mammalian cells for cell cycle analysis. *Cellular and molecular life sciences : CMLS*, 60(6):1099–1106, 2003. ISSN 1420-682X. doi: 10.1007/s00018-003-2253-2.

S. Cooper. Nocodazole does not synchronize cells. *Cell Tissue Res.*, 324:237–242, 2006.

S. Cooper and K. Shedden. Microarray analysis of gene expression during the cell cycle. *Cell & Chromosome*, 2:1–12, 2003. URL `http://www.cellandchromosome.com/content/pdf/1475-9268-2-1.pdf,AppendixI:http://www.biomedcentral.com/content/supplementary/1475-9268-2-1-S1.pdf`.

E. Cosgrave, W. Struwe, J. Kattla, M. Campbell, M. Wormland, and P. Rudd. Glycomics. In M. Moo-Young, editor, *Comprehensive Biotechnology, 2nd Edition*, pages 427–446. Pergamon, 2011. ISBN 9780444533524.

A. R. Costa, M. E. Rodrigues, M. Henriques, J. Azeredo, and R. Oliveira. Guidelines to cell engineering for monoclonal antibody production. *European Journal of Pharmaceutics and Biopharmaceuticals*, 74(2):127–138, 2010. doi: 10.1016/j.ejpb.2009.10.002.

P. Czermak. Special engineering aspects. In R. Eibl, D. Eibl, R. Pörtner, G. Catapano, and P. Czermak, editors, *Cell and Tissue Reaction Engineering*, pages 83–172. Springer-Verlag, s.l, 2008. ISBN 3540681752.

J. Dean. *Lange's Handbook of Chemistry*. McGraw Hill, Inc., 1992.

M. Dorin. Developing elutriation protocols. Technical Information. High speed centrifugation, 1994.

A. Einsele. Scaling up bioreactors. *Process Biochemistry*, 7:13–14, 1978.

J. Engasser, J. Goergen, and A. Marc. Modelling. In *Cell and Tissue Culture: Laboratory Procedures in Biotechnology*, pages 160–178. John Wiley & Sons, Inc., 1998.

I. C. Enninga, R. T. Groenendijk, A. A. van Zeeland, and J. W. Simons. Use of low temperature for growth arrest and synchronization of human diploid fibroblasts. *Mutation Research*, 130(5):343–352, 1984. ISSN 0027-5107.

M. Fiore, R. Zanier, and F. Degrassi. Reversible g(1) arrest by dimethyl sulfoxide as a new method to synchronize chinese hamster cells. *Mutagenesis*, 17(5):419–424, 2002. ISSN 0267-8357.

M. B. Fogolín, R. Wagner, M. Etcheverrigaray, and R. Kratje. Impact of temperature reduction and expression of yeast pyruvate carboxylase on hgm-csf-producing cho cells. *Journal of Biotechnology*, 109(1-2):179–191, 2004. ISSN 0168-1656. doi: 10.1016/j.jbiotec.2003.10.035.

B. Frahm, P. Lane, A. Munack, and R. Pörtner. Optimierung und Steuerung von Zellkultur-fed-Batch-Prozessen mittels einer Kollokationsmethode. *Chemie Ingenieur Technik*, 77(4):429–435, 2005.

V. C. Hass and R. Pörtner. *Praxis der Bioprozesstechnik: Mit virtuellem Praktikum*. Spektrum Akad. Verl., Heidelberg, 2 edition, 2011. ISBN 9783827428288.

C. E. Helmstetter and D. J. Cummings. Bacterial synchronization by selection of cells at division. *Proceedings of the National Academy of Sciences of the United States of America*, 50:767–774, 1963. ISSN 0027-8424.

C. E. Helmstetter, M. Thornton, A. Romero, and K. L. Eward. Synchrony in human, mouse and bacterial cell cultures–a comparison. *Cell cycle (Georgetown, Tex.)*, 2 (1):42–45, 2003. ISSN 1538-4101.

R. R. Hemrajani and G. Taterson. Mechanically stirred vessels. In E. L. Paul, V. A. Atiemo-Obeng, and S. M. Kresta, editors, *Handbook of Industrial Mixing*. Wiley-Interscience, Hoboken and N.J, 2004. ISBN 0-471-26919-0.

H.-J. Henzler. Verfahrenstechnische Auslegungsunterlagen für Rührbehälter als fermenter. *Chem.-Ing.-Tech.*, 54(5):461–476, 1982.

M. Holley. Purification of mammalian cochlear hair cells using small volume percoll density gradients. *Journal of Neuroscience Methods*, 27:219–224, 1988.

W. S. Hu and A.-P. Zeng. *Genomics and Systems Biology of Mammalian Cell Culture*, volume 127 of *Advances in Biochemical Engineering Biotechnology*. Springer Berlin Heidelberg, Berlin and Heidelberg, 2012 edition, 2012. ISBN 9783642283499. doi: 10.1007/978-3-642-28350-5.

V. Hudcova, V. Machon, and A. W. Nienow. Gas-liquid dispersion with dual Rushton turbine impellers. *Biotechnology and Bioengineering*, 34(5):617–628, 1989.

J. D. Jang and J. P. Barford. An unstructured kinetic model of macromolecular metabolism in batch and fed-batch cultures of hybridoma cells producing monoclonal antibody. *Biochemical Engineering Journal*, 4(2):153–168, 2000.

M. Jordan and N. Jenkins. Tools for high-throughput medium and process optimization. In R. Pörtner, editor, *Animal Cell Biotechnology*, pages 193–202. Humana Press Inc., Totowa and New Jersey and USA, 2007.

P. Jorgensen and M. Tyers. How cells coordinate growth and division. *Current Biology*, 14:1014–1027, 2004.

L. Ju and G. Chase. Improved scale-up strategies of bioreactors. *Bioprocess Engineering*, 8:49–53, 1992.

M. Julius, T. Masuda, and L. Herzenberg. Demonstration that antigen-binding cells are precursors of antibody-producing cells after purification with a fluorescence-activated cell sorter. *Proceedings of the National Academy of Sciences of the United States of America*, 69(7):1934–1938, 1972. ISSN 0027-8424.

B. Junker. Scale-up methodologies for escherichia coli and yeast fermentation processes. *Journal of Bioscience and Bioengineering*, 97(6):347–364, 2004.

Y. Kato, S. Hiraoka, Y. Tada, S. Shirai, T. Ue, S. T. Koh, and T. Yamaguchi. Power-consumption of horizontally shaking vessel with circulating motion. *Kagaku Kogaku Ronbunshu*, 21(2):365–371, 1995.

K. Keyomarsi, L. Sandoval, V. Band, and A. B. Pardee. Synchronization of tumor and normal cells from G1 to multiple cell cycles by lovastatin. *Cancer Research*, 51(13):3602–3609, 1991. ISSN 0008-5472.

S. H. G. Khoo and M. Al-Rubeai. Metabolomics as a complementary tool in cell culture. *Biotechnology and Applied Biochemistry*, 47(Pt 2):71–84, 2007. ISSN 1470-8744. doi: 10.1042/BA20060221.

M. Knehr, M. Poppe, M. Enulescu, W. Eickelbaum, M. Stoehr, D. Schroeter, and N. Paweletz. A critical appraisal of synchronization methods applied to achieve maximal enrichment of hela cells in specific cell cycle phases. *Experimental cell Research*, 217(2):546–553, 1995. ISSN 0014-4827. doi: 10.1006/excr.1995.1121.

M. Kraume. *Mischen und Rühren: Grundlagen und moderne Verfahren*. Wiley-VCH, Weinheim, 2003. ISBN 9783527307098.

M. Kraume and P. Zehner. Experience with experimental standards for measurements of various parameters in stirred tanks: A comparative test. *Chemical Engineering Research & Design*, 79(A8):811–818, 2001.

A. Krishan, D. Paika, and E. Frei. Cell cycle synchronization of human lymphoid cells in vitro by 2,3-dihydro-1h-imidazo[1,2-b]pyrazole. *Cancer Research*, 36(1): 138–142, 1976. ISSN 0008-5472.

A. R. Lara, E. Galindo, O. T. Ramírez, and L. A. Palomares. Living with heterogeneities in bioreactors: understanding the effects of environmental gradients on cells. *Molecular Biotechnology*, 34(3):355–381, 2006. ISSN 1073-6085. doi: 10.1385/MB:34:3:355.

T. Lindl and G. Gstraunthaler. *Zell- und Gewebekultur: Von den Grundlagen zur Laborbank*. Spektrum Akademischer Verlag, Heidelberg and Neckar, 6 edition, 2008. ISBN 3827417767.

A. Lübbert. Advanced methods for bioreactor characterization. *Journal of Biotechnology*, 25(1-2):145–182, 1992. ISSN 0168-1656.

A. Lubiniecki, D. B. Volkin, M. Federici, M. D. Bond, M. L. Nedved, L. Hendricks, P. Mehndiratta, M. Bruner, S. Burman, P. DalMonte, J. Kline, A. Ni, M. E. Panek, B. Pikounis, G. Powers, O. Vafa, and R. Siegel. Comparability assessments of process and product changes made during development of two different monoclonal antibodies. *Biologicals*, 39(1):9–22, 2011.

M. Lutz, G. Gaedicke, and W. Hartmann. Large-scale cell separation by centrifugal elutriation. *Analytical Biochemistry*, 200:376–380, 1992.

N. N. Ma, K. W. Koelling, and J. J. Chalmers. Fabrication and use of a transient contractional flow device to quantify the sensitivity of mammalian and insect cells to hydrodynamic forces (vol 30, pg 428, 2002). *Biotechnology and Bioengineering*, 81(3):379–379, 2003. doi: 10.1002/bit.10611.

C.-F. Mandenius and A. Brundin. Bioprocess optimization using design-of-experiments methodology. *Biotechnology Progress*, 24(6):1191–1203, 2008.

H. Märkl, H. Kurosawa, M. Matsumura, and H. Tanaka. New dialysis bioreactor for animal cell culture. In *Proceedings of Second Anual Meeting of Japanese Association for Animal Cell Technology*. Tsukuba and Japan, 1989.

J. Markopoulos and E. Pantuflas. Power consumption in gas-liquid contactors agitated by double-stage Rushton turbines. *Chemical Engineering & Technology*, 24 (11):1147–1150, 2001.

L. H. Matherly. A method for the synchronization of cultured cells with aphidicolin. *Analytical Biochemistry*, 182:338–345, 1989.

P. Mavros. Flow visualization in stirred vessels - a review of experimental techniques. *Chemical Engineering Research & Design*, 79(A2):113–127, 2001.

S. Miltenyi, W. Müller, W. Weichel, and A. Radbruch. *Cytometry*, 11:231–238, 1990.

J. Monod. The growth of bacterial cultures. *Annual Review of Microbiology*, 3(1):371–394, 1949. ISSN 0066-4227. doi: 10.1146/annurev.mi.03.100149.002103. URL http://www.annualreviews.org/doi/abs/10.1146/annurev.mi.03.100149.002103.

M. Monti, M. Cozzolino, F. Cozzolino, G. Vitiello, R. Tedesco, A. Flagiello, and P. Pucci. Puzzle of protein complexes in vivo: a present and future challenge for functional proteomics. *Expert review of proteomics*, 6(2):159–169, 2009. ISSN 1744-8387. doi: 10.1586/epr.09.7.

M. Moo-Young, editor. *Comprehensive Biotechnology*. Pergamon, 2 edition, 2011. ISBN 9780444533524.

A. Moore, J. Mercer, G. Dutina, C. J. Donahue, K. D. Bauer, J. P. Mather, T. Etcheverry, and T. Ryll. Effects of temperature shift on cell cycle, apoptosis and nucleotide pools in cho cell batch cultues. *Cytotechnology*, 23(1-3):47–54, 1997. doi: 10.1023/A:1007919921991.

C. Mrotzek, T. Anderlei, H.-J. Henzler, and J. Büchs. Mass transfer resistance of sterile plugs in shaking bioreactors. *Biochemical Engineering Journal*, 7(2):107–112, 2001. ISSN 1369-703X.

A. W. Nienow. On impeller circulation and mixing effectiveness in the turbulent flow regime. *Chemical Engineering Science*, 52(15):2557–2565, 1997.

J. Niklas, E. Schräder, V. Sandig, T. Noll, and E. Heinzle. Quantitative characterization of metabolism and metabolic shifts during growth of the new human cell line age1.hn using time resolved metabolic flux analysis. *Bioprocess and biosystems engineering*, 34(5):533–545, 2011. ISSN 1615-7605. doi: 10.1007/s00449-010-0502-y.

S. S. Ozturk. Engineering challenges in high density cell culture systems. *Cytotechnology*, 22(1-3):3–16, 1996.

S. S. Ozturk and B. O. Palsson. Chemical decomposition of glutamine in cell culture media: Effect of media type, ph, and serum concentration. *Biotechnology Progress*, 6:121–128, 1990.

S. J. Pirt. The maintenance energy of bacteria in growing cultures. *Proceedings of the Royal Society of London. Series B, Biological Sciences*, 163(991):224–231, October 1965. URL http://www.jstor.org/stable/75569.

O. Platas, U. Jandt, L. D. M. Phan, M. E. Villanueva, M. Schaletzky, A. Rath, S. Freund, U. Reichl, E. Skerhutt, S. Scholz, T. Noll, V. Sandig, R. Pörtner, and A.-P. Zeng. Evaluation of criteria for bioreactor comparison and operation standardization for mammalian cell culture. *Engineering in life sciences*, 12(5):518–528, 2012. doi: 10.1002/elsc.201100163.

R. Pörtner and H. Märkl. Dialysis cultures. *Applied Microbiology and Biotechnology*, (50):403–414, 1998. ISSN 1432-0614.

A. Prediger, T. Höpfner, A. Bluma, P. Lindner, M. Akin, M. Yuksel, S. Beutel, S. Timur, and T. Scheper. A multifunctional at-line

analysis system for monitoring of cell cultivations, 2011. URL http://www.tci.uni-hannover.de/index.php?eID=tx_nawsecuredl&u=0&file=uploads/tx_tkpublikationen/Waedenswil2011.pdf&t=1354625967&hash=78380219f2ceb237bdbe8c21178171bf37e2085d.

Promega. Technical bulletin: Apo-ONE homogeneous caspase-3/7 assay, 2009. URL www.promega.com/~/media/files/resources/protocols/technicalbulletins/0/apoonehomogeneouscaspase37assayprotocol.pdf?la=en.

M. Rahman. *Introduction to Flow Cytometry.* AbD Serotec a Division of Morphosys, 2006. URL http://static.abdserotec.com/uploads/Flow-Cytometry.pdf.

A. Rath. Insights into cellular energy metabolism: Connecting intracellular metabolites and maximum enzyme activities. Conference: GVC/DECHEMA Vortrags- und Diskussionstagung, 14.05.12, Freiburg, Germany, 2012.

C. Riccardi and I. Nicoletti. Analysis of apoptosis by propidium iodide staining and flow cytometry. *Nature Protocols*, 1(3):1458–1461, 2006.

D. Rickwood, T. Ford, and J. Steensgaard. Centrifugation. In D. Rickwood and B. Hames, editors, *Esential Data Series*, pages 29–41. Wiley, 1994.

M. Rieseberg, C. Kasper, K. F. Reardon, and T. Scheper. Flow cytometry in Biotechnology. *Applied Microbiology and Biotechnology*, 56(3-4):350–360, 2001. ISSN 0175-7598.

M. Rola-Pleszczynski and W. H. Churchill. Purification of human monocytes by continuous gradients sedimentation in Ficoll. *Journal of Immunological Methods*, 20:255–262, 1978.

J. H. Rushton, E. W. Costich, and H. J. Everett. Power characteristics of mixing impellers. Part I. *Chem. Eng. Prog.*, 46:395–404, 1950a.

J. H. Rushton, E. W. Costich, and H. J. Everett. Power characteristics of mixing impellers. Part II. *Chem. Eng. Prog.*, 46:467–476, 1950b.

R. Sander. Compilation of henry's law constants for inorganic and organic species of potential importance in environmental chemistry, 1999. URL http://www.mpch-mainz.mpg.de/~sander/res/henry.html.

H. Schlichting. *Boundary Layer Theory.* McGraw Hill, New York, 7th edition edition, 1979.

O. Sercinoglu. Development of a matlab-based tool for the evaluation of fed-batch process strategies in mammalian cell culture. Thesis. Master of Sciences (MSc) in Biotechnology, 2011.

P. Sharpe. Methods of cell separation. In R. Burdon and P. Knippenberg, editors, *Laboratory Techniques in Biochemistry and Molecular Biology*, volume 18. Elsevier, 1988.

C. G. Smith and P. F. Greenfield. Mechanical agitation of hybridoma suspension cultures: Metabolic effects of serum, pluronic F68, and albumin supplements. *Biotechnology and Bioengineering*, 40(9):1045–1055, 1992. ISSN 1097-0290. doi: 10.1002/bit.260400908.

P. T. Spellman and G. Sherlock. Reply: whole-culture synchronization - effective tools for cell cycle studies. *Trends in Biotechnology*, 22(6):270–273, 2004. ISSN 0167-7799. doi: 10.1016/j.tibtech.2004.04.010.

A. Srivastava and S. Gupta. Fed-batch fermentation - design strategies. In M. Moo-Young, editor, *Comprehensive Biotechnology, 2nd Edition*, pages 515–526. Pergamon, 2011. ISBN 9780444533524.

M. Takagi and K. Ueda. On-line continuous measurement of the oxygen consumption rate in mammalian cell culture. *Journal of Fermentation and Bioengineering*, 77 (6):709–711, 1994.

R.-K. Tan, W. Eberhard, and J. Buechs. Measurement and characterization of mixing time in shake flasks. *Chemical Engineering Science*, 66(3):440–447, 2011. doi: 10.1016/j.ces.2010.11.001.

P. K. Vogt and I. M. Verma. *Methods in enzymology. - 254: Oncogene techniques*. Academic Press, San Diego and Calif, 1995. ISBN 9780121821555.

W. G. Whitford. Fed-batch mammalian cell culture in bioproduction. *BioProcess International*, April, 2006.

K. F. Wlaschin and W.-S. Hu. Fedbatch culture and dynamic nutrient feeding. In T. Scheper, editor, *Advances in Biochemical Engineering / Biotechnology*, volume 101, pages 43–74. Springer-Verlag, 2006.

T. F. W.T. Shearer H.W. Schroeder A.J. Frew R.R. Rich and C. W. JR. *Clinical Immunology: Principles and Practice: Expert Consult: Online and Print (Rich, Clinical Immunology). Mosby.* 3 edition, 2008.

L. Xie and W. Zhou. Fed-batch cultivation of mammalian cells for the production of recombinant proteins. In S. S. Ozturk and W.-S. Hu, editors, *Cell Culture Technology for Pharmaceutical and Cell-Based Therapies*, pages 349–386. CRC Press. Taylor & Francis Group, Boca Raton and FL and USA, 2006.

Z. Xing, B. M. Kenty, Z. J. Li, and S. S. Lee. Scale-up analysis for a cho cell culture process in large-scale bioreactors. *Biotechnology and Bioengineering*, 103 (4):733–746, 2009. ISSN 1097-0290. doi: 10.1002/bit.22287.

A. P. Zeng and W. D. Deckwer. Mathematical modeling and analysis of glucose and glutamine utilization and regulation in cultures of continuous mammalian cells. *Biotechnology and Bioengineering*, 47(3):334–346, 1995. ISSN 1097-0290. doi: 10.1002/bit.260470308.

A.-P. Zeng and R. Pörtner. Syslogics: Systems biology of cell culture for biologics. final project report. Technische Informationsbibliothek Hannover. Förderkennzeichen: 0315275a, 2013. URL `http://www.tib-hannover.de/`.

A.-P. Zeng, W. Deckwer, and W. Hu. Determinants and rate laws of growth and death of hybridoma cells in continuous culture. *Biotechnology and Bioengineering*, 57(6):642–654, 1998a. ISSN 1097-0290. URL `http://www.ncbi.nlm.nih.gov/pubmed/10099244.PMID:10099244`.

A.-P. Zeng, W.-S. Hu, and W.-D. Deckwer. Variation of stoichiometric ratios and their correlation for monitoring and control of animal cell cultures. *Biotechnol. Prog.*, 14:434–441, 1998b.

J. Zhu. Mammalian cell protein expression for biopharmaceutical production. *Biotechnology advances*, 30(5):1158–1170, 2012. ISSN 1873-1899. doi: 10.1016/j.biotechadv.2011.08.022.